Single-arm 3-wave interferometer for measuring dispersion in short lengths of fiber

By

Michael Anthony Galle
St# 991 454 109

A thesis submitted in conformity with the requirements for the degree of Master of Applied Science at the Graduate Department of Electrical & Computer Engineering, University of Toronto

Abstract

Single-arm three wave interferometer for measuring dispersion in short lengths of fiber

Michael Anthony Galle

Master of Applied Science

Graduate Department of Electrical & Computer Engineering

University of Toronto

2007

A simple fiber-based single-arm spectral interferometer to measure the dispersion parameter in short lengths (DL) of fiber (< 50 cm) with a measurement precision of 0.0001 ps/nm is developed. Dispersion is measured by examining the envelope of the interference pattern produced by three interfering waves: two from the facets of the test fiber and one from a mirror placed behind it. The operational constraints on system parameters are discussed and a method for extending one of them is introduced. Experimental verification of this technique is carried out via comparison of measurements made on SMF28^{TM} and DCF with those made using conventional techniques. Moreover, this new technique is used to measure the dispersion of twin-hole fiber for the first time.

Acknowledgements

I would like to express my sincere gratitude to Professor Li Qian and Dr. Waleed Mohammed for their inspiration, vision, guidance and support over the last year. I would never have completed this work had it not been for their unwavering encouragement and dedication to supporting my studies and my research. For this I am truly grateful.

I would like to thank Chris Sapiano for his support and friendship throughout the years in both Undergraduate and Graduate school.

I would like to thank my friends and colleagues in graduate school for their insights, support and friendship throughout the last year. Special thanks go to Fei Ye and Jiawen Zhang.

I would like to thank my parents and family for their love, support and encouragement throughout all my years in school. I would never have come this far without their help, inspiration and guidance.

Contents

List of Figures

List of Tables

Chapter 1: Introduction

The design of photonic devices heavily depends on an accurate characterization of the components used. One of the main components in a photonic device is an optical fiber which serves as a low-loss medium for light transmission. An important characteristic of fiber is the dispersion that light experiences as it travels inside the fiber. Dispersion is the phenomenon that causes different frequencies of light to travel at different velocities. The phenomenon of dispersion is commonly observed through the spreading of light by a prism. When white light, which contains a broad spectrum of frequencies, enters a prism the different wavelengths are bent at different angles since each frequency sees a different index of refraction, a phenomenon first quantified by Newton in the 17th century [1]. Inside a fiber this variation in the index of refraction with frequency is what causes the frequency dependence of the velocity.

A more modern example of the phenomenon of dispersion is the affect it has on the performance of photonic devices used in communication systems. In these systems, dispersion, or more specifically second order dispersion, leads to a broadening of the pulses used to represent 1 or 0 in a digital communication system. Pulse broadening causes adjacent bits to overlap and leads to intersymbol interference [2]. Intersymbol interference occurs when a pulse is broadened beyond its allocated bit slot to such an extent that it begins to overlap with adjacent bits and it is no longer possible to determine whether or not a specific bit contains a 1 or a 0. This effect is illustrated in Fig. 1-1:

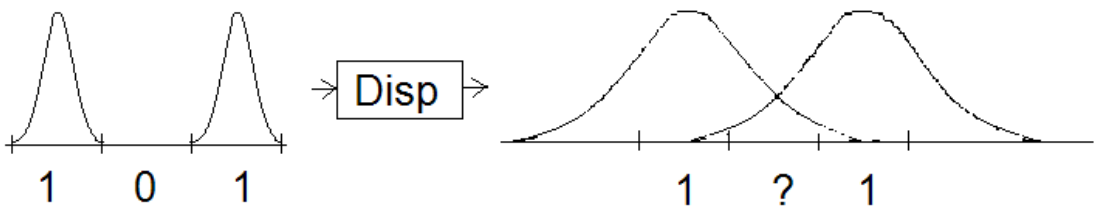

Fig. 1-1: Intersymbol interference caused by dispersion leads to reduction in system bandwidth.

As a result of intersymbol interference the allocated bit slots must be widened and this effectively lowers the number of bits that can be transmitted in a given period of time and reduces the system bandwidth [2]. As a result modern communication systems have evolved methods to mitigate the effects of dispersion.

Current methods of countering the effects of dispersion in an optical fiber use dispersion compensating devices such as chirped fiber Bragg gratings and dispersion compensating fiber (DCF) [2]. In order to effectively use these techniques it is critical to know the exact magnitude of the dispersion that is being compensated for. As a result knowledge of the dispersion in both the transmission system and the dispersion compensation system is critical to the design of the overall communication system.

For example, in order to determine the length of dispersion compensating fiber required to compensate for the dispersion incurred in a span of standard single mode fiber, one must know the dispersion in both types of fiber as well as the exact length of single mode fiber for which the dispersion is to be compensated [2]. The dispersion in the optical fiber can then be compensated by splicing a length of DCF given by:

$$L_{DCF} = \frac{L_{Fiber}\left|D_{Fiber}(\lambda)\right|}{\left|D_{DCF}(\lambda)\right|} \qquad \textbf{Eq. 1-1 [2]}$$

D is known as the second order dispersion parameter which is a function of the second order dispersion of the fiber. Its significance and its effect on an optical signal will be discussed in detail in chapter 2.

Knowledge of dispersion in a fiber is also critical for the study of fiber based nonlinear wave interaction phenomena. An optical soliton is a pulse that maintains a constant shape (width) as it propagates along a fiber (first order soliton) or has a shape that is periodic with propagation (higher order soliton) [3, 4]. This is due to the fact that the effects of dispersion and self phase modulation (SPM) are in balance [4-5]. SPM is the effect whereby the phase of a given pulse is modified by its own intensity profile [6]. Knowledge of the dispersion in an optical fiber allows for the determination of the required intensity for the formation of an optical soliton. This effect has also been used in the area of soliton effect pulse compression [5, 7, 8] where the combination of the chirping effect of SPM and subsequent distributed compression effect of negative dispersion is used to compress an optical pulse [7]. Knowledge of dispersion is also important for the study of nonlinear effects such as second harmonic generation, three-wave mixing and four-wave mixing since it determines the interaction lengths between the various wavelengths. Dispersion is particularly important in techniques that aim to extend this interaction length such as in Quasi Phase Matching (QPM) devices [9-11].

1.1 Motivation

The motivation for this thesis is to measure the dispersion parameter in short lengths of optical fiber. More accurately the method is required to measure fiber with small dispersion length products (DL). The initial need for a short length characterization scheme came from the need to measure the dispersion of a type of specialty fiber known

as the twin-hole fiber (THF) (Ch 5.6). This fiber is not easy to acquire and is expensive to produce therefore the use of conventional dispersion measurement techniques requiring long lengths of fiber (Ch. 3) are not possible. The principle reason for measuring the dispersion in THF is to study nonlinear wave interaction phenomena in these fibers. Knowledge of the dispersion was also of practical importance since we planned to use QPM to increase the interaction length [9-11]. Short length characterization was also required because the fiber geometry of THF is not uniform along its length which results in a variation of the dispersion along the fiber length. The dispersion measurement on a long length of fiber, therefore, is different than the dispersion in a given section of that fiber. Typically only a small section of THF is used in QPM experiments and therefore the dispersion of the specific section of THF used in the experiment must be measured.

Short length (small DL) characterization is not only required for THF but it is also necessary for other types of specialty fiber as well. Photonic Crystal Fiber (PCF) [12-14], for example, can be used for dispersion compensation (DC-PCF) [13]. For devices with small dispersion length (DL) products, such as fiber laser cavities [3], the length of the dispersion compensation fiber required is very short. As a result, it is necessary to measure the dispersion in the exact section of DC-PCF that will be used in the system. Recent advances in Microstructured fiber or PCF allow for a high degree of control over the dispersion [14]. This has led to a need for experimental testing to determine how close the dispersion in the fabricated device is to the predicted theoretical dispersion. Experimental verification of the theoretical dispersion is less expensive when only short lengths of this fiber are required and therefore it is both convenient and economical if dispersion can be measured on short lengths of fiber.

Gain fiber is another type of specialty fiber for which it is desirable to have a short length dispersion measurement technique. Typically short lengths of gain fiber are used to compensate for losses in a long haul optical transmission line [15]. The dispersion in these short lengths of gain fiber must be known in order for dispersion compensation schemes to accurately compensate for the dispersion produced in the entire channel. The dispersion is of particular importance when these gain fibers are used to make mode locked fiber lasers [4] since dispersion affects the group velocity of a pulse within the cavity [2] it also affects mode locking schemes.

1.2 Objectives

The primary objective of this thesis is the development of a technique to measure the dispersion parameter in fiber lengths below 50 cm (small DL products). The first objective is to develop and test the technique by comparing its results with published (or conventionally measured) dispersion parameter curves for SMF28^{TM} and Dispersion Compensating Fiber (DCF). Second, the theory for the technique will be further investigated and operational constraints will be outlined. Third, the dispersion parameter of Twin Hole fiber (THF) will be measured. The dispersion parameter for this fiber has not yet been reported in the literature. The fourth and final objective is to show that this technique is conducive to commercial development, since it can measure waveguides and optical fibers from several centimeters to a few meters in length, without the complications introduced by conventional interferometric dispersion techniques such as the dual arm techniques.

1.3 Organization of Thesis

This thesis is organized into six chapters. The first chapter introduced the topic of dispersion and the motivation and objective behind this work. The second chapter outlines the basic theory behind light propagation in a fiber and introduces the concept of chromatic dispersion. It also outlines how both the material and the waveguide dispersion are combined to yield the total chromatic dispersion in a waveguide. The third chapter surveys the conventional techniques for measuring chromatic dispersion in optical fiber.

The fourth chapter describes the theory and limitations of the novel single arm interferometer developed in this thesis for dispersion characterization of short length optical elements. It also shows how some of these limitations can be relaxed so that a larger range of fiber length can be characterized using the technique. The fifth chapter describes the experimental results used to verify and implement the new technique. Characterization is first performed on Corning SMF28^{TM} since the dispersion curves are well known and can be used to verify the validity of the theory and the technique. As a second verification the technique is applied to dispersion compensating fiber. Once the technique has been verified and tested it is used to characterize specialty fiber known as Twin Hole Fiber for which the dispersion curves have not yet been reported. The sixth chapter concludes the thesis by summarizing the benefits of the single arm interferometer and by describing the contributions this new technology can make to the field of optical characterization. The thesis is concluded with an examination of the future work that is required in order to develop a commercial device from this technology.

Chapter 2: Theory on Chromatic Dispersion of a Waveguide

Dispersion is the phenomenon whereby the index of refraction of a material varies with the frequency or wavelength of the radiation being transmitted through it [1]. The term 'Chromatic Dispersion' is often used to emphasize this wavelength dependence. The total dispersion in a waveguide or an optical fiber is a function of both the material composition (material dispersion) and the geometry of the waveguide (waveguide dispersion). This chapter outlines the contributions of both material and waveguide dispersion, identifies their physical source and develops the mathematical terminology for their description.

2.1 Dispersion in a Waveguide

When light is confined in an optical fiber or waveguide the index is a property of both the material and the geometry of the waveguide. The waveguide geometry changes the refractive index via optical confinement by the waveguide structure. The refractive index is therefore a function of both the material and waveguide contributions. For this reason in a fiber or a waveguide the index is known as an effective index.

The relationship between the effective index and the first, second and higher order dispersion can be understood mathematically via a Taylor expansion:

$$n_{eff} = n_{eff}(\lambda_o) + (\lambda - \lambda_o)\frac{dn_{eff}}{d\lambda}\Big|\lambda_o + (\lambda - \lambda_o)^2 \frac{d^2 n_{eff}}{d\lambda^2}\Big|\lambda_o + (\lambda - \lambda_o)^3 \frac{d^3 n_{eff}}{d\lambda^3}\Big|\lambda_o + \ldots$$

Eq. 2-1

The first term in Eq. 2-1 represents the linear portion of the effective index as a function of wavelength and shows how dispersion manifests itself in the wavelength dependence of the phase velocity for a wave inside a medium. The relationship between the first term and the phase velocity is described in Eq. 2-2:

$$V_p(\lambda_o) = \frac{c}{n_{eff}(\lambda_o)} \qquad \textbf{Eq. 2-2 [3]}$$

The second term in Eq. 2-1 is related to the group velocity of an optical pulse and represents the first order dispersion. The group velocity is the velocity that the envelope of an optical pulse propagates. It depends on a quantity known as the group index, N_G, which is a function of both the index of refraction and the slope of the index of refraction at a particular wavelength. The group velocity relates to the second term via Eq. 2-3 where c is the velocity of light in vacuum:

$$V_g(\lambda_o) = \frac{c}{N_G} = \frac{c}{n(\omega_o) + \omega_o \left. dn/d\omega \right|_{\omega_o}} = \frac{c}{n(\lambda_o) - \lambda_o \left. dn/d\lambda \right|_{\lambda_o}} \qquad \textbf{Eq. 2-3 [3]}$$

The third term in Eq. 2-1 represents the variation in the group velocity as a function of wavelength. This variation in the group velocity is known as Group Velocity Dispersion, GVD, which is related to the third term via Eq. 2-4, where λ_o is the particular wavelength for which the GVD is calculated and c is the speed of light in vacuum:

$$GVD(\lambda_o) = -\frac{{\lambda_o}^2}{2\pi c}\left[-\frac{\lambda_o}{c}\frac{d^2 n_{eff}}{d\lambda^2}\right] \qquad \textbf{Eq. 2-4 [2]}$$

The term in the brackets in Eq. 2-4 is known as the dispersion parameter, D, which represents second order dispersion since it describes how the second derivative of the effective index varies with respect to wavelength:

$$D(\lambda_o) = -\frac{\lambda_o}{c}\frac{d^2 n_{eff}}{d\lambda^2}\bigg|_{\lambda_o} \qquad \textbf{Eq. 2-5 [16]}$$

The dispersion parameter is important since it is related to pulse broadening which critically limits the bit rate of a communication system. Eq. 2-6 shows how an increase in the dispersion parameter directly relates to an increase in pulse broadening:

$$\Delta T = D(\lambda_o) L \Delta\lambda \qquad \textbf{Eq. 2-6 [2]}$$

In Eq. 2-6 $\Delta\lambda$ is the range of wavelengths traveling through the medium and L is the length of the medium. The dispersion parameter, $D(\lambda_o)$, which is related to pulse broadening, is the most significant parameter since it limits the bit rate of an optical communication system.

The dispersion parameter of a waveguide such as an optical fiber is given by the total dispersion due to both the material and waveguide contributions. The total dispersion is the combination of the material dispersion and the waveguide dispersion and thus the dispersion parameter of a waveguide is given by:

$$D = -\frac{2\pi c}{\lambda^2}\frac{d}{d\omega}\left(\frac{1}{V_G}\right) = D_M + D_W \qquad \textbf{Eq. 2-7 [2]}$$

The next two sections discuss the contributions that both material and waveguide dispersion make individually to the total dispersion.

2.2 Material Dispersion

Material dispersion originates from the frequency or wavelength dependent response of the atoms/molecules of a material to electromagnetic waves. All media are dispersive and the only non-dispersive medium is vacuum [1]. The source of material dispersion can be examined from an understanding of the atomic nature of matter and the frequency dependent aspect of that nature [1]. Material dispersion occurs because atoms absorb and re-radiate electromagnetic radiation more efficiently as the frequency approaches a certain characteristic frequency for that particular atom called the resonance frequency [1].

When an applied electric field impinges on an atom it distorts the charge cloud surrounding that atom and induces a polarization that is inversely proportional to the relative difference between the frequency of the field and the resonance frequency of the atom [1]. Thus the closer the frequency of the electromagnetic radiation is to the atoms resonance frequency the larger the induced polarization and the larger the displacement between the negative charge cloud and the positive nucleus. The relative displacement between the electron cloud and the nucleus is given by the Lorentz Oscillator Model [1] as:

$$\bar{x} = \frac{q_e / m_e}{(\omega_o^{\,2} - \omega^2)} \bar{E} \qquad \textbf{Eq. 2-8 [1]}$$

The induced polarization is given by:

$$\bar{P} = q_e \bar{x}$$

$$\bar{P} = (\varepsilon - \varepsilon_o)\bar{E} \qquad \textbf{Eq. 2-9 [1]}$$

The index of refraction is given by the relationship between the induced polarization and the incident electric field. It is known as the dispersion equation [1] and is given by Eq. 2-10:

$$n^2(\omega) = \frac{\varepsilon}{\varepsilon_o} = 1 + \frac{\overline{P}}{\varepsilon_o \overline{E}} = 1 + \frac{{q_e}^2}{\varepsilon_0 m_e}\left(\frac{1}{{\omega_o}^2 - \omega^2}\right) \qquad \textbf{Eq. 2-10 [1]}$$

In this equation $n(\omega)$ is known as the absolute index of refraction [1] since it is the index of refraction seen by light of frequency ω in bulk media. It illustrates mathematically how the index of refraction varies for different frequencies (wavelengths) according to how close they are to a resonance frequency of the atom.

Given this knowledge of $n(\omega)$, the group index of the material can be determined via $N_G = n(\omega_o) + \omega_o \, dn/d\omega\big|_{\omega_o} = n(\lambda_o) - \lambda_o \, dn/d\lambda\big|_{\lambda_o}$. The material dispersion is then determined by taking the derivative of the group index of the material with respect to wavelength or equivalently the second derivative of the absolute index with respect to wavelength:

$$D_M = \frac{1}{c}\frac{dN_G}{d\lambda} = -\frac{\lambda}{c}\left(\frac{d^2 n}{d\lambda^2}\right) \qquad \textbf{Eq. 2-11 [2]}$$

2.3 Waveguide Dispersion

Waveguide dispersion occurs because waveguide geometry variably affects the velocity of different frequencies of light. More technically, waveguide dispersion is caused by the variation in the index of refraction due to the confinement of light an optical mode [3]. Waveguide dispersion is a function of the material parameters of the waveguide such as the normalized core-cladding index difference, $\Delta = \left(n_{core} - n_{cladding}\right)/n_{core}$, and

geometrical parameters such as the core size, *a* [2, 17]. The index in a waveguide is known as an effective index, n_{eff}, because of the portion of the index change caused by propagation in a confined medium.

Confinement is best described by a quantity known as the V parameter, which is a function of both the material and geometry of the waveguide. The V parameter is given by Eq. 2-12:

$$V(\lambda) = \frac{2\pi}{\lambda} a(n^2{}_{core} - n^2{}_{cladding})^{1/2} \approx \frac{2\pi}{\lambda} a n_{core} \sqrt{2\Delta} \qquad \textbf{Eq. 2-12 [2]}$$

Propagation in a waveguide is described by a quantity known as the normalized propagation constant, b, which is also a function of the material and geometry of the waveguide. This quantity is given in Eq. 2-13:

$$b = \frac{n_{eff} - n_{cladding}}{n_{core} - n_{cladding}} \qquad \textbf{Eq. 2-13 [2]}$$

The contribution of the waveguide to the dispersion parameter depends on the confinement and propagation of the light in a waveguide and hence it is a function of both the V parameter and the normalized propagation constant, b. The waveguide dispersion can be calculated via knowledge of V and b via Eq. 2-14:

$$D_W = -\frac{2\pi}{\lambda^2}\left[\frac{N^2{}_{G(cladding)}}{n_{cladding}\omega}\frac{Vd^2(Vb)}{dV^2} + \frac{dN^2{}_{G(cladding)}}{d\omega}\frac{d(Vb)}{dV}\right] \qquad \textbf{Eq. 2-14 [2]}$$

In most cases the main effect of the waveguide dispersion in standard single mode fibers is a reduction in dispersion compared to dispersion in bulk [2]. In comparison to material dispersion the contribution of waveguide dispersion is quite small

and in most standard single mode fibers it only shifts the zero dispersion wavelength from 1276nm to 1310nm [2]. This effect is illustrated in Fig. 2-1:

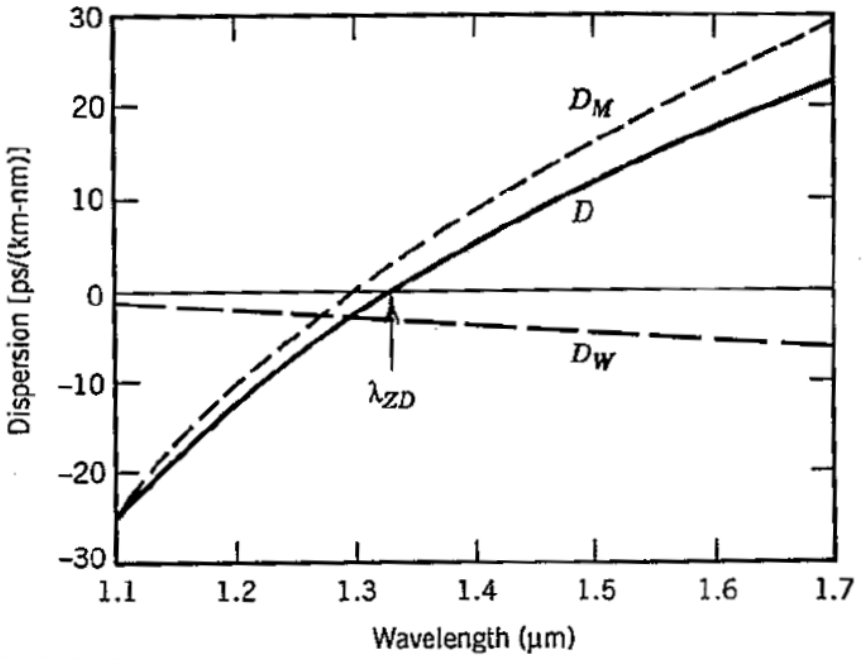

Fig. 2-1: Contributions of both waveguide and material dispersion [2]

In summary, the dispersion in a waveguide or an optical fiber is caused not only by the material but also by the effect of confinement and propagation in the waveguide. Thus accurate knowledge of the dispersion in a waveguide cannot be made by simple knowledge of the material dispersion but must include the effect of the waveguide. As a result either the dimensions of the waveguide must be known to a high degree of accuracy so that the waveguide dispersion can be calculated (which is not easy since fabrication processes are hardly perfect) or the dispersion must be measured empirically. Accurate measurement of the (total) dispersion parameter, D, is critical to the design of

photonic systems. Measurement techniques for the determination of the dispersion parameter will now be discussed in the next chapter.

Chapter 3: Conventional Measurement Techniques

There are 3 categories of dispersion measurement techniques: Time of flight (TOF) [18], Modulation phase shift (MPS) [17, 19] and Interferometric [16]. TOF and MPS are the most widely used commercial dispersion measurement techniques. Interferometric techniques are not widely used commercially but have been used in laboratories for dispersion measurements. Interferometric techniques come in two forms; temporal and spectral. This chapter surveys the existing techniques, their advantages and disadvantages and concludes with a quantitative comparison of the various dispersion measurement techniques in terms of measurement precision and fiber length requirements.

3.1 Time of Flight Technique

In the TOF technique the second order dispersion parameter, D, hereafter referred to simply as the dispersion parameter, can be determined either by measuring the relative temporal delay between pulses at different wavelengths or by measuring the pulse broadening itself. The relative temporal delay between pulses at different wavelengths is measured to determine the group velocity which can then be used to determine the dispersion parameter using Eq. 3-1:

$$D(\lambda_o) = \frac{\Delta t}{L\Delta\lambda(\lambda_o)} \qquad \textbf{Eq. 3-1 [16]}$$

The above equation can also be used to determine the dispersion parameter from the pulse broadening itself if Δt is the measured pulse broadening and $\Delta\lambda$ is the bandwidth of the wavelengths in the puilse. The measurement precision achievable by the

TOF technique is on the order of 1 ps/nm [17]. The setup for such a system is shown in the Fig. 3-1:

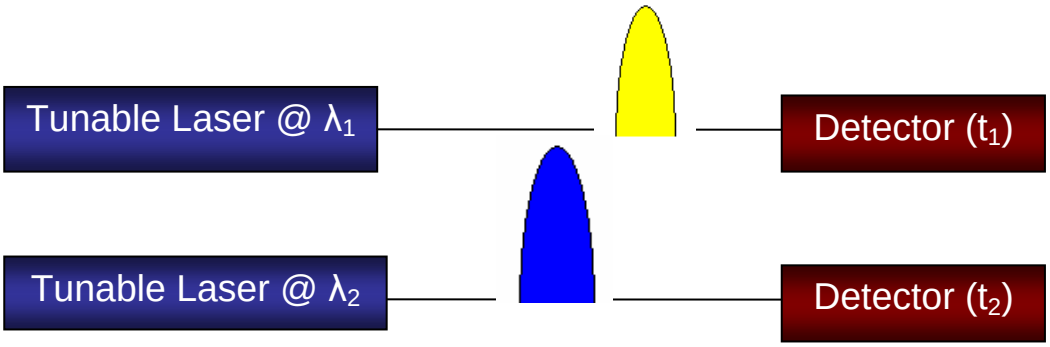

Fig. 3-1: Time of flight dispersion measurement technique

One of the main problems with the TOF technique is that it generally requires several kilometers of fiber to accumulate an appreciable difference in time for different wavelengths. Another issue with the TOF technique when the pulse broadening is measured directly is that the pulse width is affected by changes in the pulse shape which leads to errors in the measurement of the dispersion parameter. As a result, in order to measure the dispersion parameter with a precision near 1 ps/nm-km several kilometers of fiber are required [16]. Another long fiber measurement technique is now discussed in the next section.

3.2 Modulation Phase Shift Technique

The MPS technique is another dispersion characterization technique that requires long lengths of fiber. In the MPS technique, a continuous-wave optical signal is amplitude modulated by an RF signal, and the dispersion parameter is determined by measuring the RF phase delay experienced by the optical carriers at the different wavelengths. A diagram of the experimental implementation of this technique is shown in Fig. 3-2:

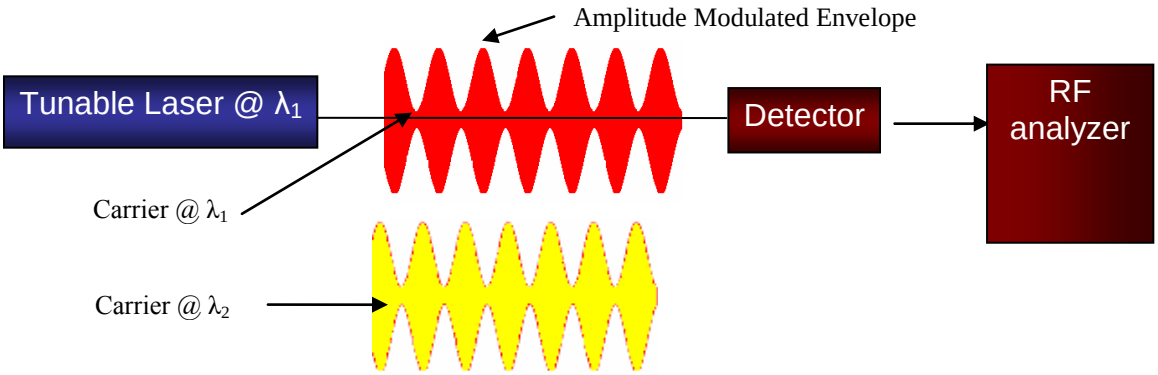

Fig. 3-2: Modulation Phase Shift Dispersion Measurement Technique

The RF phase delay information is extracted by this technique, and by taking the second derivative of the phase information, the dispersion parameter can be determined. Measurement precision achievable by the MPS technique is on the order of 0.07 ps/nm [20]. Due to its higher precision, MPS has become the industry standard for measuring dispersion in optical fibers. However, MPS, has several disadvantages. The first is that it is expensive to implement since the components required such as an RF analyzer and a tunable laser, are costly. The second is that its precision is limited by both the stability and jitter of the RF signal [21, 22].

MPS has several limitations on the minimum device length that it is capable of characterizing. In the MPS method the width of the modulated signal limits the minimum characterizable device length. This method also typically requires fiber lengths in excess of tens of meters to obtain a precision to better than 1 ps/nm-km [16]. Therefore it is not desirable for the characterization of specialty fibers or gain fibers [23], of which long fiber lengths are expensive to acquire or not available. Also, when fiber uniformity changes significantly along its length, the dispersion of a long span of fiber cannot be used to accurately represent that of a short section of fiber. In such cases, dispersion

measurement performed directly on short fiber samples is desirable. As a result a technique for measuring the dispersion of short lengths of fiber is desired.

3.3 Dispersion Measurements on Short Length Fiber

Interferometric techniques are capable of characterizing the dispersion on fiber lengths below 1m [16] (fiber with small DL products). There are two categories of interferometric techniques for making dispersion measurements on fiber of short length: temporal and spectral. These two categories will be discussed in detail in the following sections.

3.3.1 Temporal Interferometry (Fourier Transform Spectroscopy)

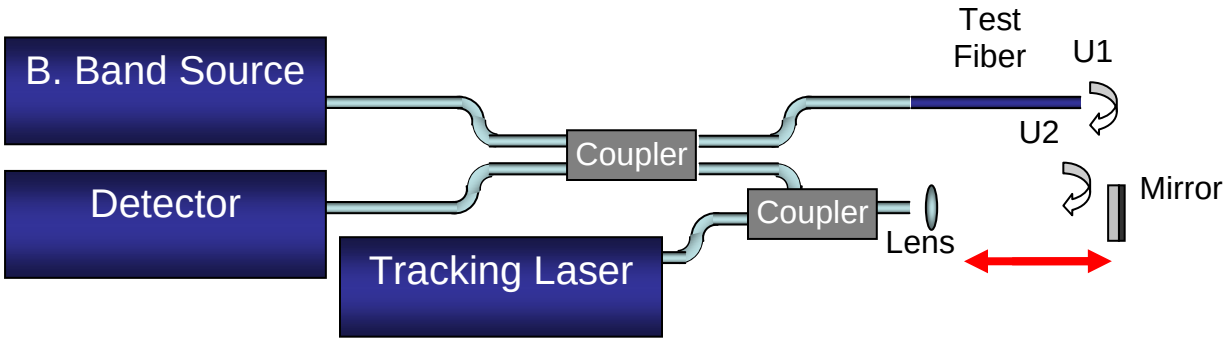

Fig. 3-3: Experimental setup for dual arm temporal interferometry

Dual Arm temporal interferometry employs a broadband source and a variable optical path to produce a temporal interferogram between a fixed path through the test fiber and variable air path. It involves moving one arm of the interferometer at a constant speed and plotting the interference pattern as a function of delay length (time) [23-32]. The spectral amplitude and phase are then determined from the Fourier transform of the temporal interferogram. A sample temporal interference pattern is shown in Fig. 3-4:

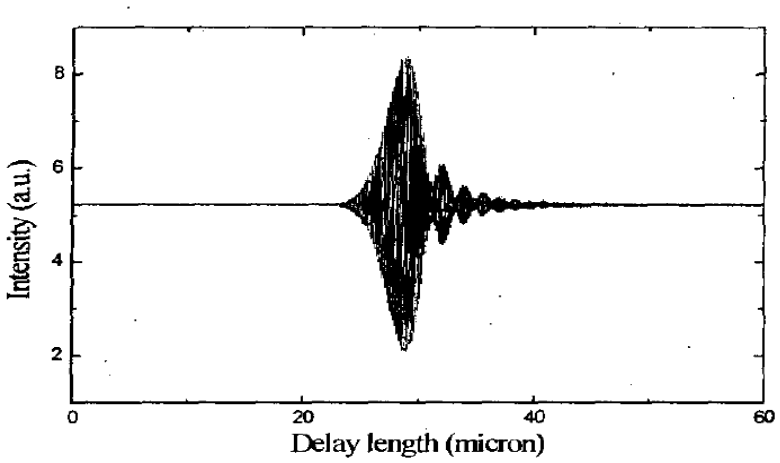

Fig. 3-4: Sample Temporal Interferogram [24]

A temporal interferogram gives the phase variation as a function of time. The spectral phase variation can be extracted from the temporal interferogram if a Fourier Transform is applied to it. The spectral phase contains the dispersion information which can be indirectly obtained by taking the second derivative of the spectral phase. A precision of 0.0015 ps/nm measured on a 0.814-m-long photonic crystal fiber [29] was recently reported using temporal interferometry. The main disadvantage of temporal interferometry is that it is susceptible to noise resulting from both translation inaccuracy and vibration of the optics in the variable path. A tracking laser is typically required to calibrate the delay path length [26, 29]. Another problem with this technique is that a second derivative of the phase information must be taken to obtain the dispersion parameter which means that it is less accurate than a method that can obtain the dispersion parameter directly. A method for obtaining the dispersion parameter directly is now discussed in the next section.

3.3.2 Spectral Interferometry

Spectral interferometry, like temporal interferometry, is capable of characterizing the dispersion in short length fiber (< 1m) (or fiber with a small DL product). In spectral interferometry, instead of stepping the length of one of the arms, a scan of the wavelength domain performed to produce a spectral interferogram. Spectral interferometry is generally more stable than temporal interferometry since the arms of the interferometer are kept stationary. Thus it is simpler than temporal interferometry since no tracking laser is necessary.

There are two types of spectral interferometry, one is general and does not require balancing, and another, the special case, is ‘balanced’. In the balanced case it is possible to directly measure the dispersion parameter from the interferogram. This makes it more accurate than temporal interferometry and it is for this reason that spectral interferometry is discussed as a dispersion measurement technique. We first examine the more general case of spectral interferometry.

General Case: Unbalanced

In general spectral interferometry the dispersion parameter is obtained from the interference spectrum produced by two time delayed light pulses/beams in an unbalanced dual arm interferometer. Two pulses/beams from the two arms of the interferometer are set up to interfere in a spectrometer and a spectral interferogram is produced. The interference pattern produced for a given time or phase delay is given by:

$$I(\omega) = \left|E_o(\omega) + E(\omega)\exp(i\omega\tau)\right|^2$$
$$= \left|E_o(\omega)\right|^2 + \left|E(\omega)\right|^2 + E_o{}^*(\omega)E(\omega)\exp(i\omega\tau) + E_o(\omega)E^*(\omega)\exp(-i\omega\tau)$$
$$= \left|E_o(\omega)\right|^2 + \left|E(\omega)\right|^2 + f(\omega)\exp(i\omega\tau) + f^*(\omega)\exp(-i\omega\tau)$$

Eq. 3-2 [33]

The last two terms in Eq. 3-2 result in spectral interference pattern via a $\cos(\Delta\phi(\omega) + \omega\tau)$ term. This interference pattern is seen in Fig. 3-5.

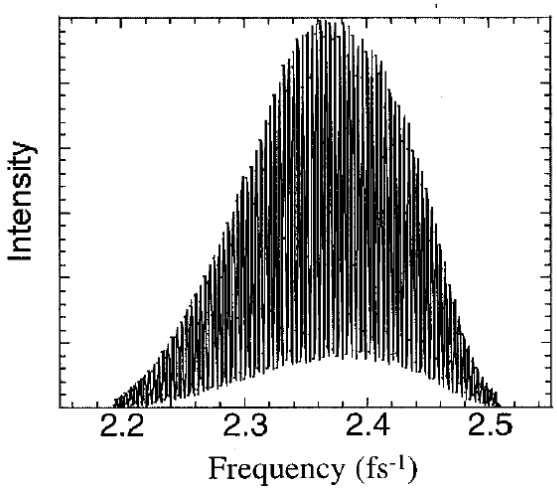

Fig. 3.5: Interference pattern produced by two time delayed pulses [34]

There are several ways to extract the phase information from the cosine term but the most prevalent way to do so is to take the Inverse Fourier transform of the spectral interference pattern. Note that $f(\omega) = F.T.f(t) = \left|E^*{}_o(\omega)E(\omega)\right|\exp(i\Delta\phi(\omega))$ [33] contains all the phase information on the spectral phase difference $\Delta\phi(\omega)$. Therefore, if $f(\omega)$ can be extracted from the interference pattern then the phase difference information can be known. If an Inverse Fourier Transform of the spectral interference is performed on the interference pattern the following is obtained:

$$F.T.^{-1}(I(\omega)) = E^*{}_o(-t) \otimes E_o(t) + E^*(-t) \otimes E(t) + f(t-\tau) + f(-t-\tau)^*$$

Eq. 3-3 [33]

If all terms except the $f(t-\tau)$ term get filtered out via a band pass filter then the phase information can be extracted from a Fourier Transform on $f(t-\tau)$. A graphical description of this process is given in Fig. 3-6:

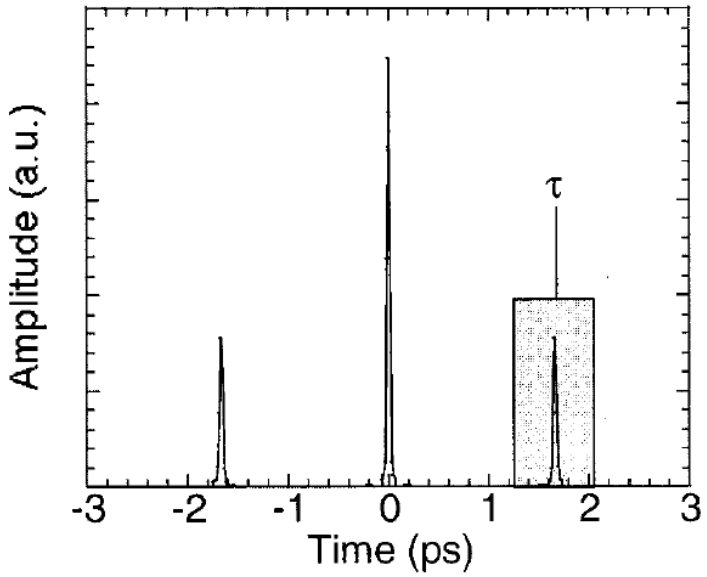

Fig. 3-6: Filtering out all but the *f(t-τ)* terms so that the phase information can be extracted [34]

The phase information can then be extracted if a Fourier Transform is applied to the filtered component *f(t-τ)* to transfer it back to the spectral domain. The complex amplitude therefore becomes $f(\omega) = |E_o(\omega)||E(\omega)|\exp(i\Delta\phi(\omega) + \omega\tau)$ [33, 34]. The phase of this complex amplitude minus the linear part (ωτ) that is due to the delay, yields the spectral phase difference between the two pulses as a function of ω and is independent of the delay between the two pulses [33, 34]. In this way the phase difference between the two pulses can be obtained. A sample plot of the amplitude and phase information retrieved using this method is shown in Fig. 3-7:

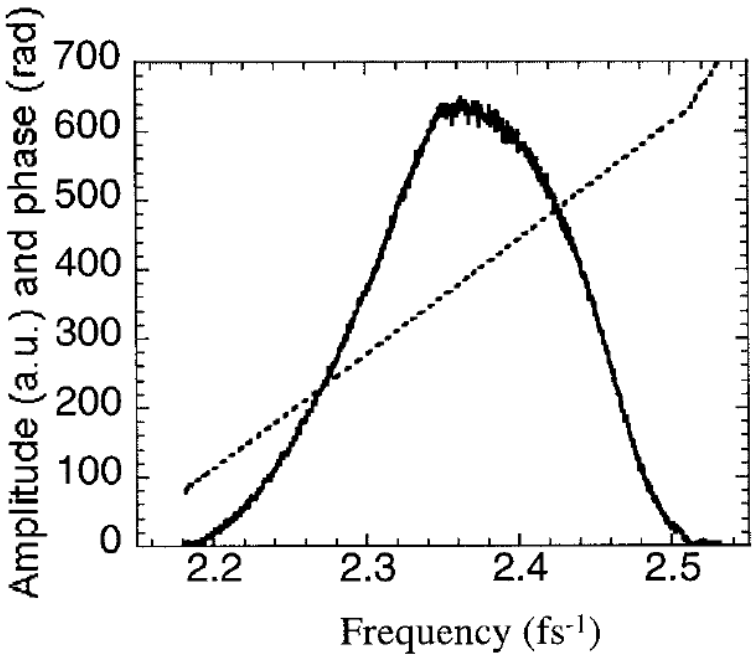

Fig. 3-7: Amplitude and phase spectrum of *f(ω)* [34]

If one of the pulses travels through a non-dispersive medium such as air and the other pulse travels through a dispersive medium such as an optical fiber then the phase difference spectrum will be directly related to the dispersion in the fiber. Thus the dispersion parameter plot can be determined by taking the second derivative of the phase difference spectrum with respect to wavelength.

The main issue with this form of spectral interferometry, however, is that the dispersion parameter is not determined directly but rather via a second order derivative of the phase information with respect to wavelength. Therefore, like temporal interferometry, this general unbalanced form of spectral interferometry is not as accurate as the method capable of measuring the dispersion parameter directly which will be discussed in the next section on balanced interferometry.

Special Case: Balanced

In balanced spectral interferometry the arm lengths of an interferometer are kept constant and they are balanced for a given wavelength called the central wavelength such that the group delay in both arms is the same. This allows for the removal of the effect of the large linear dispersion term in the interferogram. Balanced interferometry measures the dispersion parameter D at the wavelength at which the group delay is the same in both arms. This wavelength is henceforth referred to as the central wavelength. The dispersion parameter in this case can be directly determined from the phase information in the spectral interferogram without differentiation of the phase. For this reason it is more accurate than both unbalanced general spectral interferometry and temporal interferometry. As a result balanced spectral interferometry is often used to obtain accurate dispersion measurements in short length waveguides and fibers. A precision of 0.00007 ps/nm has been reported on a 1 m long SMF using this technique [16]. The experimental setup for balanced spectral interferometry is shown in Fig. 3-8.

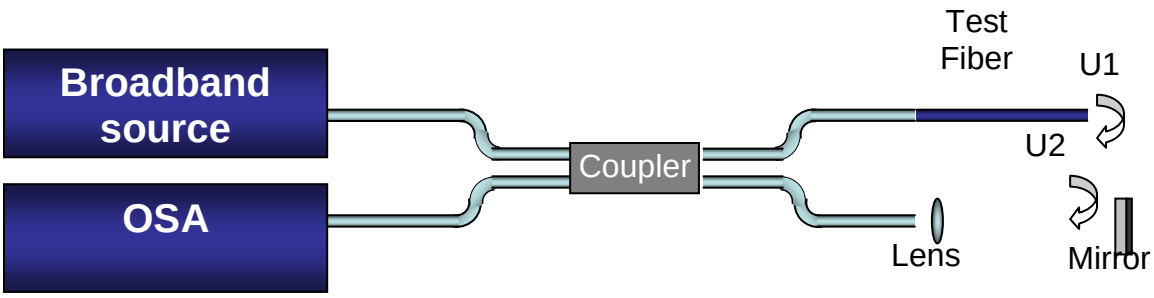

Fig. 3-8: Experimental setup for Spectral Interferometry

A sample spectral interference pattern produced from the setup in Fig. 3-8 is shown in Fig. 3-9. The central wavelength can be seen in this interferogram and is

labeled $\hat{\lambda}$. The dispersion parameter can be determined at the central wavelength, $\hat{\lambda}$, from the phase information given by the wavelength separation between the peaks/troughs of the interferogram [16].

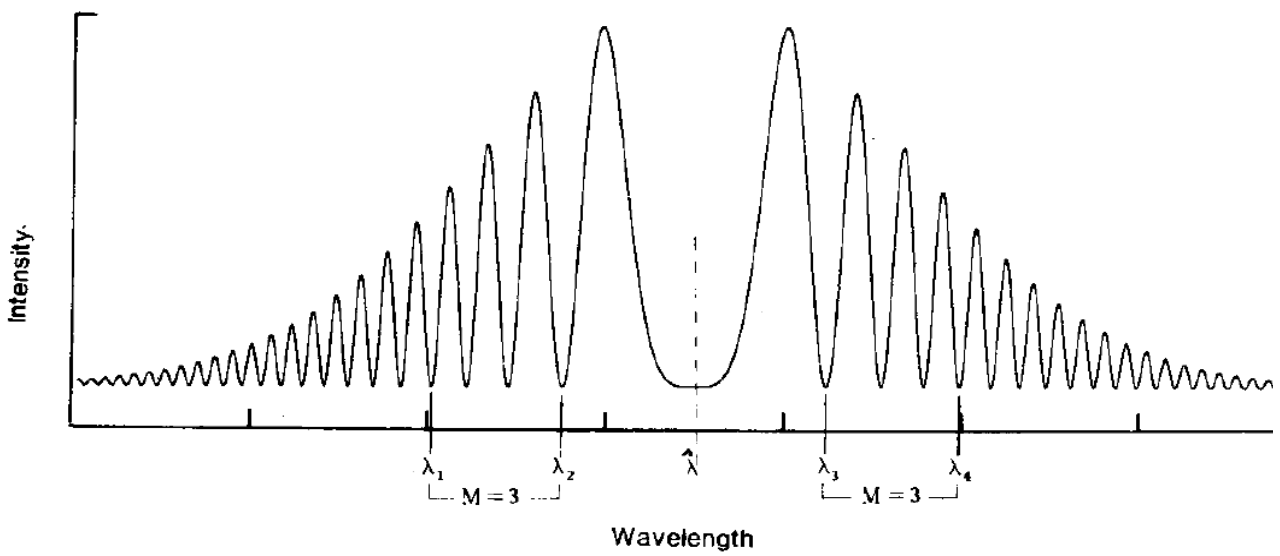

Fig. 3-9: Sample spectral interferogram [16]

Both forms of spectral interferometry are considered to be less susceptible to noise since the arms of the interferometer are kept still and there are no moving parts. It is for this reason that spectral interferometry in general is considered to be more accurate than temporal interferometry. Spectral interferometry is therefore considered to be the technique of choice for measuring the dispersion of photonic components [34-37] and spectral depth resolved optical imaging [38, 39]. One well known and important class of spectral interferometry is optical coherence tomography (OCT) [40-45].

The resolution of balanced spectral interferometry, in particular, can be improved by replacing the combination broadband source and Optical Spectrum Analyzer shown in Fig. 3-8 with a tunable laser and detector system. Current tunable laser technology allows

for a bandwidth of 130 nm and a 1 picometer resolution. This improves the range of fiber lengths that can be measured using this technique. Also of note is that the use of tunable lasers for dispersion measurement is becoming more widespread [46] as they decrease in cost.

Balanced dual arm spectral interferometers are typically in a Michelson or a Mach Zehnder configuration in which the path lengths are equalized at the given wavelength in which the dispersion is to be measured [23, 24, 32]. The most often used configuration, however, is the Michelson and the discussion that follows considers the Michelson interferometer. In a balanced Michelson interferometer the dispersion is measured from the interference between two waves: one that passes through the test fiber and another that passes through an air path. Balancing the air path length with the fiber eliminates the effect of the group index of the fiber in the interference pattern. This allows for the measurement of the second derivative of the effective index with respect to wavelength *directly* from the interference pattern [16].

The main disadvantage of this configuration is that, for this to work, two types of path balancing must occur simultaneously. The first type of path balancing is coupler arm balancing illustrated in red in Fig. 3-10:

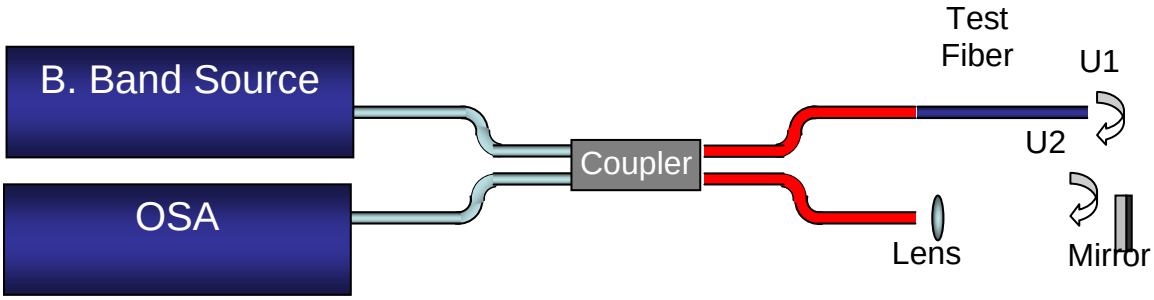

Fig. 3-10: Balanced path requirements for a Michelson interferometer

The path lengths of both arms coming out of the coupler (highlighted in red) need to be balanced exactly or an extra set of interference fringes will be created from the reflections at the two end facets of the coupler arms as shown in Fig. 3-11.

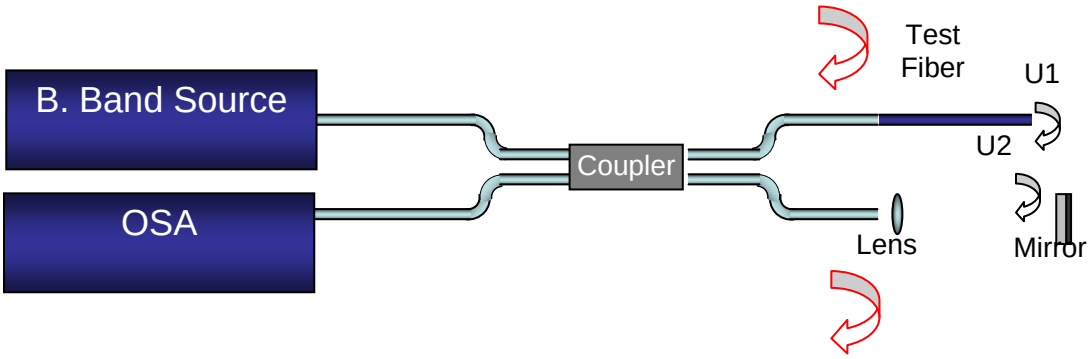

Fig. 3-11: Interference of the coupler arm reflections

The second type of balancing is test fiber-air path balancing to ensure that the group delay in the air path exactly equals that of the fiber for a given central wavelength. This ensures that the central wavelength in the interference pattern is within the viewable bandwidth of the OSA.

The main problem in implementing a Michelson interferometer is that the arms of the coupler cannot be balanced *exactly* and as a result the effect of the extra set of reflections produced at the coupler facets cannot be removed.

One method of canceling out the extra set of fringes produced at the facets of the coupler arms is by having a relatively long difference between the coupler arms as shown in Fig. 3-12:

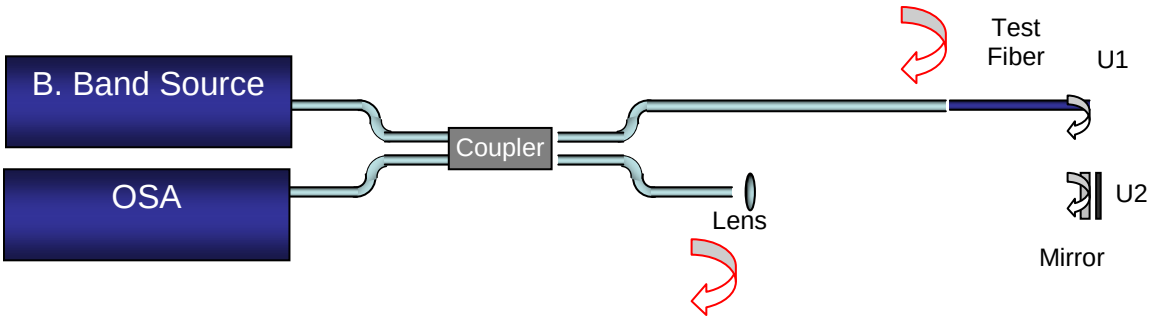

Fig. 3-12: Fringe cancellation technique for a Michelson interferometer

This fringe cancellation technique, depicted in Fig. 3-12, dramatically reduces the period of the fringes produced by the extra set of reflections from the coupler facets to a level in which they are smaller than the resolution of the OSA. As a result they become low-pass filtered by the OSA and do not show up in the plot of the interference. This technique, however, requires compensation of the added dispersion due to the optical path difference between the coupler arms. To do this, however, requires knowledge of the exact difference in length between the two arms of the coupler and the exact dispersion parameter curve for the arms of the coupler. Both of which are generally not easy to determine accurately. Also of note is that this technique requires a much longer air path which introduces more noise into the measurement due air path disturbances.

As a result of the difficulties inherent in the fringe cancellation technique I will introduce a new method (which is a subset of balanced spectral interferometry) for the measurement of dispersion. This new method, known as Single Arm Interferometry, will not require the cancellation of any extra fringes as was the case for the Michelson. In the next section I compare the performance of Single Arm Interferometry to the conventional techniques in order to show how it is a natural progression in the development of dispersion measurement technology. The performance of Single Arm Interferometry is

introduced before the details of the technique are described in order entice the reader study the technical/theoretical discussion in chapter 4.

3.4 Comparison of Dispersion Measurement Techniques

There have been several techniques developed for the measurement of chromatic dispersion in fiber. Especially important are those developed for the measurement of short lengths of fiber [16, 47]. One reason that short length characterization techniques are important stems from recent developments in the design and fabrication of specialty fiber.

Specialty fiber such as Twin Hole Fiber (THF) [48] and Photonic Crystal Fiber (PCF) [29] have made short length fiber characterization desirable due to their high cost. Because of this it is not economical to use TOF and MPS techniques to characterize these types of fiber. Another impetus for short length characterization comes from the fact that in many specialty fibers the geometry is often non-uniform along its length. As a result of this non-uniformity the dispersion in these fibers varies with position. Thus measurement of the dispersion in a long length of this fiber will be different than that measured in a section of the same fiber.

In the last few sections several dispersion measurement techniques have been discussed and it has been shown that it is desirable to seek a short length characterization scheme. The techniques discussed for short length dispersion characterization were temporal and spectral interferometry. Temporal interferometry and unbalanced general spectral interferometry are both capable of characterizing short length fiber, however, since they obtain the dispersion parameter indirectly via second order differentiation of the phase term they are not as accurate as balanced spectral interferometry which directly

measures the dispersion parameter. As a result the technique of choice for dispersion measurement is balanced spectral interferometry since it will provide the most accurate measurements. As a result the new technique will employ balanced spectral interferometry.

The two important parameters in comparing dispersion measurement techniques is the minimum device length that each is capable of characterizing and the precision to which the characterization is achieved. It is generally desirable to characterize as short a fiber as possible with as high a precision as possible. It is also desirable to perform the measurement in the simplest way possible. A summary of the length requirements and the precision of the various dispersion measurement techniques is summarized in Table 3-1:

Table 3-1: Summary of the various dispersion measurement techniques and their precision

Technique	Measures Short Fiber?	Precision (Shortest length)	Reference	Comments
Time of Flight (Film laser pulse)	No	1 ps nm^{-1} (7.8 m)	40	-Need km's of fiber
Modulation Phase Shift	No	0.1 ps nm-1 (1.2 km) [19] 0.07 ps nm^{-1} (Agilent 86038B) [20]	19, 20, 22	-Need 10's of meters of fiber -System is expensive esp. RF components
Temporal Interferometry	Yes <1 m	0.01 ps nm^{-1} (1 m) [16], 0.0015 ps nm^{-1} (0.814m) [49]	16, 49	-Noise due to translation of mirror: -Stepping accuracy, drift in position, vibration -Less accurate, Indirect measure of D
Dual Arm Spectral Interferometry (Balanced)	Yes <1 m	0.00007 ps nm^{-1} (1 m)	16	-No moving parts → less noise -More accurate, directly measures D -Technique of choice
Single Arm Interferometry (Balanced Spectral Interferometry)	Yes <0.5 m	0.0001 ps nm^{-1} (0.395 m)	This work	-Subset of Balanced SI but simpler -Details in the next chapter

*Note that in calculating the resolution of the Single Arm Interferometry technique the standard deviation of the measurement for single mode fiber (0.28 ps/nm-km) was multiplied by the length of SMF used (0.000395 km).

In the summary given in Table 3-1 it is evident that the order of magnitude for the measurement in dual arm spectral interferometry [16] is the same as the order of magnitude reported for Single arm Interferometry. The technique used in single arm interferometry, however, is significantly simpler as will be shown in the next chapter. The next chapter introduces the theory and implementation of Single Arm Interferometry and outlines the parameters affecting performance.

Chapter 4: Theory of Single Arm Interferometry

A Single Arm Interferometer (SAI) can be produced by folding the two arms of a Michelson interferometer together into a common path (as in a common path interferometer) and placing a mirror behind the test fiber. This configuration was designed to eliminate the calibration step required by dual arm interferometers in which the coupler arms are made to be disproportionate in length to eliminate the effect of the extra reflections from the coupler-test fiber/coupler-air path facets. Since calibration is not required this technique is also more accurate than a dual arm interferometer.

4.1 A New Concept

This chapter introduces a balanced Single-Arm Interferometer (SAI) for the direct measurement of dispersion in short fibers. A balanced SAI is depicted in Fig. 4-1. This configuration is not only much simpler than a dual arm interferometer but it also eliminates the need for system calibration (assuming the dispersion introduced by the collimating lens is negligible and the air path is stable). Its simpler construction also makes it less susceptible to polarization and phase instabilities.

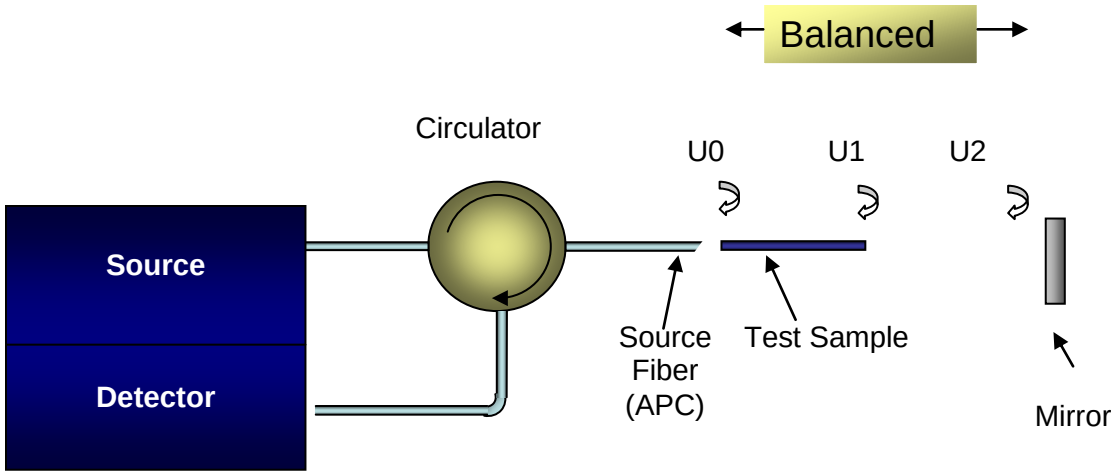

Fig. 4-1: Single-arm interferometer where three waves interfere; Uo, U1 and U3.

The SAI is a balanced interferometer since the group delay in the fiber is the same as the group delay in the air path. It will be shown mathematically that this balancing of the group delay in each path allows the dispersion parameter to be measured directly from the interference pattern. The conceptual difference between SAI and Dual Arm interferometers is that, in SAI, the interference pattern is produced by *three* waves: two from the reflections at the facets of the test fiber and one from a mirror placed behind it (as shown by U_o, U_1, and U_2 in Fig. 4-1). The beating between the interference fringes produced by the test fiber and those by the air path generates an *envelope* which is equivalent to the interference pattern produced by two waves (U_1 and U_2 in Fig. 4-1) in a dual-arm interferometer.

From the phase information in this envelope the dispersion parameter can be extracted. Both dual and single arm balanced interferometers have in common this ability to directly measure the dispersion parameter from the interference pattern.

The SAI configuration appears similar to common path interferometers, often used for depth imaging as in Common-Path Optical Coherence Tomography (CP-OCT)

[50, 51]. The SAI, however, is fundamentally different from CP-OCT since it utilizes 3 reflections, and extracts the *dispersion* parameter directly from the *envelope* of the interference pattern. The main difference between common path interferometers and single arm interferometers is the fact that there is a path balancing of the group delay in the fiber path and the air path. The differences between the Michelson Interferometer, CP-OCT and balanced Single Arm Interferometry are outlined in Table 4-1:

Table 4-1: Differences & Similarities between the Michelson Interferometer, CP-OCT and the Single Arm Interferometer

	Balanced Michelson Interferometer	CP-OCT (Common path)	Balanced SAI
# of interfering waves	2	2	3
# of longitudinally separate paths	2	1	1
Path balancing	yes	no	yes
Dispersion information	entire interferogram	n/a	envelope of interferogram
Dispersion parameter measured	directly	n/a	directly
Measures	dispersion parameter	optical path length difference	dispersion parameter

In the next section, we will briefly present the theoretical representation of the interference pattern, the phase between the adjacent peaks/troughs of the envelope, and its relationship to the dispersion.

4.2 Mathematical Description

4.2.1.1 Equal Amplitude Case

Dispersion measurements can be made using a single-arm interferometer by extracting the second derivative of the effective index with respect to wavelength from the *envelope* of the interference pattern generated by three waves U_o, U_1 and U_2 depicted in Fig. 4-2:

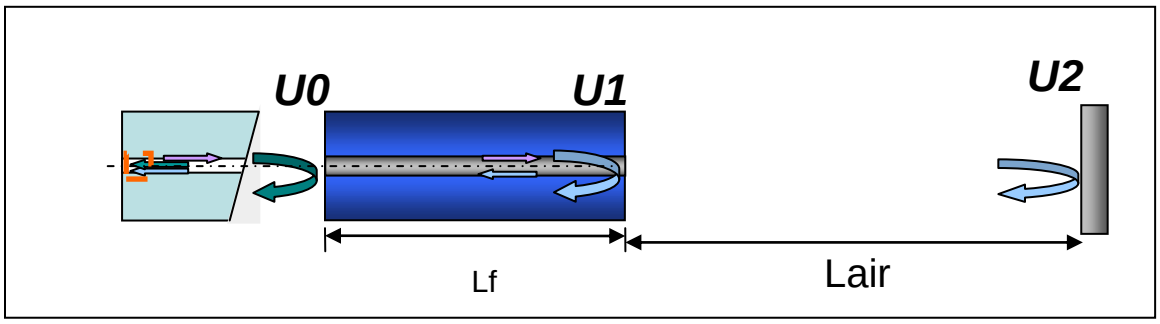

Fig. 4-2: Interference when reflections from the facets and mirror have equal amplitudes

The extra reflection from the source fiber is eliminated using angle polished fiber as shown in Fig. 4-2. Note that this method is insensitive to the loss introduced by the angle polished connector since the dispersion information is contained within the phase of the three reflected waves. The optical path length of the air path is made to cancel out the strong linear effective group index term of the test fiber at a central wavelength, λ_o. The amplitudes of U_o and U_1 are assumed to be equal to the magnitude of the reflection at the fiber end facets. The amplitude of U_2 depends on the amount of light coupled back to the fiber. This coupling efficiency can be adjusted by varying the alignment of the mirror such that U_2 has the same amplitude as U_o and U_1. In this simplified presentation:

$$U_1 = U_0 e^{-j2\beta L_f}$$
$$U_2 = U_0 e^{-j2\beta L_f - j2k_0 L_{air}} \qquad \textbf{Eq. 4-1}$$

In Eq. 4-1, L_f and L_{air} are the lengths of the test fiber and the air path, respectively. β and k_o are the propagation constant of the fundamental mode in the fiber and the propagation constant in free space. The interference pattern is produced by the interference of the three reflections is given by Eq. 4-2:

$$I_o = \left|U_0 + U_1 + U_2\right|^2$$
$$= U_o{}^2\left(3 + 2\cos(2\beta L_f + 2k_o L_{air}) + 4\cos(\beta L_f + k_o L_{air})\cos(\beta L_f - k_o L_{air})\right)$$

Eq. 4-2

Eq. 4-2 contains two fast terms, with a phase $\phi_1 = (\beta L_f + k_o L_{air})$ and $\phi_2 = 2(\beta L_f + k_o L_{air})$. Since ϕ_1 is slower than ϕ_2 it will amplitude modulate the faster term. As a result the period of the 'carrier' will be that of the slowest of the fast terms, $\phi_{carrier} = \phi_1$. This carrier is then itself amplitude modulated by the slower term $\phi_{envelope} = (\beta L_f - k_o L_{air})$ to produce the 'envelope' of the interference pattern. This envelope is equivalent to the interference pattern produced by Michelson interferometer [16] and it can be written as:

$$U_o{}^2\left(5 + 4\left|\cos(\phi_{envelope})\right|\right) \qquad \textbf{Eq. 4-3}$$

The calculated interference pattern generated by the setup for a 39.5 cm SMF28^{TM} test fiber is shown in Fig. 4-3. It depicts the envelope function (highlighted) which is a good approximation of the envelope of the actual envelope of the carrier.

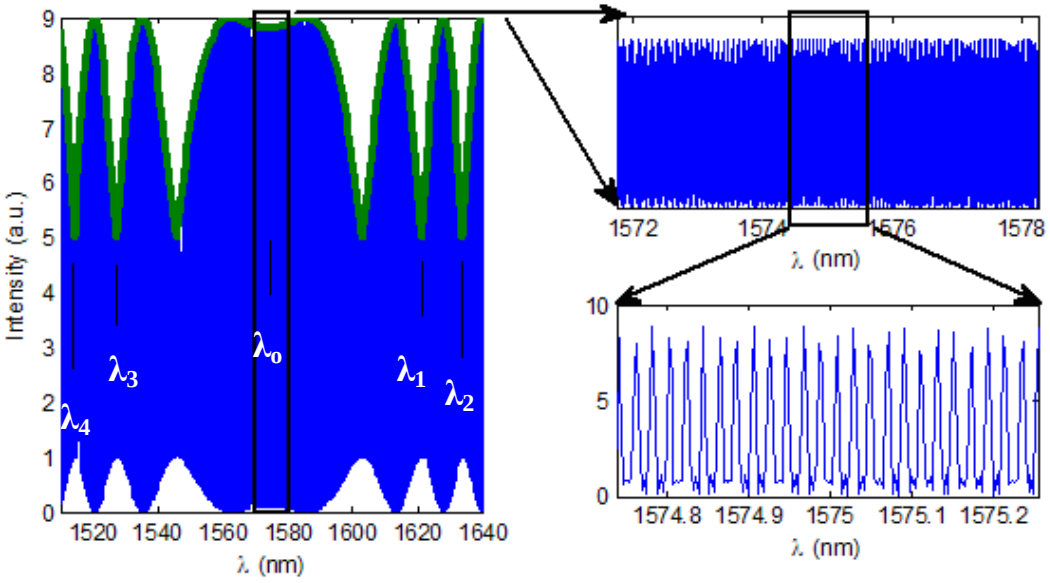

Fig. 4-3: Calculated 3 wave interference pattern and envelope for a 39.5 cm piece of SMF28™

Applying a Taylor expansion to the phase of the slow envelope and replacing β with $2\pi n_{eff}/\lambda$, where n_{eff} is the effective index of the fiber, gives the phase relation in Eq. 4-4:

$$\phi_{envelope}(\lambda) = 2\pi\left\{\frac{1}{\lambda}\left[\left(n_{eff}(\lambda_o) - \lambda_o \left.\frac{dn_{eff}}{d\lambda}\right|_{\lambda_o}\right)L_f - L_{air}\right] + L_f \left.\frac{dn_{eff}}{d\lambda}\right|_{\lambda_o}\right.$$
$$\left. + L_f \frac{(\lambda-\lambda_o)^2}{2!\lambda}\left.\frac{d^2 n_{eff}}{d\lambda^2}\right|_{\lambda_o} + L_f \frac{(\lambda-\lambda_o)^3}{3!\lambda}\left.\frac{d^3 n_{eff}}{d\lambda^3}\right|_{\lambda_o} + \cdots\right\}$$

Eq. 4-4

The first term in Eq. 4-4 (in the square brackets) disappears when L_{air} is adjusted to balance out the group delay of the test fiber at λ_o, the balanced wavelength. Taking the difference between the phases at two separate wavelengths; λ_1 and λ_2 results in [16]:

$$\begin{aligned}\Delta\phi_{envelope} &= \left|\phi_{envelope}(\lambda_2) - \phi_{envelope}(\lambda_1)\right| \\ &= 2\pi\left(\left[\frac{(\lambda_2-\lambda_0)^2}{2!\lambda_2} - \frac{(\lambda_1-\lambda_0)^2}{2!\lambda_1}\right]\frac{d^2 n_{eff}}{d\lambda^2}\bigg|_{\lambda_0} + \left[\frac{(\lambda_2-\lambda_0)^3}{3!\lambda_2} - \frac{(\lambda_1-\lambda_0)^3}{3!\lambda_1}\right]\frac{d^3 n_{eff}}{d\lambda^3}\bigg|_{\lambda_0}\right)L_f \\ &= m\pi\end{aligned}$$

Eq. 4-5

Note that *m* is the number of fringes between the two wavelengths. If this phase difference is taken using a different pair of peaks/troughs (i.e. λ_3 & λ_4) the result is a system of equations in which $d^2 n_{eff}/d\lambda^2\big|_{\lambda_o}$ and $d^3 n_{eff}/d\lambda^3\big|_{\lambda_o}$ can be solved directly [16]. Since the troughs in the interference pattern are more sharply defined it is more accurate to choose the wavelength locations of the troughs of the envelope as the wavelengths used in Eq. 4-5.

Note that, if we ignore the third-order dispersion, then only two wavelengths (e.g., λ_1 and λ_2) are required to calculate the second-order dispersion. This, however, would be less accurate. The dispersion parameter D can then be found as follows:

$$D(\lambda_o) = -\frac{\lambda_o}{c}\frac{d^2 n_{eff}}{d\lambda^2}\bigg|_{\lambda_o} \qquad \textbf{Eq. 4-6}$$

The next section presents a more general analysis of the interference pattern and details the effect of having variable reflection magnitudes from each of the facets. It will show how the variation in the magnitude of the reflections has no effect on the phase information in the envelope and as such the simplified analysis presented here is generally applicable.

4.2.1.2 Unequal Amplitude Cases

To prove that this method is insensitive to the loss introduced by the angle polished connector since the dispersion information is contained within the phases of the three reflected waves we will now show the effect that is obtained if the reflections do not have equal magnitudes. The interference pattern produced by three reflections with unequal amplitudes is not as simple as presented in the previous section. Here we show that despite this fact the previous results still hold since the locations of the troughs of the envelope, which are used to obtain the dispersion information, remain the same even though the fringe contrast varies.

In general the reflections from the facet and the mirror, shown in Fig. 4-2, do not have the same magnitude and we express the magnitudes of the reflections in terms of the first reflection in the following way.

$$U_1 = aU_0 e^{-j2\beta L_f}$$
$$U_2 = bU_0 e^{-j2\beta L_f - j2k_0 L_{air}} \qquad \textbf{Eq. 4-7}$$

In Eq. 4-7 L_f and L_{air} are the lengths of the test fiber and the air path, respectively. β and k_o are the propagation constant of the fundamental mode in the fiber and the propagation constant in free space. '*a*' is the fraction of the amplitude reflected from the second facet in terms of the first and '*b*' is the fraction of the amplitude reflected from the mirror in terms of the fraction reflected from the first facet. The interference pattern of the spectral interferogram can be expressed as:

$$\begin{aligned} I_o &= |U_0 + U_1 + U_2|^2 \\ &= U_o{}^2\{1 + a^2 + b^2 + 4a\cos(\beta L_f + k_o L_{air})\cos(\beta L_f - k_o L_{air}) \\ &+ 2a(b-1)\cos(2k_o L_{air}) + 2b\cos(2(\beta L_f + k_o L_{air}))\} \end{aligned} \qquad \textbf{Eq. 4-8}$$

The expression in Eq. 4-8 can be treated as a fast-varying "carrier" (with respect to frequency or wavelength) modified by an upper and a lower slow-varying envelope, as shown in Fig. 4-3, which depicts the simulated spectral interferogram generated by the 3-wave SAI with a 39.5-cm SMF28 fiber as the test fiber. Upon closer examination (Fig. 4-3, lower right), the "carrier" is not a pure sinusoidal function, because there are three fast-varying phases in Eq. 4-8, $2(\beta L_f + k_o L_{air})$, $(\beta L_f + k_o L_{air})$, and $2k_o L_{air}$, all of which vary much faster than the phase of the envelope ($\phi_{envelope}$), which equals $\beta L_f - k_o L_{air}$. When γ is large (>0.5), it can be shown that the upper envelope is approximated by

$$U_o{}^2\left(1 + a^2 + b^2 + 2a(b-1) + 2b + 4a\left|\cos(\phi_{envelope})\right|\right) \qquad \textbf{Eq. 4-9}$$

It will now be shown that although the magnitude of the interference pattern is not the same as the envelope for cases in which $b \neq 1$, the peak and trough locations of the two match exactly. As a result the phase information of the interferogram is preserved and the dispersion information can be extracted from the interferogram. Note that $a = b = 1$ is a special case of this more general analysis and was presented in the previous section. Several cases will be shown for the variation in the magnitudes of the reflections from each of the facets. The Matlab code used to generate these interference patterns is presented in Appendix A.1.

The first few cases will be shown to determine the effect of the variation of a while keeping b constant. Figs. 4-4 to 4-6 show that the variation of a does not change the interference pattern and the envelope in Eq. 4-3 still matches the upper peaks interference pattern produced using Eq. 4-2. In the figures below the envelope function as determined by Eq. 4-9 is plotted along with the fringe pattern to show that it is a good

approximation of the actual upper envelope of the carrier and that the locations of the peaks and troughs are the same.

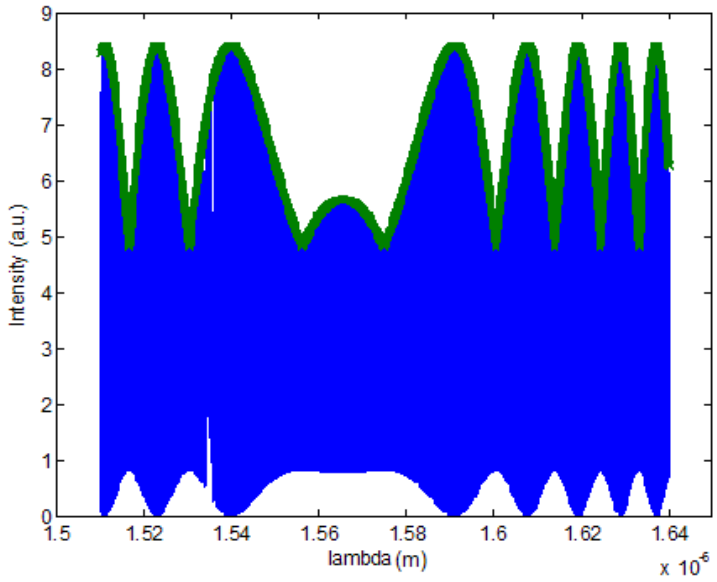

Fig. 4-4: Simulated interference pattern produced by the setup in Fig. 4-1 for a 30-cm-long SMF28™ test fiber, with *a* =0.9, *b* =1. The parameters used for the SMF28™ is published in [Appendix B]. The envelope calculated by Eq. 4-9 is superimposed on the fringe pattern in a thick line, which is a close approximation of the upper envelope.

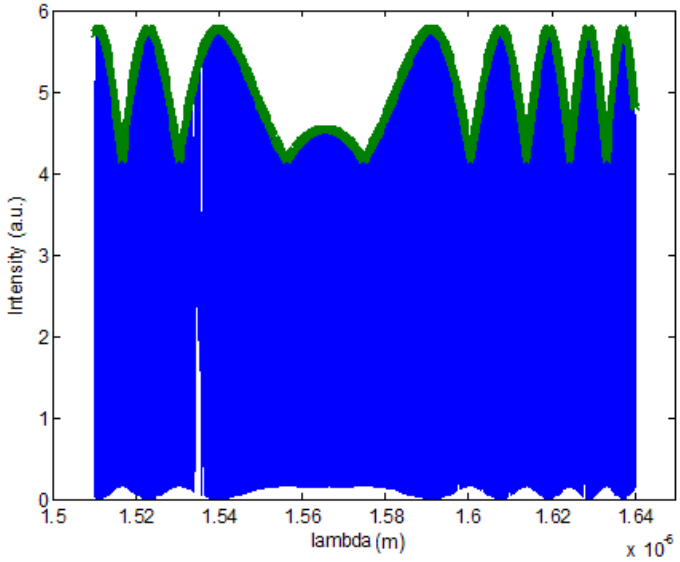

Fig. 4-5: Simulated interference pattern produced by the setup in Fig. 4-1 for a 30-cm-long SMF28™ test fiber, with *a* =0.4, *b* =1. The parameters used for the SMF28™ is published in Appendix B. The envelope calculated by Eq. 4-9 is superimposed on the fringe pattern in a thick line, which is a close approximation of the upper envelope.

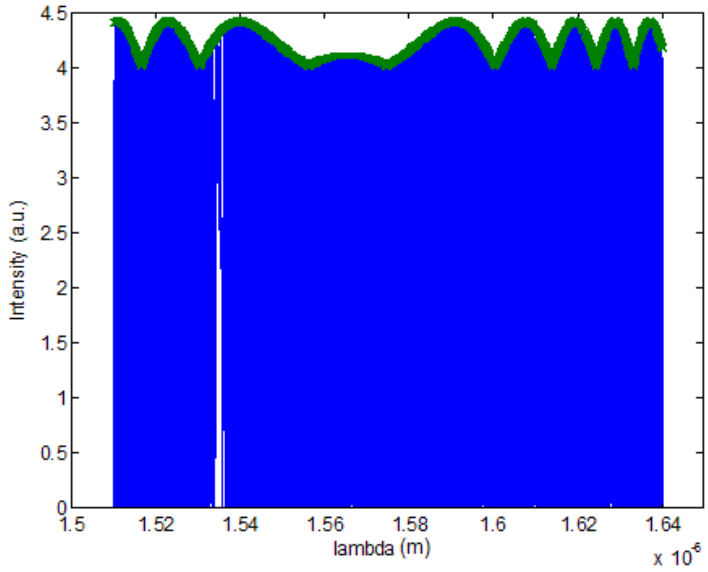

Fig.4-6: Simulated interference pattern produced by the setup in Fig. 4-1 for a 30-cm-long SMF28™ test fiber, with *a* =0.1, *b* =1. The parameters used for the SMF28™ is published in [Appendix B]. The envelope calculated by Eq. 4-9 is superimposed on the fringe pattern in a thick line, which is a close approximation of the upper envelope.

The next few cases will show the effect of a variation of *b* while keeping *a* constant. Figs. 4-7 to 4-9 show that the variation of *b* does change the magnitude of the interference pattern and the magnitude of the envelope in Eq. 4-9 does not match the upper peaks of the interference pattern produced using Eq. 4-8 but that the phases of both equations still match. Since the dispersion information is contained within the phase of the interference pattern it can still be used as in section 4.3.1 to determine the dispersion.

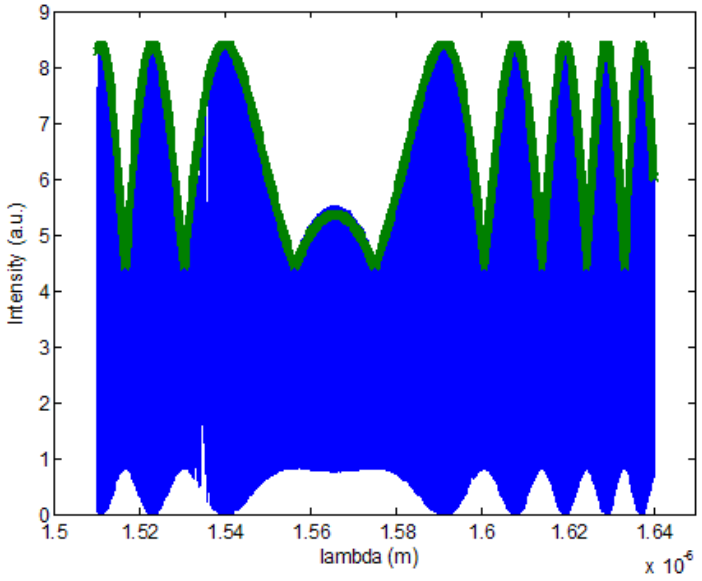

Fig. 4-7: Simulated interference pattern produced by the setup in Fig. 4-1 for a 30-cm-long SMF28™ test fiber, with *a* =1, *b* =0.9. The parameters used for the SMF28™ is published in [Appendix B]. The envelope calculated by Eq. 4-9 is superimposed on the fringe pattern in a thick line, which is a close approximation of the upper envelope.

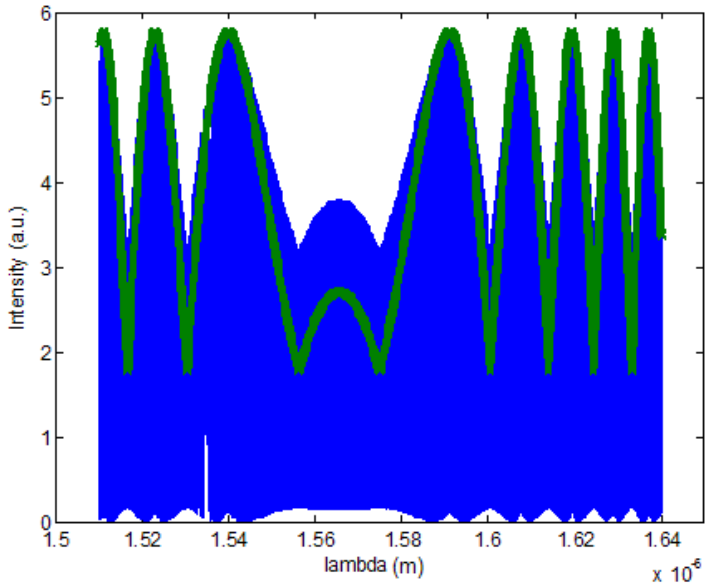

Fig. 4-8: Simulated interference pattern produced by the setup in Fig. 4-1 for a 30-cm-long SMF28™ test fiber, with *a* =1, *b* =0.4. The parameters used for the SMF28™ is published in [Appendix B]. The envelope calculated by Eq. 4-9 is superimposed on the fringe pattern in a thick line, which is a close approximation of the upper envelope.

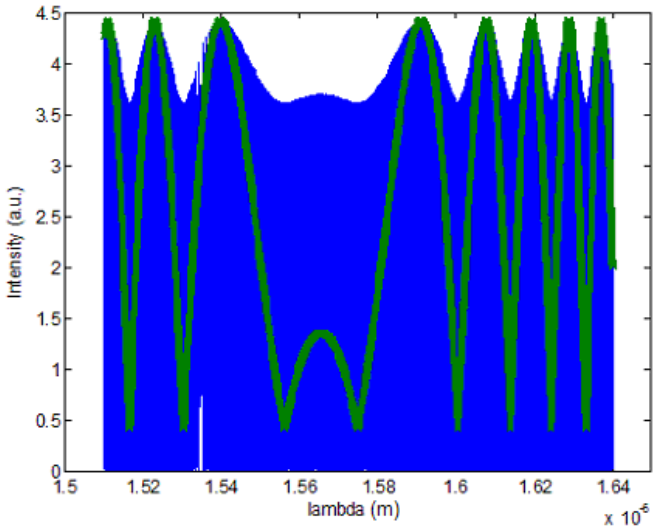

Fig. 4-9: Simulated interference pattern produced by the setup in Fig. 4-1 for a 30-cm-long SMF28™ test fiber, with *a* =1, *b* =0.1. The parameters used for the SMF28™ is published in [Appendix B]. The envelope calculated by Eq. 4-9 is superimposed on the fringe pattern in a thick line, which is a close approximation of the upper envelope.

Since the phase of the upper envelope, $\varphi_{envelope}$ (and therefore the dispersion information) is unaffected by the magnitude of the reflections from the facets and the mirror, the method for determining the dispersion parameter as presented in Eqs. 4-4 to 4-6 is valid even in the general case. The dispersion parameter, therefore, can always be obtained from an SAI.

As mentioned earlier, the main difference between the fringes produced in this setup and those produced by dual arm interferometers is the presence of a fast carrier (Eq. 4-8) slowly modulated by the desired envelope. The presence of this carrier sets extra operational constraints that will be discussed in the next section.

4.3 System Parameters

There are four factors of interest with regard to the dispersion measurement system. These factors are important since they will determine the quality and range of the output of the dispersion measurements. The first factor of interest is the wavelength resolution of the measurement, the second is the minimum required bandwidth of the source, the third is the measurable bandwidth of the dispersion curve and the fourth is the test fiber length. The sections that follow discuss how each of these factors affect the output of the dispersion measurement.

4.3.1 Wavelength Resolution of the Dispersion Measurement

The wavelength resolution of the points in the plot of the dispersion parameter is determined by the minimum step size of the translation stage. With smaller step increments in the translation stage there are smaller step increments in the plot of the dispersion parameter vs. wavelength. This is because variation of the air path changes the wavelength where the air path and test fiber are balanced and produces a new interferogram from which the dispersion parameter can be determined. Examination of Eq. 4-4 shows that the first term can be removed if the group delay in the air path is equal to that in the fiber path for the central wavelength, λ_o (central wavelength at which the group delay in fiber and air paths are balanced). The relationship between the air path length and the fiber length at the wavelength λ_o is given by Eq. 4-10:

$$L_{air} = \left(n_{eff}(\lambda_o) - \lambda_o \left. \frac{dn_{eff}}{d\lambda} \right|_{\lambda_o} \right) L_f \qquad \textbf{Eq. 4-10}$$

Taking the derivative of L_{air} with respect to λ_o and using the definition given by Eq. 4-6, we obtain:

. $$\left.\frac{dL_{air}}{d\lambda}\right|_{\lambda_o} = \left(-\lambda_o \left.\frac{d^2 n_{eff}}{d\lambda^2}\right|_{\lambda_o} \right) L_f = cD(\lambda_o) L_f \qquad \textbf{Eq. 4-11}$$

Therefore the change of λ_o with respect to the change of L_{air} can be written as

$$\frac{d\lambda_o}{dL_{air}} = \frac{1}{cL_f D} \qquad \textbf{Eq. 4-12}$$

Thus, the relationship between a change in the central (balanced) wavelength and the change in the air path length is given by:

$$d\lambda_o = dL_{air} \frac{1}{cL_f D} \qquad \textbf{Eq. 4-13}$$

The minimum amount by which we can change the air path sets the minimum increment of the central wavelength in the interferogram. This amount must be several times smaller than the bandwidth of the source. Thus the minimum step size of the air path sets the wavelength resolution of the measured dispersion curve. Note the wavelength resolution is also inversely proportional to the dispersion-length product of the test fiber.

I will now show the dependence of the wavelength resolution on the dispersion length product. As a numerical example, for a step size of 0.1μm, assuming a 50-cm-long SMF28^{TM} test fiber, the wavelength resolution is 0.1nm, which is sufficient for most applications. As a graphical example the wavelength resolution is plotted against the dispersion-length product of standard SMF28^{TM} fiber.

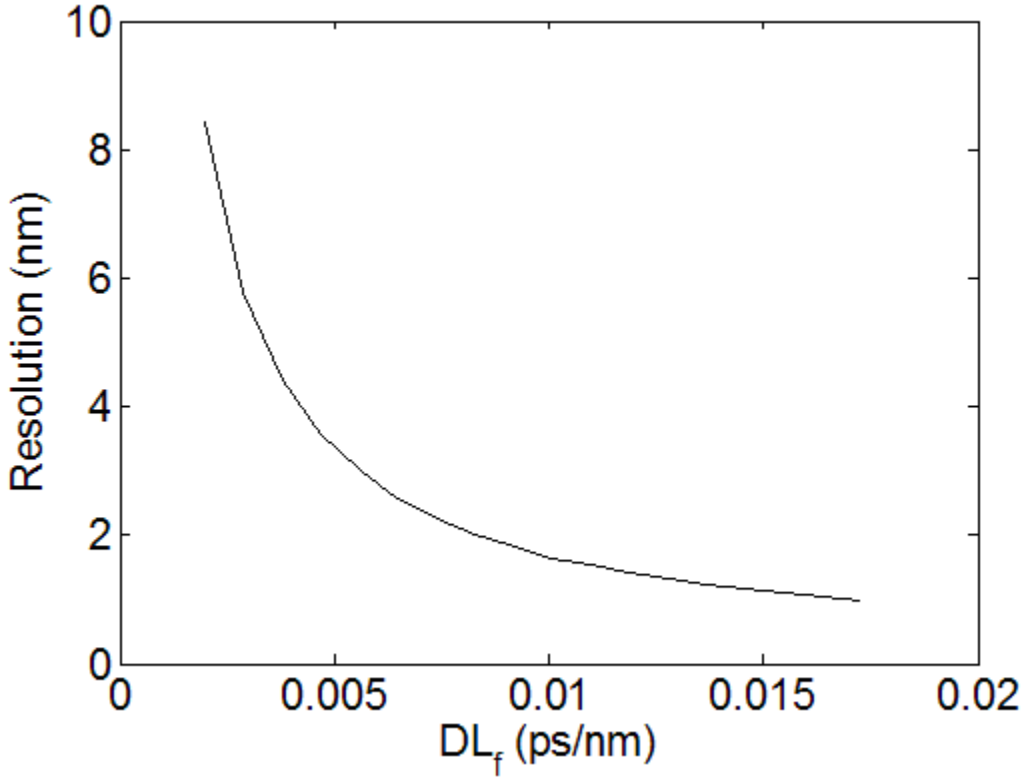

Fig. 4-10: Dependence of the wavelength resolution on the dispersion-length product. Note we assume the values λ_o = 1550nm and δL_{air} = 5µm and B_{source} = 130nm.

4.3.2 Minimum Required Source Bandwidth

A minimum number of *envelope* fringes are required for accurate measurements of dispersion. As long as the balanced wavelength, λ_0, and four other wavelengths corresponding to the peaks (or troughs) of the envelope fringes are captured within the source bandwidth, B_{source}, (Fig. 4-11), it is sufficient to determine dispersion $D(\lambda_0)$. It is found in practice that more accurate measurements require selecting two peaks (or troughs) on either side of λ_0, as indicated by B_{min} on Fig. 4-11.

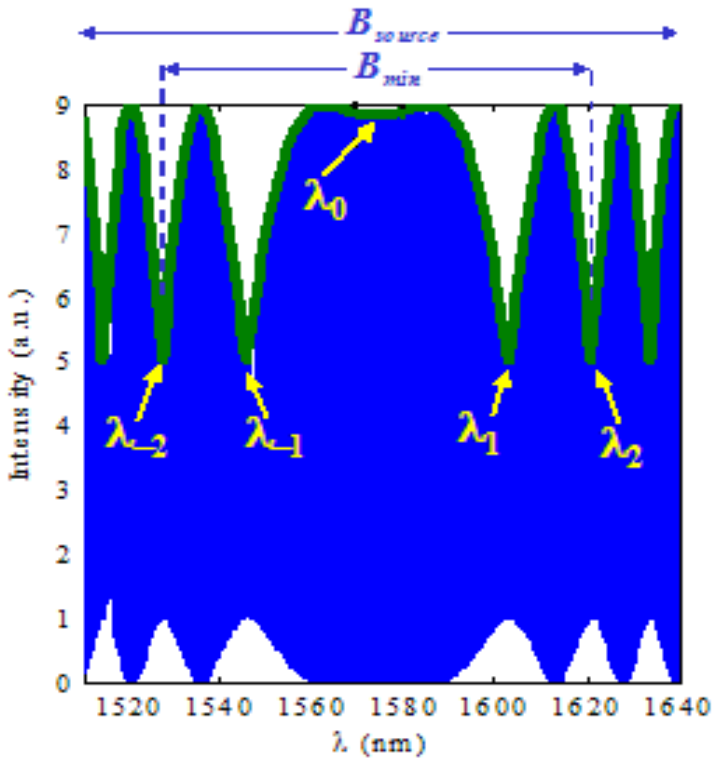

Fig. 4-11: Minimum required source bandwidth and the locations of the troughs

For a given test fiber, the dispersion-length product is fixed. Therefore, the only factor that limits the number of *envelope* fringes is the source bandwidth, B_{source}. The longer the fiber, or the larger the dispersion, the more closely spaced the envelope fringes, and hence the smaller the required bandwidth. In order to determine B_{min} quantitatively, we need to determine the maximum value for the wavelength spacing $(\lambda_2-\lambda_0)$, as shown in Fig. 4-11. From Eq. 4-4, ignoring the 3rd-order term, we can obtain the envelope phase difference $|\phi_{envelope}(\lambda_1) - \phi_{envelope}(\lambda_0)|$, which has an upper bound of π, since the first trough occurs at λ_1:

$$\left|\phi_{envelope}(\lambda_1)-\phi_{envelope}(\lambda_0)\right| = 2\pi \frac{(\lambda_1-\lambda_0)^2}{2!\,\lambda_1}\left.\frac{d^2 n_{eff}}{d\lambda^2}\right|_{\lambda_0} L_f \le \pi \qquad \textbf{Eq. 4-14}$$

Applying the definition of dispersion in Eq. 4-6, we can therefore find the upper bound of the wavelength spacing ($\lambda_1-\lambda_0$):

$$\lambda_1 - \lambda_0 \le \frac{\lambda_0}{\sqrt{cDL_f}} \qquad \textbf{Eq. 4-15}$$

Next, we examine the wavelength spacing between λ_1 and λ_2. From 4-5, ignoring the 3rd-order term and applying Eq. 4-6 gives,

$$(\lambda_2 - \lambda_0)^2 - (\lambda_1 - \lambda_0)^2 \approx \frac{\lambda_o^2}{cDL_f} \qquad \textbf{Eq. 4-16}$$

Combining Eqs. 4-15 and 4-16, we get the upper bound for the wavelength spacing $\lambda_2-\lambda_0$:

$$(\lambda_2 - \lambda_0)^2 = [(\lambda_2 - \lambda_1) + (\lambda_1 - \lambda_0)]^2 \le \frac{2\lambda_o^2}{cDL_f} \qquad \textbf{Eq. 4-17}$$

The minimum required source bandwidth B_{min} should be not less than the upper bound of $2(\lambda_2-\lambda_0)$, therefore,

$$B_{\min} = 2\sqrt{2}\frac{\lambda_0}{\sqrt{cDL_f}} \qquad \textbf{Eq. 4-18}$$

It is clear that the dispersion-length product of the test fiber also affects the minimum required bandwidth. Using a similar numerical example, assuming a 50-cm-long SMF test fiber and 1.55μm as the balanced wavelength, the minimum required bandwidth is 85 nm. As a graphical example the minimum bandwidth required is plotted against the dispersion-length product for a standard single mode fiber and the values assumed for the calculation are Note we assume the values λo = 1550nm and dLair = 5μm and Bsource = 130nm.

.

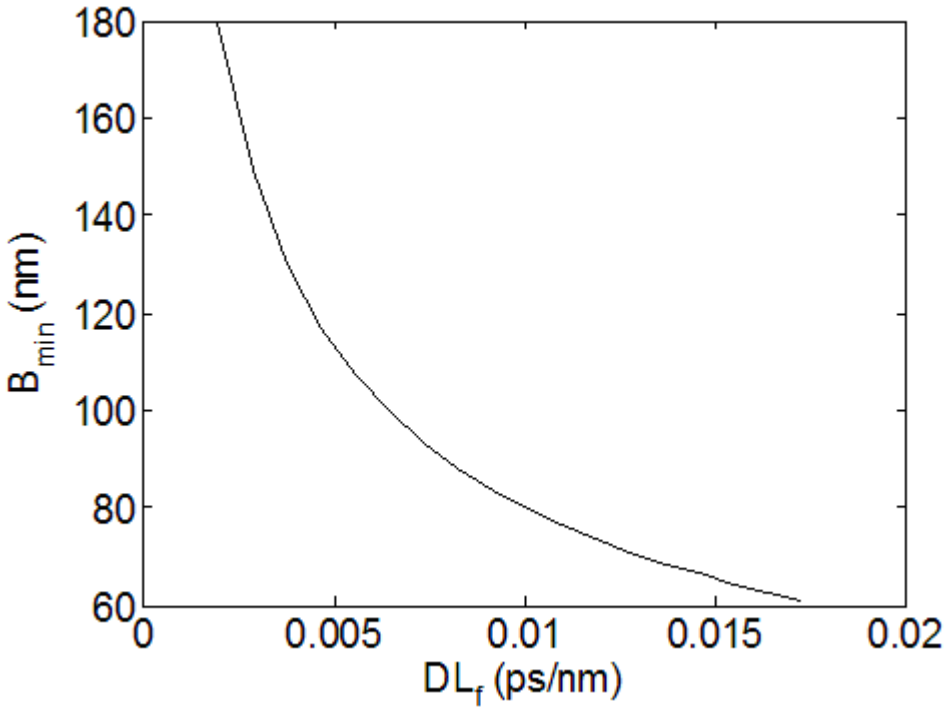

Fig. 4-12: Minimum bandwidth required as a function of the dispersion length product. Note we assume the values λ_0 = 1550nm and δL_{air} = 5µm and B_{source} = 130nm.

4.3.3 Measurable bandwidth of the dispersion curve B_{mea}

Since each spectral interferogram produces one dispersion value at the balanced wavelength, λ_0, to obtain dispersion versus wavelength, a number of interferograms are recorded at various balanced wavelengths by setting the appropriate air path lengths. Since each interferogram should be taken over a bandwidth of at least B_{min}, from Fig. 4-11 one can see that the measurable bandwidth of the dispersion curve is the difference between the available source bandwidth B_{source} and the minimum required bandwidth B_{min}, that is,

$$B_{mea} = B_{source} - B_{\min} \geq B_{source} - 2\sqrt{2}\frac{\lambda_0}{\sqrt{cDL_f}} \qquad \textbf{Eq. 4-19}$$

Alternatively, if we do not require two of the troughs to be on each side of λ_0, then the measurable bandwidth B_{mea} can be larger. In order to accurately determine λ_0, the central fringe (from λ_{-1} to λ_1 in Fig. 4-11) is required to be entirely visible within the measured spectral range. Therefore,

$$B_{mea} = B_{source} - 2(\lambda_1 - \lambda_0) \geq B_{source} - 2\frac{\lambda_0}{\sqrt{cDL_f}} \qquad \textbf{Eq. 4-20}$$

Equation 4-19 or 4-20 gives the lower bound for the measurable bandwidth, which assumes the widest possible central fringe. In practice, since $\phi_{\text{envelope}}(\lambda_0)$ cannot be controlled, the width of the central fringe can be anywhere between zero and twice the limit of Eq. 4-20. Therefore, B_{mea} can be as large as B_{source} in certain cases.

Examination of Eq. 4-19 or 4-20 shows that increasing the dispersion-length product of the test fiber increases B_{mea}. Note that for a given measurement system, B_{source} is fixed, so the only parameter that can be used to extend B_{mea} is L_f. The dispersion length product is, in fact, the main independent variable in determining the system parameters. As a graphical example the minimum measurable bandwidth is plotted against the dispersion-length product for a standard single mode fiber.

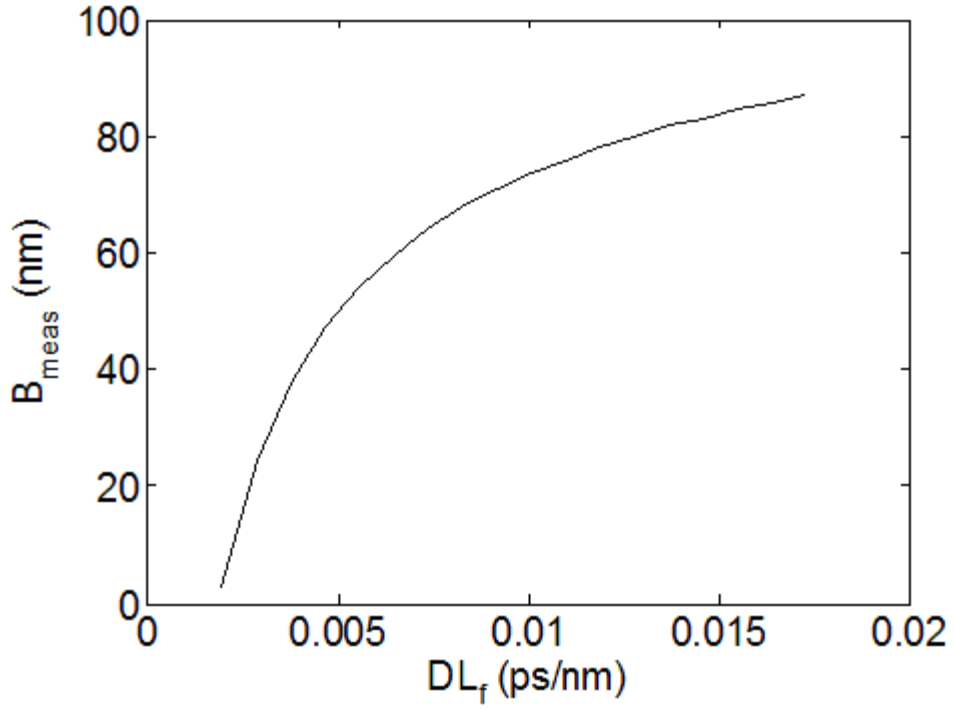

Fig. 4-13: The dependence of the measurable bandwidth (B_{mea}), on the DL_f product. Note we assume the values λ_o = 1550nm and δL_{air} = 5µm and B_{source} = 130nm.

The dispersion length-product has been shown to be the main independent variable in determining the measurable bandwidth and the minimum bandwidth. But the range of this parameter is itself affected by the source used. The bandwidth of the source determines the minimum fiber length that can be characterized using this technique and the minimum wavelength step of the source leads to a maximum characterizable fiber length. The next section discusses how the source bandwidth and minimum wavelength step size affect the range of fiber lengths that can be measured using the SAI technique.

4.3.4 Minimum Fiber Length

The bandwidth of the source determines the minimum fiber length that can be characterized using SAI. A smaller fiber length produces a wider spectral interferogram as determined by Eq. 4-18. Thus in order for a certain fiber length to be characterizable using SAI the interferogram produced must fit inside the source bandwidth. Therefore the requirement is that,

$$B_{\min} \le B_{source} \qquad \textbf{Eq. 4-21}$$

Using Eq. 4-18, we have:

$$L_f \ge \frac{8\lambda_o^{\,2}}{cDB_{source}^{\,2}} \qquad \textbf{Eq. 4-22}$$

Note that for a longer fiber there will be a greater measurement bandwidth (according to Eq. 4-19 or 4-20) and a higher wavelength resolution (Eq. 4-13). As a numerical example, for a source bandwidth of 130nm, the minimum length for a SMF28 fiber is 0.23m. The maximum fiber length is plotted as a function of the source bandwidth in Fig. 4-14.

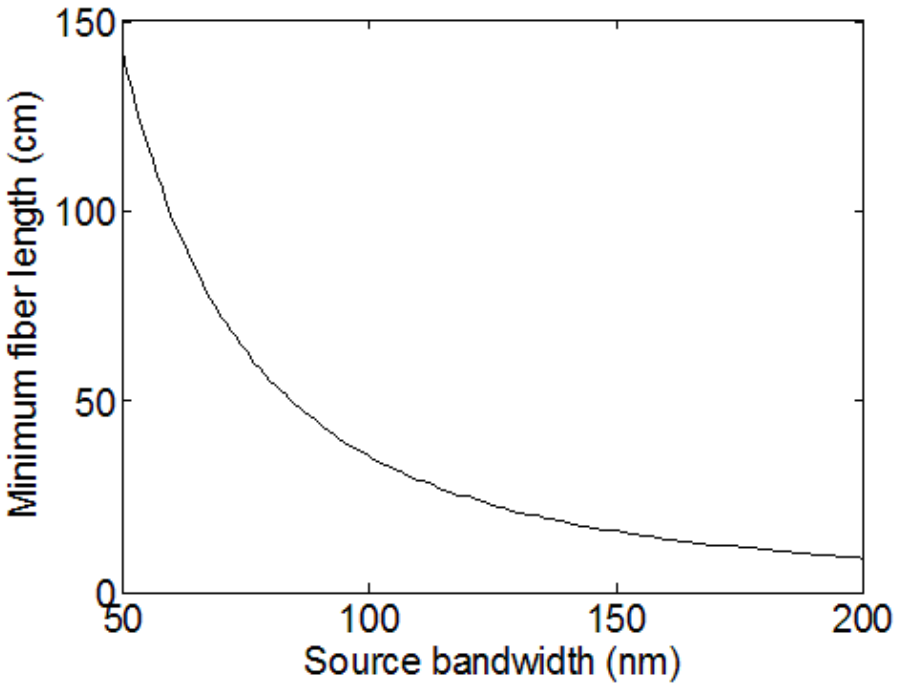

Fig. 4-14: Minimum fiber length vs. source bandwidth. Note λ_o = 1550 and D = 18 ps/nm-km.

4.3.5 Maximum Fiber Length

The SAI method uses the slow-varying envelope function to obtain dispersion. Though the "carrier" fringes are not of interest, they still need to be resolved during measurement otherwise the envelope shape cannot be preserved. The carrier fringe spacing is directly affected by the length of the fiber under test, L_f. A longer fiber will lead to narrower carrier fringes.

The minimum step size of the tunable laser, however, sets a limit on the minimum carrier fringe period that can be detected due to aliasing. Since a longer fiber length has a higher frequency carrier this minimum detectable fringe period results in a limit on the maximum fiber length. The carrier fringe period is the wavelength difference that causes

the fast varying phase to shift by 2π. The Fast phase term in Eq. 4-2 for a balanced air path, $L_{air} = N_g(\lambda_o)L_f$, can be written as:

$$\phi = (k_o n_{eff} L_f + k_o N_g(\lambda_o) L_f) \quad \textbf{Eq. 4-23}$$

Using a first order approximation of n_{eff} and N_g

$$N_g(\lambda_o) \approx n_{eff} \approx n \quad \textbf{Eq. 4-24}$$

Where n is the core index, the phase term is written as

$$\phi = \frac{4\pi n L_f}{\lambda_o} \quad \textbf{Eq. 4-25}$$

The fringe period, $\Delta\lambda$, corresponds to a 2π phase shift

$$\Delta\phi = \frac{4\pi n L_f}{\lambda_o^{\,2}} \Delta\lambda = 2\pi \quad \textbf{Eq. 4-26}$$

Hence,

$$\Delta\lambda = \frac{\lambda_o^{\,2}}{2nL_f} \quad \textbf{Eq. 4-27}$$

In order to detect one fringe accurately, we apply the Nyquist criterion that at least 2 sample points have to be included in one fringe. This sets the following limit over the fiber length:

$$L_f \leq \frac{\lambda_o^{\,2}}{4n\,\Delta\lambda} \quad \textbf{Eq. 4-28}$$

Where $\Delta\lambda$ is the minimum wavelength step size of the tunable laser.

If the fiber length limit is exceeded aliasing occurs. The maximum fiber length for aliasing to be avoided is plotted as a function of step size in Fig. 4-15.

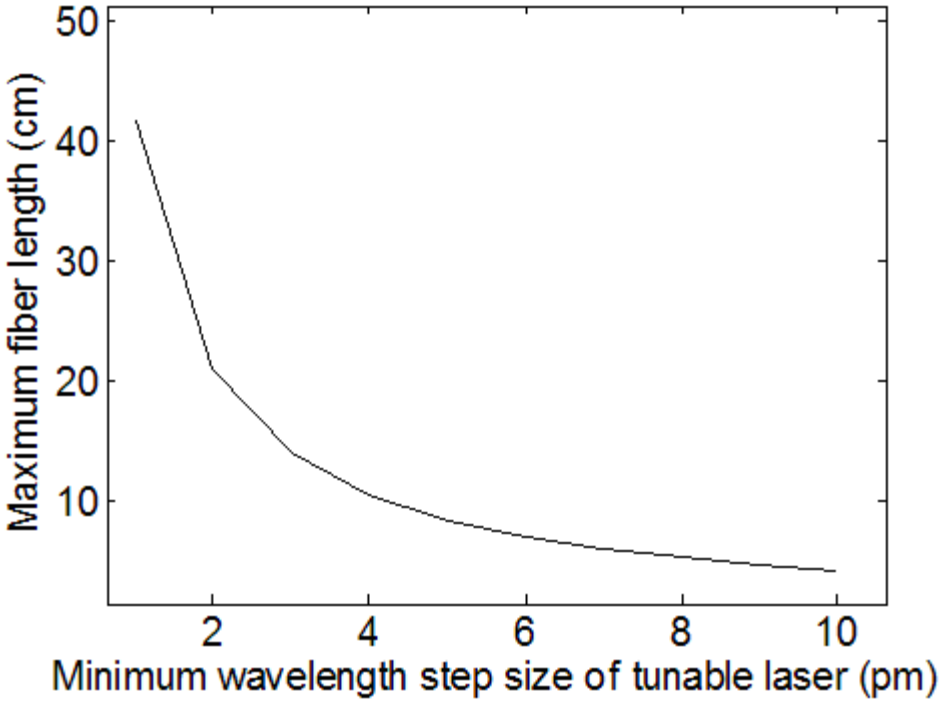

Fig. 4-15: The maximum measurable fiber length, L_f as a function of the step size of the tunable laser. The detector resolution is 1 picometer, λo=1550 nm and n = 1.44.

The preceding analysis assumes that it is necessary to avoid aliasing to ensure that *all* of the peaks of the interferogram are sampled in order to accurately plot the envelope of the interferogram. It is this assumption that leads to the upper limit in the fiber length given in Eq. 4-28. This upper limit however can be exceeded by dividing the interferogram into small window sections and selecting a single point in each window to plot the envelope. The theory behind this technique, called wavelength windowing, will be explained in detail in the next section.

4.4 The Effect of Wavelength Windowing

The problem with trying to measure a fiber longer than Eq. 4-28 allows is that the period of the carrier gets shorter with increasing fiber length. According to Nyquist theory the sampling period, determined by the average step size of the tunable laser, must be at least 2 times smaller than the period of the carrier in order to avoid aliasing. This ensures that *all* the sampled peaks of the carrier match the true envelope of the interference pattern.

Aliasing is a phenomenon that prevents *every* peak of the carrier from being sampled but it does not mean that *some* of the peaks in a given wavelength window range will not be sampled. We can therefore divide the interferogram into small window sections, as shown in Fig. 4-16, each containing many sampled points. Thus when aliasing does occur there will be a certain probability that at least one of the sampling points will land on a peak of the interferogram within each wavelength window (assuming a slow variation in the envelope within that window). Therefore, the envelope of the interferogram can be plotted under conditions where aliasing does occur by taking the maximum in each wavelength window and connecting them together, as shown in Fig. 4-16.

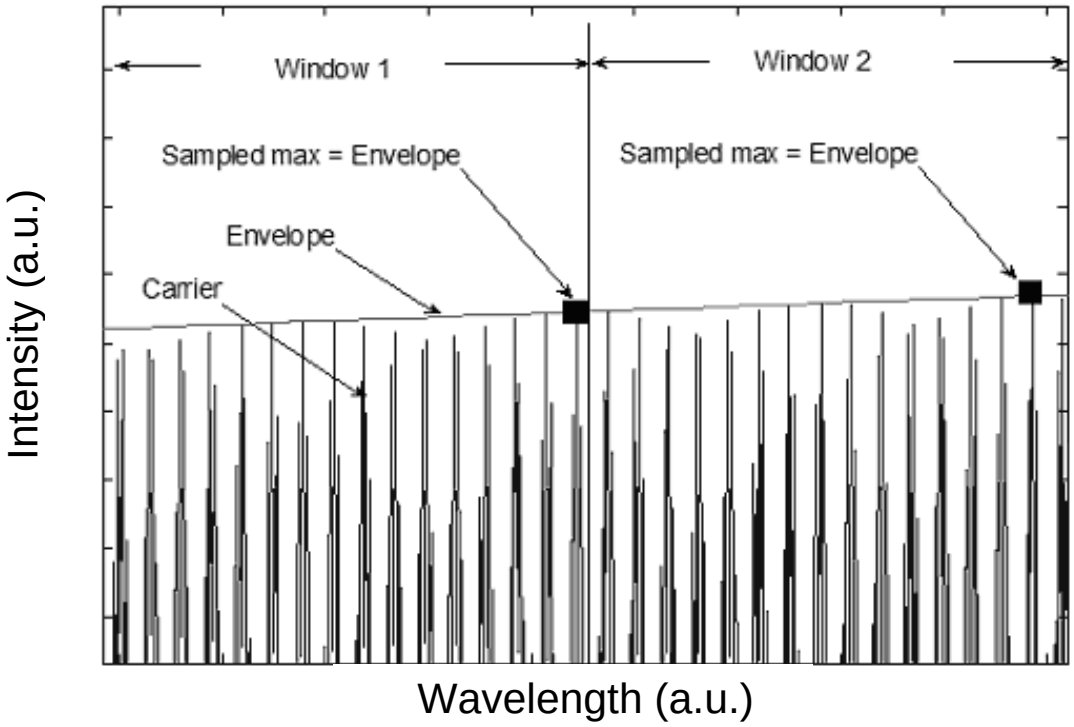

Fig. 4-16: Tracing the envelope of the interferogram by wavelength windowing.

Detailed statistical analysis (developed in the next section) shows how the probability that *at least one* of the peaks will be sampled within a wavelength window is determined. This technique shows that the upper limit in Eq. 4-28 can be exceeded by many folds by wavelength windowing.

4.5 Model Development

This technique uses a tunable laser system to sample the peaks of an interferogram. A real world tunable laser system, however, does not step the wavelength with equal step sizes but has a certain standard deviation in its step size. In order to produce an accurate modeling of a real world process this variation in the step size of the tunable laser must be taken into account by the model. The tunable laser system used in the experiments was

the Agilent 8164A which has an average step size of 1 pm and a standard deviation of 0.17 pm as determined from the histogram and the Gaussian PDF in Fig. 4-17:

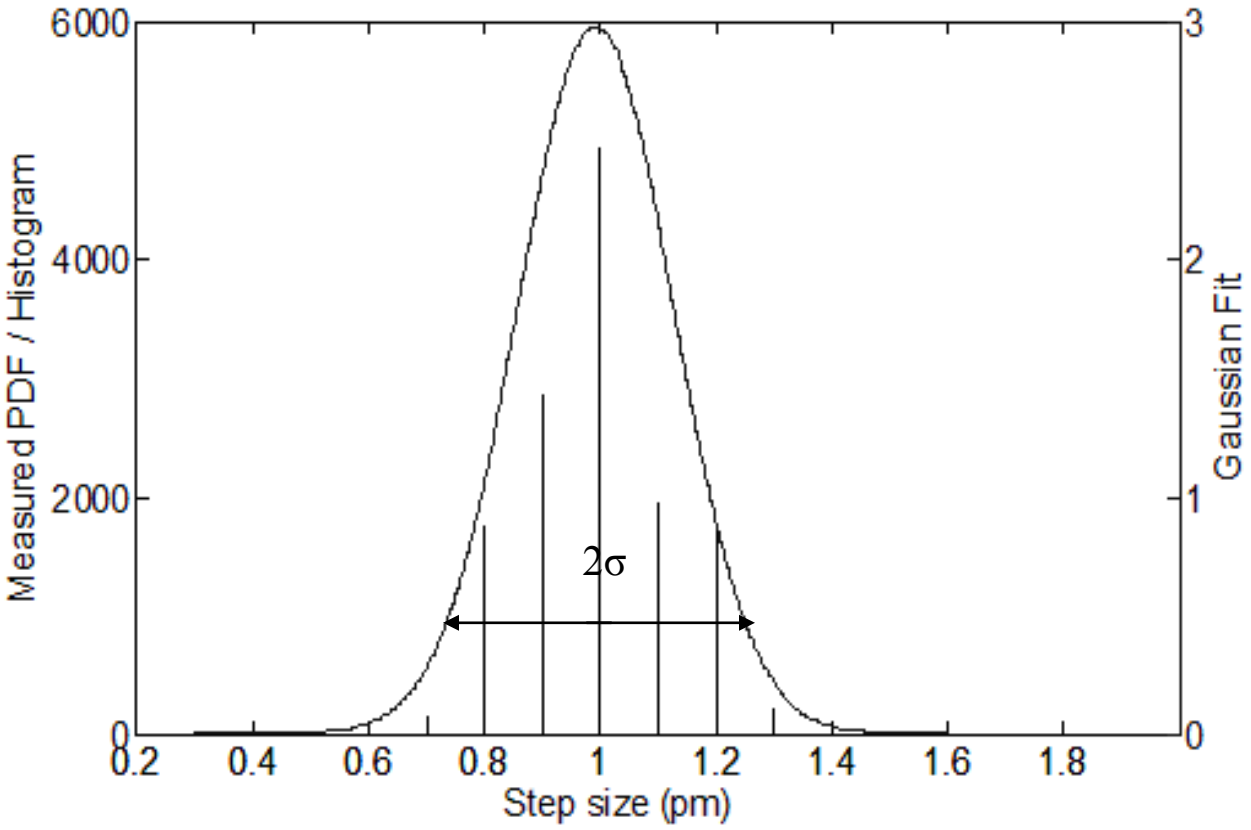

Fig. 4-17: Measured Probability density function (histogram) and a Gaussian fit for the step size of the Agilent 8164A tunable laser.

In order for the model to accurately determine the probability of a sampled point matching at least one peak of the carrier wave within a certain wavelength window, certain parameters must be determined. The model that will be developed requires knowledge of the fiber length, the width of wavelength window, the average step size of the tunable laser, the standard deviation of this step size and the tolerance in detecting the peak as a percentage of the carrier period.

In this model we will designate the fiber length as L_f, the wavelength window within which we wish to detect a peak as W, the average step size of the tunable laser as μ, the standard deviation of the step size of the tunable laser as σ and the tolerance in detecting the peak as a percentage of the carrier period as ε. If we call λ_o the separation between the first carrier peak and the maximum sampling probability density of the first step, as shown in Fig. 4-18, then the wavelength location of the next maximum sampling probability occurs at $\lambda_o + \mu$ and the following one occurs at $\lambda_o + 2\mu$ and so on. Fig. 4-18 illustrates the probability density functions along with the carrier functions.

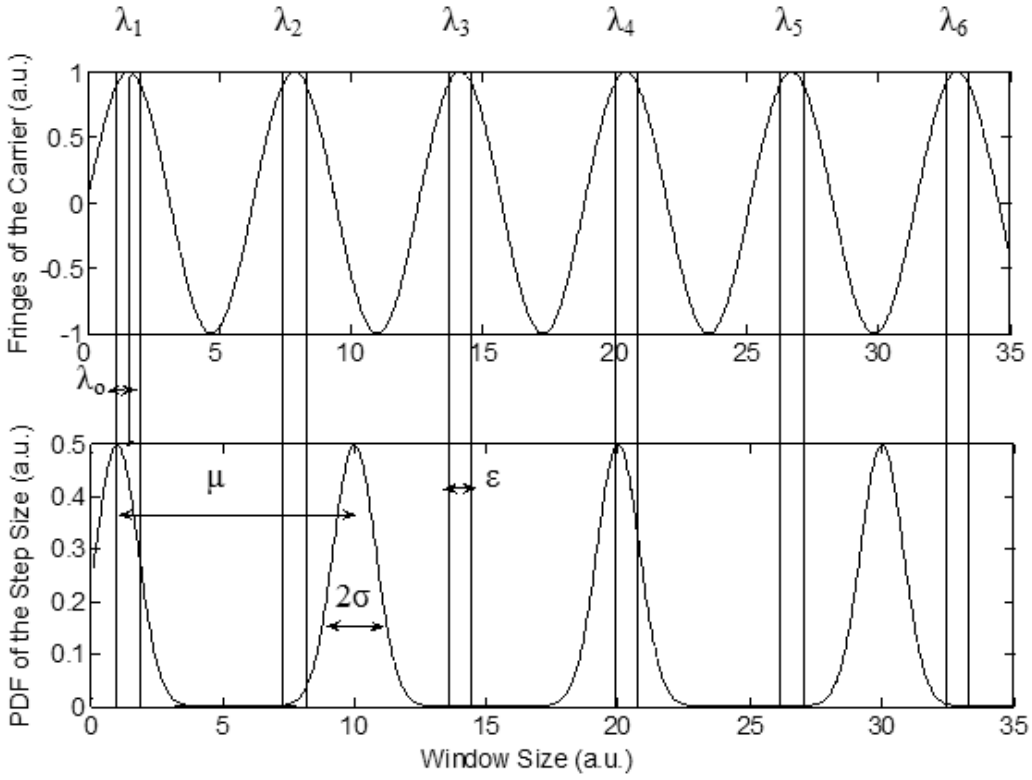

Fig. 4-18: Model showing the probability density functions for the step size and the carrier for determining the probability of hitting a peak in a given wavelength window. The probability density functions for the step size and the carrier fringes are shown. Note that even with aliasing the tunable laser has a chance of hitting the peaks of the carrier at least once for a given wavelength window since the period of the peaks of the carrier is different than the period of the wavelength steps of the tunable laser.

Fig. 4-18 also illustrates the fact that even with aliasing, where all the peaks of the interferogram are not sampled, there is still a chance that at least one of the peaks of the interferogram will be sampled for a given wavelength window since the period of the peaks of the carrier is different than the period of the wavelength steps of the tunable laser. Thus, for any given window size there will be a number of peaks of the carrier.

If we assume the location of the first carrier peak to be at λ_1, as shown in Fig. 4-18, then the probability that this first peak is sampled by the first step of the tunable laser is given by:

$$P_{11} = \int_{\lambda_1 - \frac{\varepsilon}{2}}^{\lambda_1 + \frac{\varepsilon}{2}} \frac{1}{\sqrt{2\pi}\sigma} e^{\left(-\frac{(\lambda-\lambda_o)^2}{2\sigma^2}\right)} d\lambda \qquad \textbf{Eq. 4-29}$$

Therefore the probability that the first peak is <u>not</u> sampled by the first step is:

$$\overline{P_{11}} = 1 - P_{11} = 1 - \int_{\lambda_1 - \frac{\varepsilon}{2}}^{\lambda_1 + \frac{\varepsilon}{2}} \frac{1}{\sqrt{2\pi}\sigma} e^{\left(-\frac{(\lambda-\lambda_o)^2}{2\sigma^2}\right)} d\lambda \qquad \textbf{Eq. 4-30}$$

Here ε, shown in Fig. 4-18, is a fraction of the width of the carrier period and this measure translates into a tolerance in the measurement of the peak amplitude.

If we let N be the number of steps of the tunable laser in a given window size then the probability of *not* sampling the first peak with *any* of the N steps is given by:

$$\begin{aligned} \overline{P_N} &= \overline{P_{11}}\,\overline{P_{12}} \ldots \overline{P_{1N}} \\ &= \prod_{n=1}^{N} \left[1 - \frac{1}{\sqrt{2\pi}\sigma} \int_{\lambda_1 - \frac{\varepsilon}{2}}^{\lambda_1 + \frac{\varepsilon}{2}} \frac{1}{\sqrt{2\pi}\sigma} e^{\left(-\frac{(\lambda-(\lambda_o+n\mu)^2}{2\sigma^2}\right)} d\lambda \right] \end{aligned} \qquad \textbf{Eq. 4-31}$$

If we let M be the number of peaks of the carrier in a given window size then the probability of *not* sampling *any* of the M peaks with *any* of the N steps is given by:

$$\begin{aligned}\overline{P_{NM}} &= \prod \overline{P_{nm}} \\ &= \prod_{m=1}^{M}\prod_{n=1}^{N}\left[1-\frac{1}{\sqrt{2\pi}\sigma}\int_{\lambda_m-\frac{\varepsilon}{2}}^{\lambda_m+\frac{\varepsilon}{2}}\frac{1}{\sqrt{2\pi}\sigma}e^{\left(-\frac{(\lambda-(\lambda_o+n\mu)^2}{2\sigma^2}\right)}d\lambda\right] \\ &= \prod_{m=1}^{M}\prod_{n=1}^{N}\left[1-\frac{1}{2}\left[erf(\Lambda_+)-erf(\Lambda_-)\right]\right]\end{aligned} \qquad \textbf{Eq. 4-32}$$

Where λ_m is the location of the mth peak in the wavelength window and is given by m λ_1 and Λ_+ and Λ_- are the normalized wavelength parameters given by:

$$\Lambda_{m\pm} \equiv \frac{\left(\lambda_m \pm \frac{\varepsilon}{2}\right)-\left(\lambda_o+n\mu\right)}{\sqrt{2}\sigma} \qquad \textbf{Eq. 4-33}$$

Since the model assumes a fixed relationship between the first carrier peak and the maximum of the probability density function this probability should be averaged for λ_o varying over one carrier wave period. This gives the probability that no carrier peak is sampled in a given window for a random alignment between the carrier peaks and the maximum of the probability density function. The result is given as:

$$\left\langle\overline{P_{NM}}\right\rangle = \left\langle\prod_{m=1}^{M}\prod_{n=1}^{N}\left[1-\frac{1}{2}\left[erf(\Lambda_+)-erf(\Lambda_-)\right]\right]\right\rangle \qquad \textbf{Eq. 4-34}$$

Thus the probability that *at least one* of the peaks is sampled for a given window size is determined as:

$$\left\langle P\right\rangle = 1-\left\langle\prod_{m=1}^{M}\prod_{n=1}^{N}\left[1-\frac{1}{2}\left[erf(\Lambda_+)-erf(\Lambda_-)\right]\right]\right\rangle \qquad \textbf{Eq. 4-35}$$

4.6 Simulation Results

The calculated effective index and dispersion of SMF28^{TM} is used in the following sections to determine the probability that at least one peak is sampled as one of five parameters is varied. The parameters varied are the window size, the step size, the fiber length (which determines the peak spacing), and the tolerance (which determines the how close the sampled peak is to the actual carrier amplitude). The results are shown in the following five sections. The parameters held constant in these simulations are chosen to be the same as the experimental conditions that will be implemented in section 5.2 in the experiment on SMF28^{TM}. The Matlab code used to perform these simulations is given in Appendix A.2.

4.6.1 Probability vs. Window Size

The probability that at least one peak is sampled in a given window size, W, is shown in Fig 4-19, as a function of the window size. The parameters held constant for this simulation are the fiber length (Lf = 39.5 cm), the average step size (μ = 1 pm) and the tolerance (ε = 0.02 x average carrier period). The probability is plotted for 3 different cases of the standard deviation in Fig. 4-19: σ = 0.05pm, which is as close to the σ = 0 case (i.e. constant step size case) that we can get using the model since σ = 0 leads to a $\Lambda_{m\pm}$ = 1/0 (undefined) in Eq. 4-33. The other two cases plotted in Fig. 4-19 are σ = 0.17pm, and σ = 1pm.

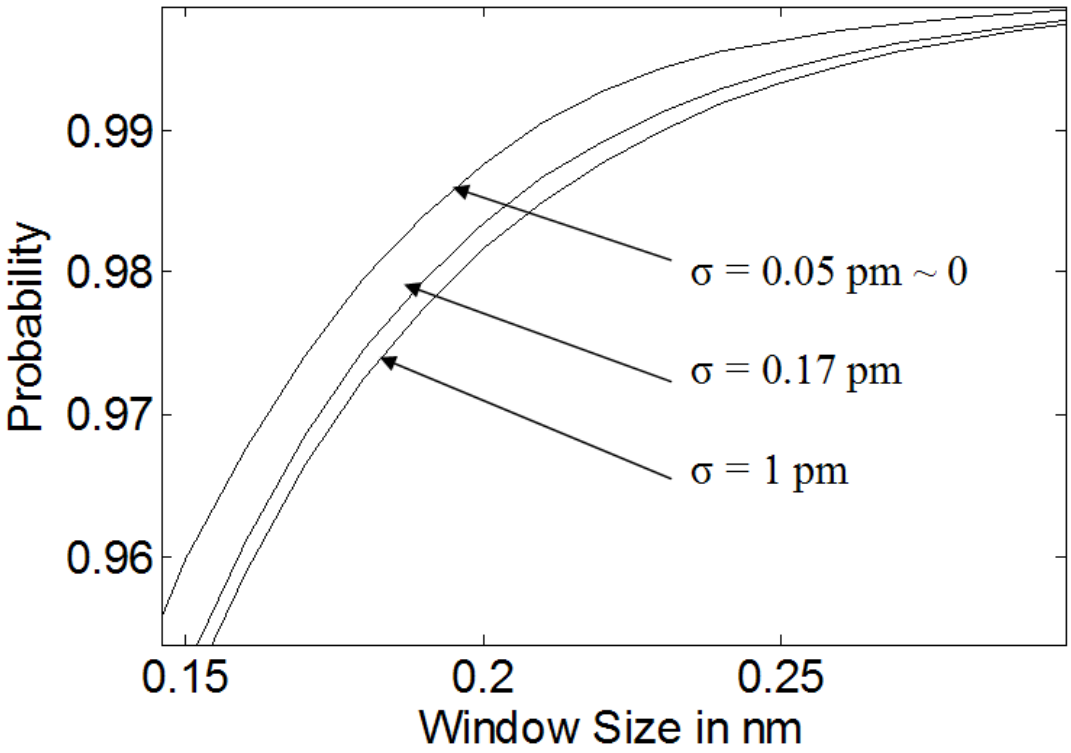

Fig. 4-19: Probability vs. window size. The parameters held constant for this simulation are the fiber length (L_f = 39.5 cm), the average step size (μ = 1 pm) and the tolerance (ε = 0.02 x average carrier period). The probability is plotted for 3 different cases of the standard deviation: σ = 0.05pm, σ = 0.17pm, and σ = 1 pm

Fig. 4-19 shows that for the given parameters a unity probability can be obtained for a window size of > 0.29nm. The window size, however, is not the only parameter that affects the probability that the tunable laser step will sample the peak of the interferogram in a given window. The next section shows that the average step size of the tunable laser also affects this probability.

4.6.2 Probability vs. Average Step Size

The probability that at least one peak is sampled in a given window size, W, is shown in Fig. 4-20 as a function of the average step size, μ, of the tunable laser. The parameters held constant for this simulation are the fiber length (L_f = 39.5cm), the window size (W = 0.25 nm) and the tolerance (ε = 0.02 x average carrier period). The probability is plotted for 3 different cases of the standard deviation in Fig. 4-20: σ = 0.05pm, which is as close to the σ = 0 case (i.e. constant step size case) that we can get using the model since σ = 0 leads to a $\Lambda_{m\pm}$ = 1/0 (undefined) in Eq. 4-33, σ = 0.17pm, and σ = 1pm.

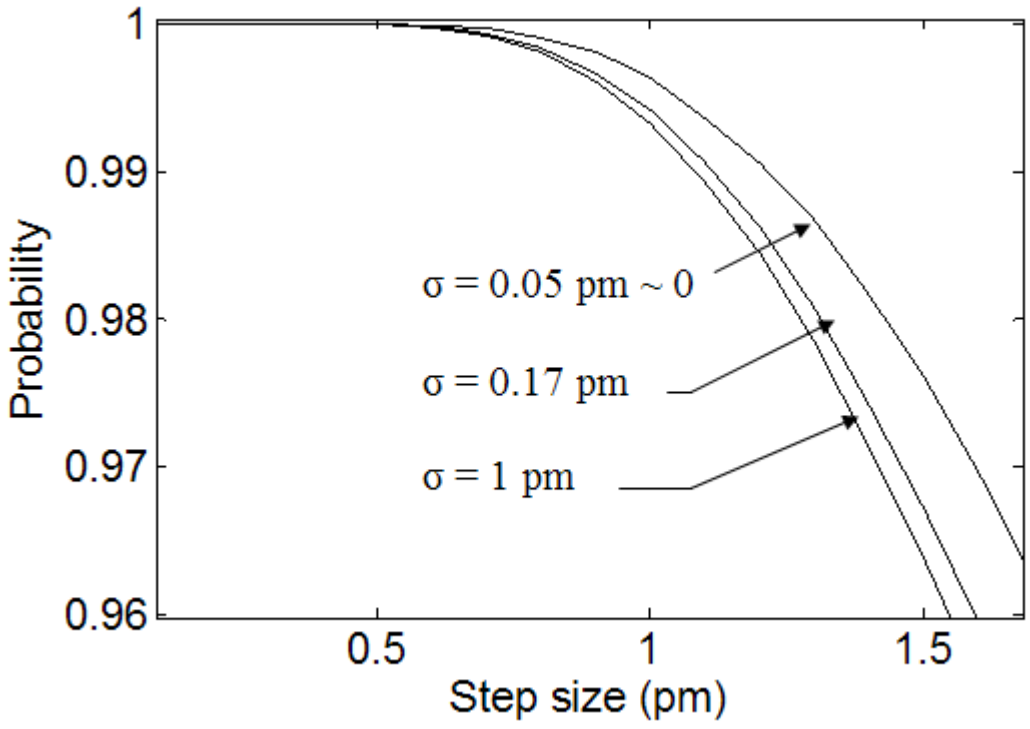

Fig. 4-20: Probability vs. Step Size. The parameters held constant for this simulation are the fiber length (L_f = 39.5cm), the window size (W = 0.25 nm) and the tolerance (ε = 0.02 x average carrier period). The probability is plotted for 3 different cases of the standard deviation: σ = 0.05pm, σ = 0.17pm and σ = 1 pm

Fig. 4-20 shows that for the given parameters there is a near unity probability for an average step size below 0.5 pm and that it decreases as the step size increases. The average step size of the tunable laser, however, is not the only parameter that affects the probability that the tunable laser step will sample the peak of the interferogram in a given window. The next section shows that the length of the test fiber also affects this probability.

4.6.3 Probability vs. Fiber Length

The probability that at least one peak is sampled in a given window size, W, is shown in Fig 4-21 as a function of the fiber length, L_f. The parameters held constant for this simulation are the average step size of the tunable laser (μ = 1 pm), the window size (W = 0.25 nm) and the tolerance (ε = 0.02 x average carrier period). The probability is plotted for 3 different cases of the standard deviation in Fig. 4-21: σ = 0.05pm, which is as close to the σ = 0 case (i.e. constant step size case) that we can get using the model since σ = 0 leads to a $\Lambda_{m\pm}$ = 1/0 (undefined) in Eq. 4-33, σ = 0.17 pm and σ = 1 pm.

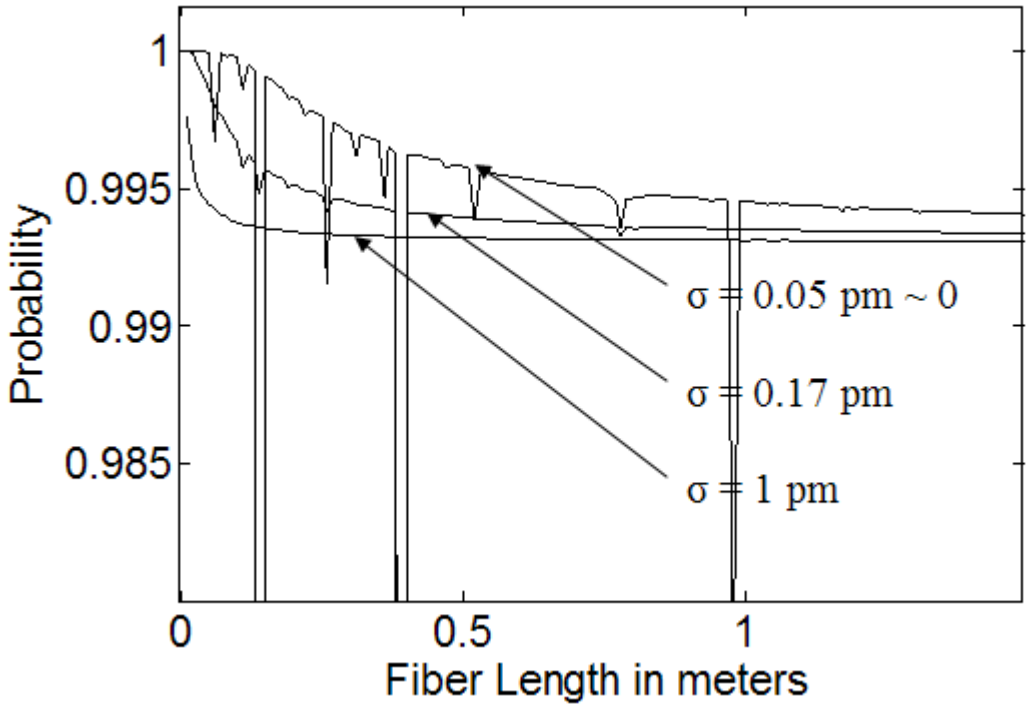

Fig. 4-21: Probability that at least one peak is sampled in a given window vs. fiber length. The parameters held constant for this simulation are the average step size of the tunable laser (μ = 1 pm), the window size (W = 0.25 nm) and the tolerance (ε = 0.02 x average carrier period). The probability is plotted for 3 different cases of the standard deviation: σ = 0.05 pm, σ= 0.17 pm, and σ=1 pm.

Fig. 4-21 shows some peculiar dips where the probability drops to zero for the cases where the standard deviation is small ($\sigma = 0.05$ pm and $\sigma = 0.17$ pm). We can see that when the standard deviation is high ($\sigma = 1$pm) these dips disappear. We also notice from Fig. 4-21 that for higher standard deviation the probability curves drop more quickly to the asymptotic value. Thus a lower standard deviation in the step size of the tunable laser produces curves with higher initial probabilities, but large dips in the probability curve where the probability drops to zero. A higher standard deviation in the step size produces curves with lower initial probabilities but eliminates the dips where the probability drops to zero. It is therefore beneficial to have some amount of variation in the step size of the tunable laser in order to eliminate these dips in the probability.

These dips where the probability drops to zero can be explained by the fact that certain fiber lengths lead to a carrier spacing that is a multiple of the wavelength step size and as a result none of the peaks in a window get sampled. Fig. 4-22 shows the probability as a function of fiber length for $\sigma = 0.05$pm and for two different step sizes $\mu = 1.3$pm (plotted in blue and $\mu = 1$pm (plotted in green). Fig. 4-22 shows that the location of the dips are different for each case since the dips occur at different fiber lengths (different carrier spacing).

The dips occur whenever the carrier spacing is a certain multiple of the step size of the tunable laser. This multiple is given in Eq. 4-36.

$$G = \frac{n}{2^m} \qquad \textbf{Eq. 4-36}$$

n and m are positive integers. Whenever the carrier period is a multiple of *G* there is a high probability that none of the peaks get sampled.

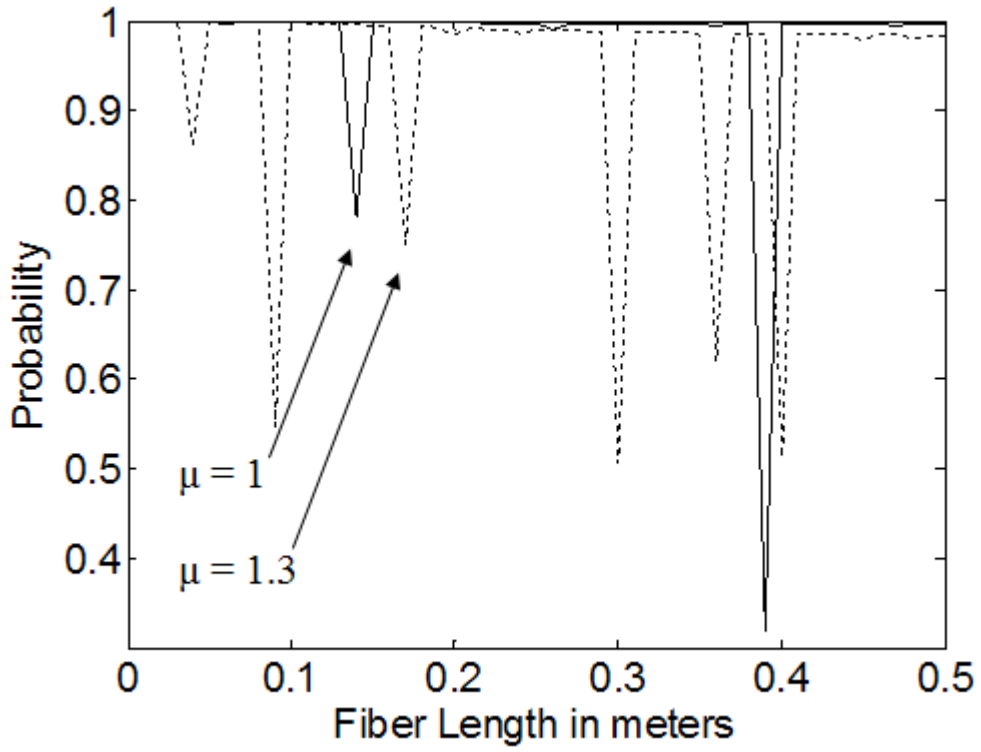

Fig. 4-22: Probability vs. Fiber length for the σ = 0.05pm case for a step size of μ = 1 pm and for the step size of μ = 1.3 pm. The location of the dips in probability occur at different fiber lengths (carrier periods) for different step sizes. They occur when the carrier period is a certain multiple of the step size and there is a chance that none of the peaks within the window get sampled. The parameters held constant for this simulation are the window size (W = 0.25 nm), the tolerance (ε = 0.02 x average carrier period) and the standard deviation of the step size σ = 0.05 pm.

The average carrier period is determined by taking the average of all the carrier period in the bandwidth as described by Eq. 4-37:

$$\lambda_p = \left\langle \frac{\lambda^2}{2n_{eff} L_f} \right\rangle_{Bandwidth} \qquad \textbf{Eq. 4-37}$$

This is easily calculated using the Matlab program written in Appendix A.2.5. As a numerical example Fig. 4-22 shows several dips where the probability drops to zero. In the case where μ = 1.3 pm in Fig. 4-22 when the fiber length is 0.05m the average carrier period is determined to be 13 pm which is 10 times the step size. Table 4-2 shows several other numerical examples using the dips in Fig. 4-22.

Table 4-2: The dips where the probability drops to zero in Fig. 4-22 occur when the carrier period is a multiple of $G = n/2^m$ the step size.

Fiber length	Step Size	Carrier Period	m	n	Multiple
0.04 m	1.3 pm	20.8 pm	0	16	16
0.0916 m	1.3 pm	9.1 pm	0	7	7
0.139 m	1 pm	6 pm	0	6	6
0.171	1.3 pm	4.878 pm	2	15	3.75
0.3 m	1.3 pm	2.6 pm	0	2	2
0.365 m	1.3 pm	2.285 pm	2	7	1.75
0.3925	1	2.125	3	17	2.125
0.425 m	1.3 pm	1.95 pm	1	3	1.5

Note that a dip occurs whenever the period of step size approaches G times the carrier period (for the cases with low standard deviation). This is not illustrated in Fig. 4-22 since it is impossible to get a high enough resolution so that the simulated points fall exactly on the fiber length where every dip occurs. This is also the reason that the dips in Fig. 4-22 do not fall completely to zero.

We also notice that for the given parameters that we have held constant in this simulation the probability of sampling a peak asymptotically approaches a constant value as the length is increased. We notice that this constant is the same, regardless of the standard deviation of the step size. The conclusion, therefore, is that this technique can be used to measure the dispersion of long lengths of fiber (assuming of course that a long enough air path can be produced by the experimental setup and that the period of the carrier peaks is still above the laser linewidth).

4.6.4 Probability vs. Tolerance

The probability that at least one peak is sampled in a given window size is shown in Fig. 4-23 as a function of the tolerance. The parameters held constant for this simulation are the average step size of the tunable laser (μ = 1 pm), the window size (W = 0.25 nm), and the fiber length L_f = 39.5 cm. The probability is plotted for 3 different cases of the standard deviation in Fig. 4-23: σ = 0.05pm, which is as close to the σ = 0 case (i.e. constant step size case) that we can get using the model since σ = 0 leads to a $\Lambda_{m\pm}$ = 1/0 (undefined) in Eq. 4-33, σ = 0.17 pm and σ = 1 pm.

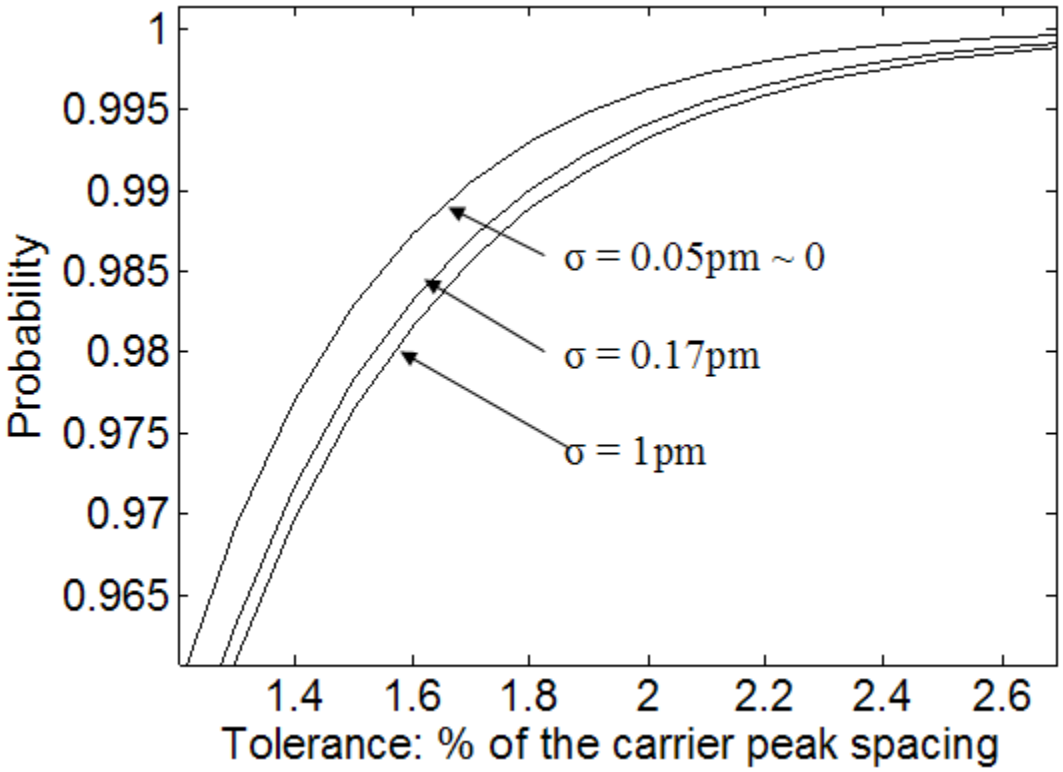

Fig. 4-23: Probability vs. Tolerance. The parameters held constant for this simulation are the average step size of the tunable laser (μ = 1 pm), the window size (W = 0.25 nm) and the fiber length L_f = 39.5 cm. The probability is plotted for 3 different cases of the standard deviation: σ= 0.05pm, σ = 0.17pm and σ = 1pm.

Fig. 4-23 shows that the probability of hitting a ‘peak’ increases as the definition of where the peak actually is becomes relaxed. As the tolerance is increased the degree to which the peaks of the envelope match the amplitude of the actual interference pattern is reduced. It can be seen from this figure that the minimum probability of hitting a peak is zero and that it approaches unity if the tolerance is 2.6% for the given parameters that are held constant.

This chapter has developed the theory of single arm interferometry, discussed how it is implemented and how it can be explained via rigorous mathematical analysis of three wave interference. The technical limits of the SAI have been discussed by showing the effects on the dispersion measurements of four factors of interest. The range of characterizable fiber lengths can be extended via a wavelength windowing technique in which the envelope is plotted by selecting a few points in a given bandwidth. The result of this range extension is that the ultimate limit on the test fiber length is the laser linewidth (which should be much smaller than the carrier fringe period) and the maximum air path length. The next chapter will describe the practical application of the theory that has been developed in this chapter.

Chapter 5: Experiments & Analysis

In this chapter the results of experiments using Single Arm Interferometry are presented to substantiate the theory of single arm interferometry, introduced in the last chapter. An outline of the steps in the experimental process is first provided to give an overview of the experimental process. Then the challenges encountered during the setup of the Single arm interferometry experiments are described. Following these challenges is a description of the instruments used in the experiments and their specific limitations. The last three sections of this chapter outline the results of the experiments performed to characterize three different types of fiber: Single mode fiber (SMF28^{TM}), Dispersion Compensating Fiber (DCF) and Twin Hole Fiber (THF).

5.1 Experimental Process

The experiments in this chapter were carried out to validate the theory presented in the previous chapter and to characterize the dispersion of a Twin Hole fiber for which the dispersion has never been published. The first step in the experiment is to set up the Single Arm Interferometer and to assemble the control and data acquisition hardware. The second step in the experiment is to test the technique by using it to measure the dispersion of fibers for which the dispersion curves are known or that can easily be measured using conventional techniques. To do this, the dispersion curves of Single Mode Fiber (SMF28^{TM}) and Dispersion Compensating Fiber (DCF) were measured. After careful analysis of the results for the experiments on SMF28^{TM} and DCF the new technique was then used to measure the dispersion of a fiber that has never before been

characterized. The entire experimental process for this project is outlined in Fig. 5-1 below.

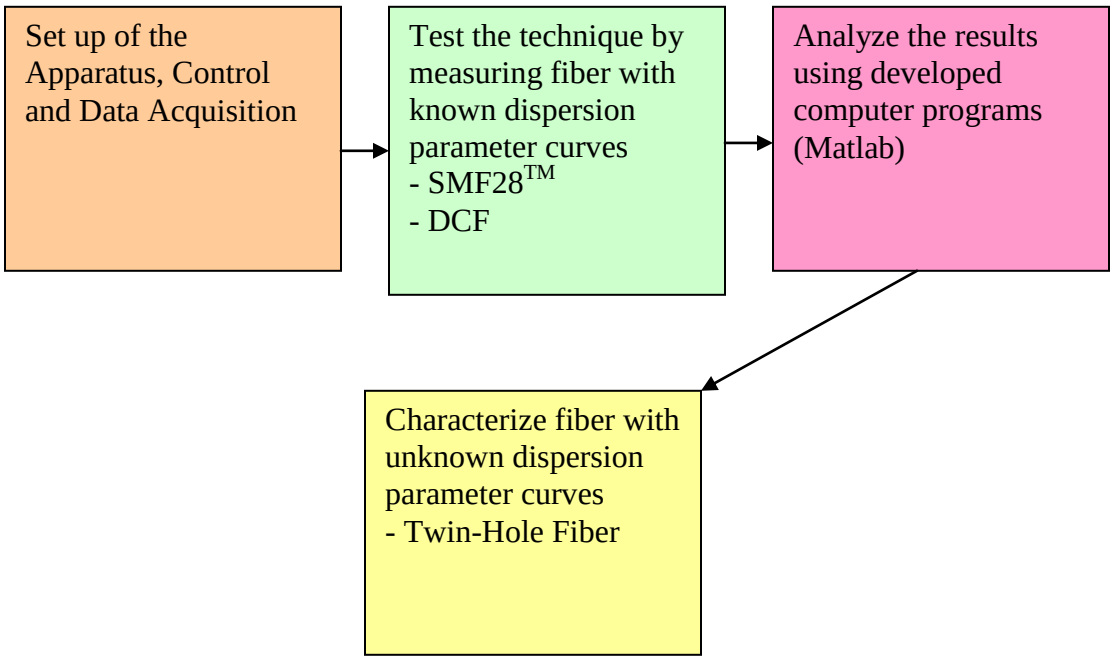

Fig. 5-1: Experimental process for the development and testing of the Single Arm Interferometer. The first step is to set up the apparatus as well as the control and data acquisition hardware and software. The second and third steps test the technique and the fourth step uses the verified technique to characterize a fiber with unknown dispersion.

5.2 Experimental Challenges

In order to compare Single Arm Interferometry to other dispersion measurement techniques the challenges of setting up such an interferometer must also be well understood. There were several challenges associated with the setup of the system and the implementation of the experiments.

One challenge in the setup included alignment of the APC connector with the test fiber which was especially difficult for Twin-hole fiber since the fiber was different in size to SMF so core to core alignment was not easy. Using a bare fiber adapter and a fiber

to fiber connector helped but coupling was still a difficult task since the core of THF is slightly off centre (see Fig. 5-6) whereas the core of SMF28^{TM} is at the centre of the fiber. Another challenge is to prevent the angle polished connector (APC) from being broken by being pushed too forcefully against the flat polished connector (FPC). One way to eliminate the possibility of this occurrence is to produce the APC with a locking pin to prevent a standard FPC from breaking it.

Another challenge in the setup was placing the test fiber at the right location in the bare fiber adapter so that light could be properly collimated by the collimating lens. Trial and error using an infrared card and a pinhole to collimate the beam helped in this regard.

Another challenge was alignment of the mirror such that the beam could be reflected back exactly into the collimating lens and thus back to the detector with a magnitude on the same order as the reflections from the facets of the test fiber. Trial and error was used to achieve maximum fringe visibility.

Air flow in the air path is an effect that leads to changes in the density and therefore the optical path length in the air path. To solve this problem the system was encased in a container to reduce air flow in the air path.

Because of its simplicity the challenges presented in the set up of a single arm interferometry experiment are rather straightforward and it is for this reason that it will be very competitive as a dispersion measurement technique. This simplicity coupled with the advantage of high precision make the SAI a powerful method for characterizing the dispersion of short length fibers. The next section outlines the instruments and tools used in the setup of an SAI and their specific limitations.

5.3 Experimental Instrumentation & Specific Limits

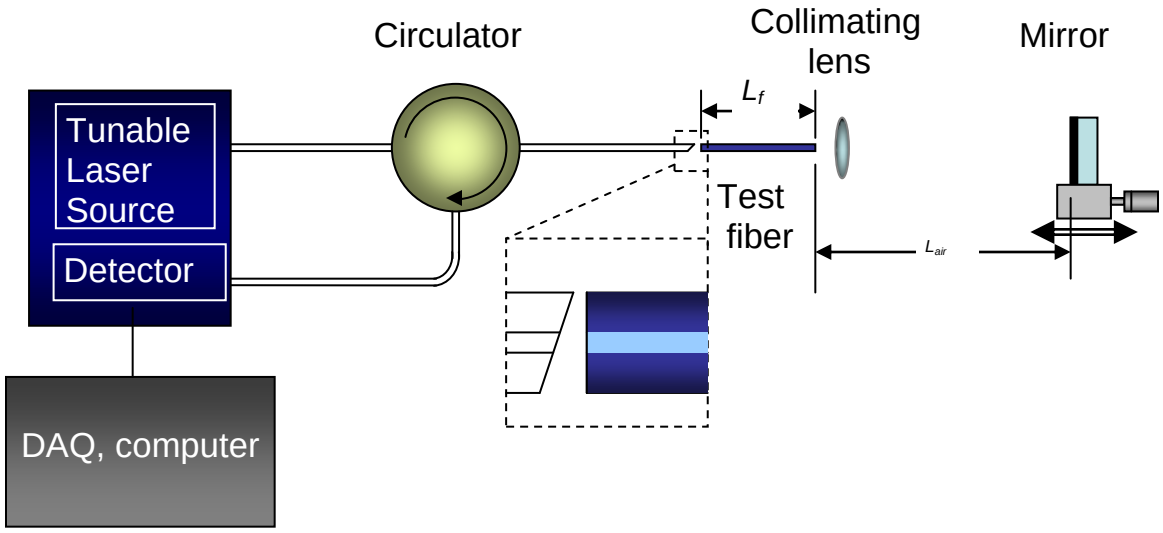

Fig. 5-2: Experimental Setup of a Single Arm Interferometer for dispersion characterization. The tunable laser source and detector used are the Agilent 8164A Lightwave Measurement System with a bandwidth of 130 nm centered around 1550 nm, and a minimum *average* wavelength step of 1 pm (standard deviation 0.17 pm). An angle-polished connector is used at the launch fiber to eliminate the reflection from this facet. The reflections from the collimation lens surfaces are suppressed by using an antireflection coated lens. The mirror tilt is adjusted to obtain maximum fringe visibility. The mirror translation is controlled manually, and the minimum step is approximately 5μm.

The experimental set up is shown in Fig. 5-2. The tunable laser source and detector used are plug-in modules of the Agilent 8164A Lightwave Measurement System. The source has a bandwidth of 130 nm centered around 1550 nm, and a minimum *average* wavelength step of 1 pm (standard deviation σ = 0.17 pm). The unit records the detector readings and the wavelength readings as the source wavelength is swept. The spectral interference pattern is then analyzed. The fibers are aligned by a standard connector or using a bare fiber adapter in cases where the fiber is not connectorized. An angle-polished connector (APC) is used at the launch fiber as shown in Fig. 5-2 in order to eliminate the reflection from this facet. A locking mechanism can be used to prevent the APC from being broken by the FPC. The reflections from the collimation lens surfaces

are suppressed by using an antireflection coated lens. The dispersion of the lens is negligible. The mirror tilt is adjusted to obtain maximum fringe visibility. The mirror translation is controlled manually, and the minimum step is approximately 5μm.

In the following sections, we will apply the SAI technique to measure the dispersion of three different fibers: a standard SMF28^{TM} single mode fiber, a Dispersion Compensating Fiber (DCF) and a Twin-Hole Fiber (THF). In measuring the envelope of the spectral interferogram, the total scanning region is divided into 0.25-nm-wide wavelength windows, over which the envelope is considered constant. The peak value within each band is extracted to produce the spectral envelope as described in sections 4.5.1 – 4.5.3.

5.4 Experiments

5.4.1 Single Mode Fiber

The dispersion properties of SMF28^{TM} are well known and hence it was used to verify the theory of single arm interferometry. In this experiment we used a 39.5±0.1 cm piece of the SMF28^{TM} fiber in a SAI in order to characterize its dispersion. Fig. 5-3 shows a plot of both the experimental dispersion parameter points and the simulated dispersion of SMF28^{TM}. From this figure we can see that the slope of the measured dispersion points closely match the simulated dispersion curve. The simulated dispersion curve for SMF28^{TM} was calculated using the dispersion equation given in Appendix B:

$$D(\lambda) = \frac{S_o}{4}\left[\lambda - \frac{\lambda_o{}^4}{\lambda^3}\right] \qquad \textbf{Eq. 5-1}$$

Where λ_0 = 1313 nm and S_o = 0.086 ps/nm-km and $D(\lambda)$ is measured in ps/nm-km.

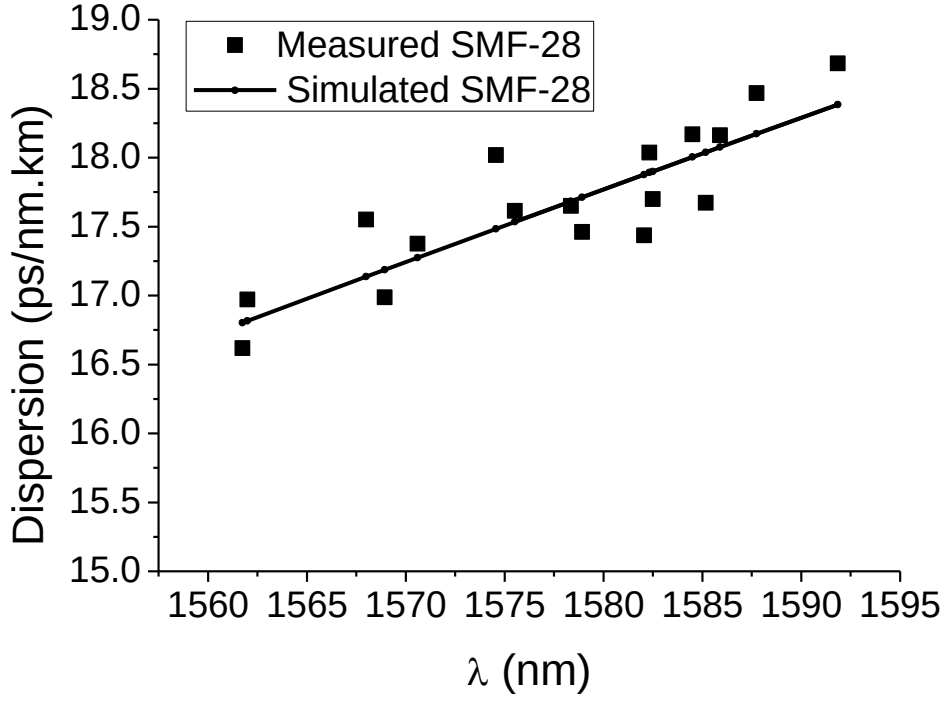

Fig. 5-3: Measured dispersion compared to published dispersion equation [Appendix B] for a 39.5±0.1cm SMF28™ fiber. The standard deviation of the measured dispersion is determined using a linear fit and calculating the standard deviation of the difference between the measured values and the linear fit. The simulation is calculated using the Matlab code in Appendix A.3.1 to be is 0.28 ps/nm-km (corresponding to a relative error of 1.6%). When this standard deviation is multiplied by the length of the fiber, this translates into a standard deviation of 0.0001 ps/nm.

The wavelength resolution of the measured dispersion curve, as determined by Eq. 4-13, is 2.4 nm. The measurable bandwidth according to Eq. 4-20 is 30nm, which is the bandwidth actually used, as shown in Fig. 5-3. The standard deviation of the measured dispersion is calculated by taking the difference between the measured points and a linear fit and then calculating the standard deviation from the difference. The standard deviation, as calculated using the Matlab code in Appendix A.3.1, is 0.28 ps/nm-km (this corresponds to a relative error of 1.6%). When this standard deviation is multiplied by the length of the fiber, this translates into a standard deviation of 0.0001 ps/nm. A comparison between the measured and simulated interference patterns for SMF28™ is shown in Figs. 5-4 (a) and (b).

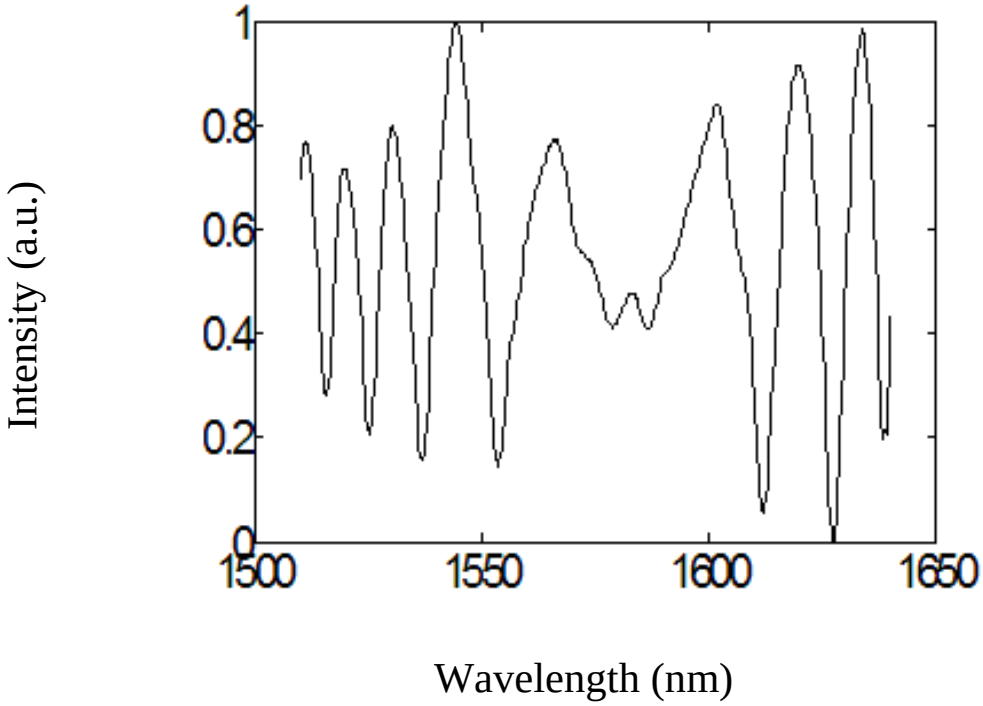

(a)

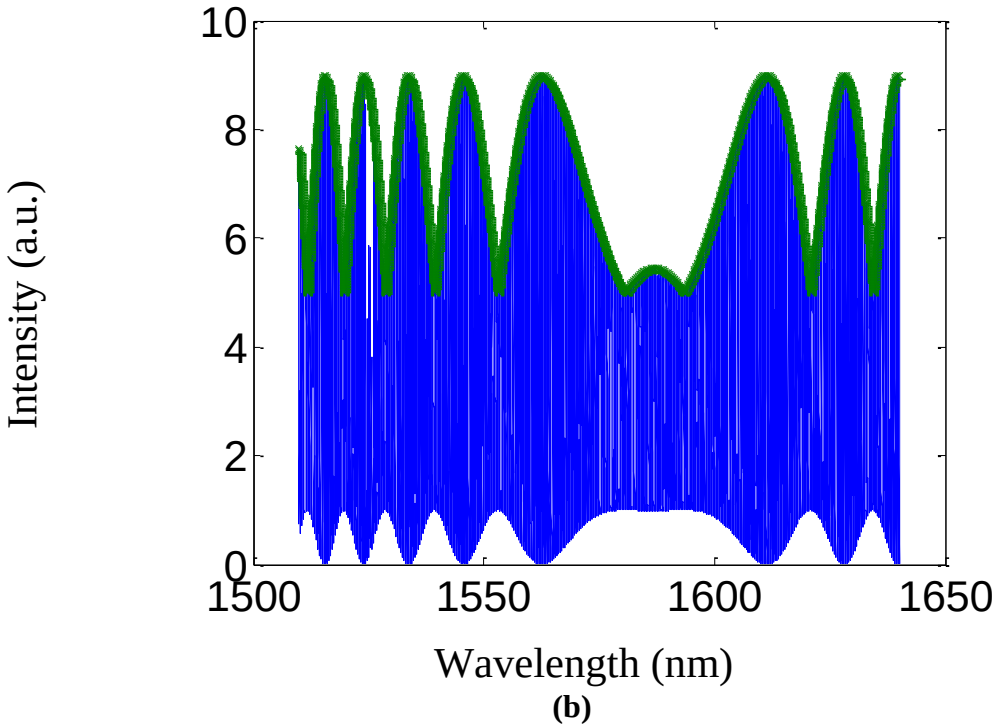

(b)

Fig. 5-4: (a) Measured *upper* envelope (experimental) fringe pattern. (b) Simulated interference pattern and upper envelope. The experimental and simulated conditions are: fiber length L_f = 0.395m effective group index at central wavelength = 1.472469, L_{air} = 1.472469L_f.

The simulated interference pattern is generated using Eq. 4-8 and the envelope of the interference pattern is generated using Eq. 4-9. The Matlab code used in the simulation is given in Appendix A.1. In the simulation a fiber length of 0.395 m is assumed in order to match the experimental conditions. The path length of the air path is determined via a calculation of the effective group index of the fiber was determined to be 1.472469 at the central wavelength, λ_o, via Eq. 5-2:

$$\frac{(\kappa(\lambda)\alpha)J_{l+1}(\kappa(\lambda)a)}{J_l(\kappa(\lambda)a)} = \frac{(\gamma(\lambda)a)K_{l+1}(\kappa(\lambda)a)}{K_l(\kappa(\lambda)a)} \qquad \textbf{Eq. 5-2}$$

Where

$$\kappa(\lambda) = \sqrt{n_{core}(\lambda)^2 - n_{eff}(\lambda)^2}$$
$$\gamma(\lambda) = \sqrt{n_{eff}(\lambda)^2 - n_{cladding}(\lambda)^2} \qquad \textbf{Eq. 5-3}$$

Note that *a* is the core size of the fiber and *J* and *K* are Bessel functions of the first and second kind. The locations of equality in Eq. 5-2 determine the values of $\kappa(\lambda)$ and $\gamma(\lambda)$ as well as a mode of the fiber. The first of these modes is called the *fundamental* mode of the fiber. The values of $n_{core}(\lambda)$ and $n_{cladding}(\lambda)$ are the index of bulk glass with the composition of the core and cladding respectively. The effective group index as a function of wavelength in SMF28^{TM} fiber is determined using the simulation in Appendix A.1.2.

In Fig 5-4 there are differences between the upper envelope of the experimental fringe pattern and the upper envelope of the simulated fringe pattern. These differences are in the contrast and amplitude of the experimental fringe pattern. The larger contrast in the experimental data is due to the fact that in the experiment the magnitude of the reflections from the facets of the fiber and the mirror were not equal. The aim of the

experiment was to simply maximize the fringe visibility so that the locations of the peaks/troughs of the envelope could be determined so that the dispersion could be calculated. The simulation has a different contrast since it assumes equal reflections from the fiber facets and the mirror. The analysis that shows how the differences in the reflections from the facets and the mirrors lead to variation in the fringe contrast was presented in chapter 4.3.1.2. The variable amplitude in the experimental fringe pattern is due to the fact that there is a background amplitude spectrum that has not been removed from the measurement.

5.4.2 Dispersion Compensating Fiber

As a second method of verification, we measured dispersion on a short piece of DCF, whose dispersion value is approximately one order of magnitude higher than that of SMF28^{TM}, and has an opposite sign. We used a 15.5$\pm$0.1 cm piece of DCF fiber, and the measurement results are given in Fig. 5-5. To verify the accuracy of our measurement, we also measured dispersion on an identical 100$\pm$0.5m DCF using a commercial dispersion measurement system (Agilent 83427A), which employs the MPS technique. Again, our measured dispersion values are in good agreement with those measured by the commercial device, though the fiber length we used is almost 3-orders of magnitude smaller.

The standard deviation of the measured dispersion is calculated by taking the difference between the measured points and a linear fit and then determining the standard deviation of the difference. The standard deviation of the measured data (as calculated using the Matlab code in Appendix A.3.2) is 0.99 ps/nm-km, which corresponds to a

relative error of 0.9%. When multiplied by the length of the fiber, this translates into a standard deviation of 0.00015 ps/nm.

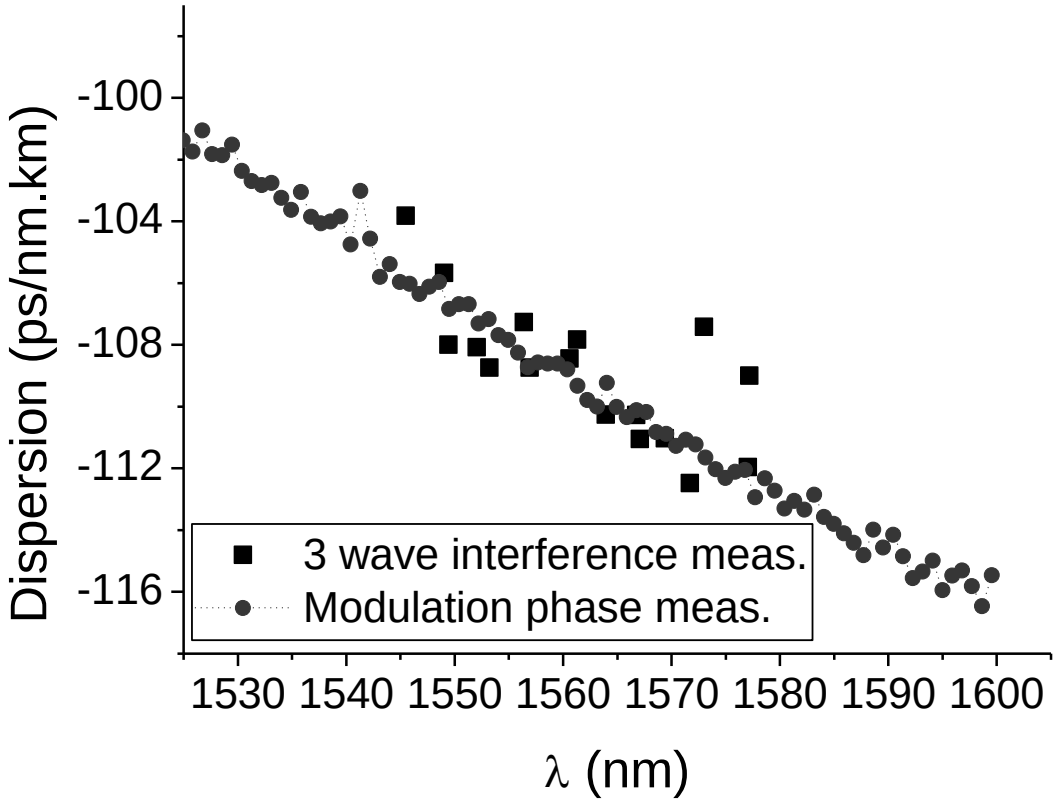

Fig. 5-5: Measured dispersion parameter plot for DCF using the Agilent 83427A and Single Arm interferometry. The standard deviation of the measured data (as calculated using the Matlab code in Appendix A.3.2 - with reference to a linear fit) using the SAI is 0.99 ps/nm-km, which corresponds to a relative error of 0.9%. When multiplied by the length of the fiber, this translates into a standard deviation of 0.00015 ps/nm.

Since DCF has negative dispersion values a procedure for determining the sign of the dispersion was developed. By examination of Eq. 4-13 repeated below for convenience

$$d\lambda_o = dL_{air}\frac{1}{cL_f D} \qquad \textbf{Eq. 5-4}$$

We can see that if the sign of the dispersion is negative then the location of the central wavelength will decrease as the path length of the air path is increased. This is a quick method for determining the sign of the dispersion.

5.4.3 Twin Hole Fiber

Twin Hole Fiber (THF) has been used in fiber poling to facilitate parametric generation in fibers [48, 52] or making fiber-based electro-optic switching devices [53]. In such nonlinear applications, dispersion of the fiber is an important parameter to be determined. The dispersion properties of THF, however, have never been reported. This is partly due to the lack of uniformity in the diameter of the THF along its length. The fiber has a 3-μm-diameter core and a numerical aperture that is higher than that of SMF28TM. The cross section of a typical THF is shown in Fig. 5-6:

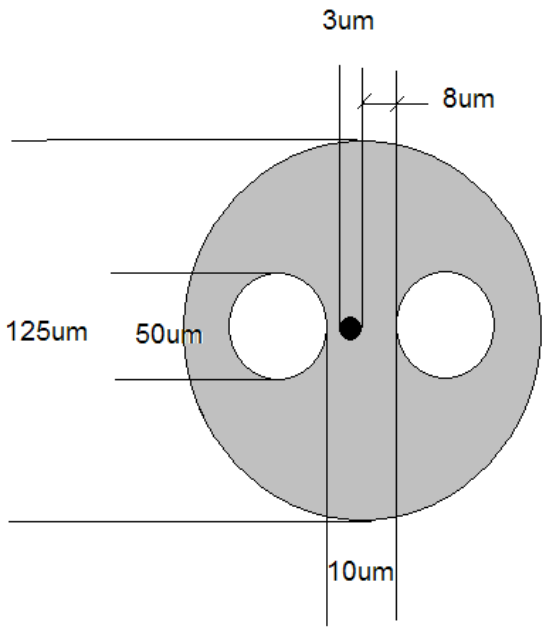

Fig. 5-6: Cross section of a typical Twin-Hole Fiber

The core is Ge-doped silica, and has an index similar to that of SMF28^{TM}. Therefore, we expect the dispersion of THF to be slightly lower than that of SMF28^{TM}. Since we did not know the magnitude of the dispersion for THF we decided to choose the largest length of THF available to increase the chance that the minimum bandwidth

required for a measurement would fit in the available bandwidth of the tunable laser source. The largest length of THF available was 45±0.1 cm. This length of fiber is slightly longer than the length allowed by Eq. 4-28 but since we used the technique of wavelength windowing described in sections 4.5.1-4.5.3 the measurement of the envelope was still possible in this experiment.

The measurement results from the experiment on THF are given in Fig. 5-7. The standard deviation of the measured dispersion is calculated by taking the difference between the measured points and a linear fit and then calculating the standard deviation from the difference. The standard deviation of the measured data, as calculated using the Matlab code in Appendix A.3.3, is 0.375 ps/nm-km (which corresponds to a relative error of 2.9%). When multiplied by the fiber length, this standard deviation translates into a precision of 0.00017 ps/nm. The slightly larger standard deviation compared to those for the SMF and DCF measurement is due to the higher loss in fiber coupling between the SMF and the THF, and hence the lower and more noisy signal level during the THF measurement.

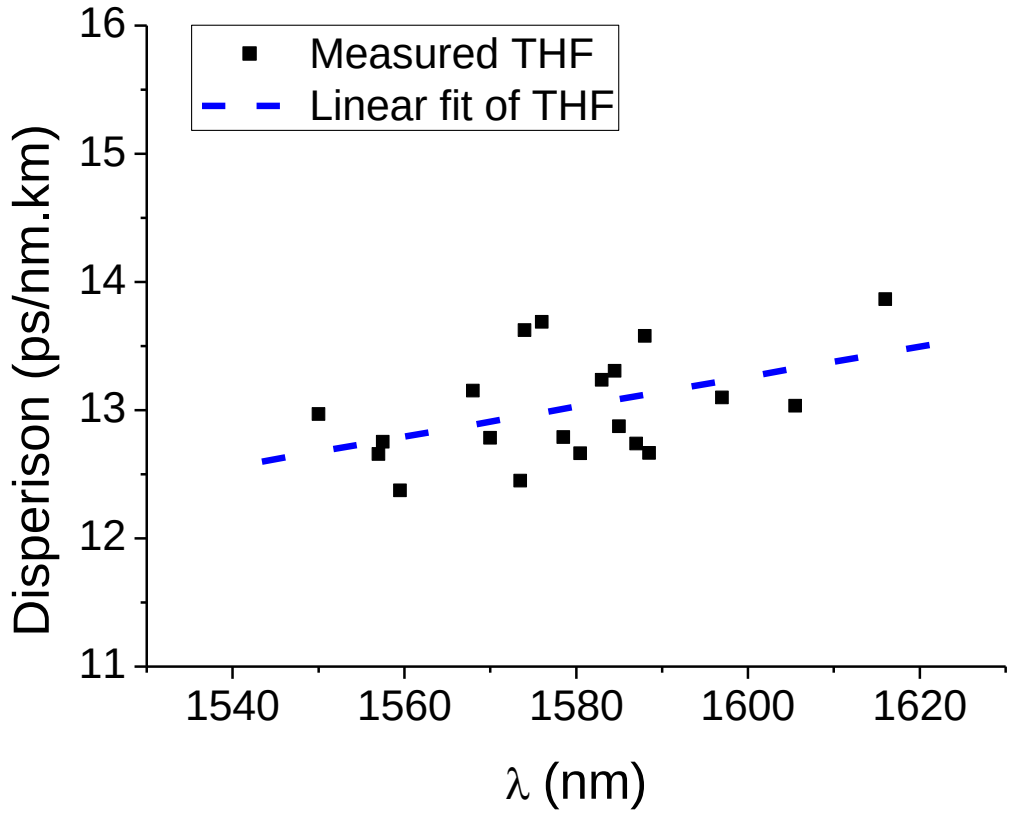

Fig. 5-7: Measured dispersion for the 45±0.1cm Twin-Hole Fiber performed using Single Arm Interferometry. The standard deviation of the measured data (as calculated using the Matlab code in Appendix A.3.3 - with reference to the linear fit) is 0.375 ps/nm-km, which corresponds to a relative error of 2.9%. Multiplied by the fiber length, this translates into a standard deviation of 0.00017 ps/nm.

An important aspect of the previous three sections is the error associated with the measurement of each point in the dispersion parameter plots. The next section outlines the source and magnitude of the error associated with the measurement of the dispersion parameter.

5.5 Error Analysis

It is important to understand the source and magnitude of the error in the measurement of the dispersion parameter in the previous experiments to gain an understanding of the precision and accuracy that can be attained with an SAI. There are several sources of error in the measurement of the dispersion parameter.

Errors introduced by the environment in which the experiment takes place are the first types of errors in the experiment. These errors are not quantifiable so they were mitigated by encasing the system in a sealed container in which the temperature and density of the air was stabilized. Encasing the system in a sealed container mitigates the error that causes a variation in the optical path length of the air path due to air currents and the error that causes a variation in the length of the fiber due to temperature fluctuations in the air.

There are three other quantifiable sources of error in the experiment. Instrument error in accurately measuring the wavelength of the tunable laser is the first, human error in measuring the lengths of the fiber used in the experiment is the second, and systematic error due to the wavelength windowing process (which puts an uncertainty with a magnitude of $\pm$ one half the window size on the points in the envelope) is the third. Instrument error in the measurement of the wavelength is much smaller than the wavelength window used to plot the envelope and as a result, it can be ignored in comparison to the systematic error.

Thus the major quantifiable contributions to the error in measuring the dispersion parameter are human error and systematic error. How these two quantities combine to

produce an overall error in the measurement of the dispersion parameter is now discussed.

The dispersion parameter is measured (at the central wavelength, λ_0) using equation Eq. 2-5:

$$D(\lambda_o) = -\frac{\lambda_o}{c}\underbrace{\left.\frac{d^2 n_{eff}}{d\lambda^2}\right|_{\lambda_o}}_{B} \qquad \textbf{Eq. 5-5}$$

There are two sources of error in this calculation; the error in the measurement of the location of the central wavelength, λ_0, due to systematic error caused by the use of wavelength windowing to plot the envelope and the error in the measurement of the second derivative of the effective index with respect to wavelength. For simplicity this quantity is henceforth referred to as *B*.

When two measurements are made independently the errors are added in quadrature. For example, given the function $z = f(x, y)$ the error in z can be calculated:

$$\Delta z = \sqrt{\left(\frac{df}{dx}\right)^2 (\Delta x)^2 + \left(\frac{df}{dy}\right)^2 (\Delta y)^2} \qquad \textbf{Eq. 5-6}$$

B and λ_0 are not independent since *B* depends on λ_0, however, for simplicity we assume that the two are independent and later we will show that the error in λ_0 is much smaller than the error in *B* and thus the error in measuring the dispersion parameter, *D*, really only depends on the error in measuring *B*. At this point, however, we proceed with the analysis assuming that the measurement of λ_0 and *B* are independent. Under this assumption the error in the dispersion parameter can be found via the addition of the errors in quadrature:

$$\Delta D = \sqrt{\left(\frac{dD}{d\lambda_o}\right)^2 (\Delta\lambda_0)^2 + \left(\frac{dD}{dB}\right)^2 (\Delta B)^2} = \sqrt{\left(\frac{B}{c}\right)^2 (\Delta\lambda_0)^2 + \left(\frac{\lambda_0}{c}\right)^2 (\Delta B)^2} \quad \textbf{Eq. 5-7}$$

Where $\Delta\lambda_o$ is the error associated with measuring the central wavelength, which is $\pm$ half the wavelength window and ΔB is the error in calculating the second derivative of the effective index with respect to wavelength. Since B is calculated using the phase information in the envelope of the interference pattern via Eq. 4-5 we use this equation in order to determine ΔB. In order to simplify the calculation of ΔB, we ignore the third order dispersion term so that Eq. 4-5 becomes:

$$\Delta\phi = m = 2L_f \left[\frac{(\lambda_2 - \lambda_0)^2}{\lambda_2} - \frac{(\lambda_1 - \lambda_0)^2}{\lambda_1}\right] \left.\frac{d^2 n_{eff}}{d\lambda^2}\right|_{\lambda_0} = 2L_f \underbrace{\left[\lambda_2 - \lambda_1 + \lambda_0{}^2\lambda_2{}^{-1} - \lambda_0{}^2\lambda_1{}^{-1}\right]}_{A(\lambda_0,\lambda_1,\lambda_2)} \underbrace{\left.\frac{d^2 n_{eff}}{d\lambda^2}\right|_{\lambda_0}}_{B}$$

Eq. 5-8

So that:

$$B = mL_f{}^{-1} A(\lambda_0, \lambda_1, \lambda_2)^{-1} \quad \textbf{Eq. 5-9}$$

Thus if we assume that all variables in the experiment are independent then their errors can be added in quadrature:

$$\Delta B = \sqrt{\left(\frac{dB}{dA}\right)^2 (\Delta A)^2 + \left(\frac{dB}{dL_f}\right)^2 (\Delta L_f)^2} = \sqrt{\left(\frac{m}{L_f A^2}\right)^2 (\Delta A)^2 + \left(\frac{m}{L_f{}^2 A}\right)^2 (\Delta L_f)^2} \quad \textbf{Eq. 5-10}$$

ΔB is the total error in measuring the second derivative of the effective index with respect to wavelength, B, and it is due to both ΔA and the human error in measuring the length of the test fiber, L_f.

ΔA is the error in calculating the B due to the error in locating the peaks of the envelope as shown in Fig. 5-8. The magnitude of this error is again $\pm$ half the width of

the wavelength window used to plot the envelope, i.e. it is the systematic error. ΔA is calculated by adding the error in measuring the location of the troughs in quadrature:

$$\Delta A = \sqrt{\left(\frac{dA}{d\lambda_o}\right)^2 (\Delta\lambda_0)^2 + \left(\frac{dA}{d\lambda_1}\right)^2 (\Delta\lambda_1)^2 + \left(\frac{dA}{d\lambda_2}\right)^2 (\Delta\lambda_2)^2}$$

$$= \sqrt{\left(2\lambda_0\left(\frac{1}{\lambda_2} - \frac{1}{\lambda_1}\right)\right)^2 (\Delta\lambda_0)^2 + \left(\left(\frac{\lambda_0}{\lambda_1}\right)^2 - 1\right)^2 (\Delta\lambda_1)^2 + \left(1 - \left(\frac{\lambda_0}{\lambda_2}\right)^2\right)^2 (\Delta\lambda_2)^2} \quad \textbf{Eq. 5-11}$$

In order to reduce the systematic error it is best to choose the wavelength locations λ_o, λ_1 and λ_2 to be the troughs of the envelope since their locations are more sharply defined. Therefore this is the reason why the troughs of the envelope locations were used in the experiments instead of the peaks. The systematic error is illustrated in Fig 5-8.

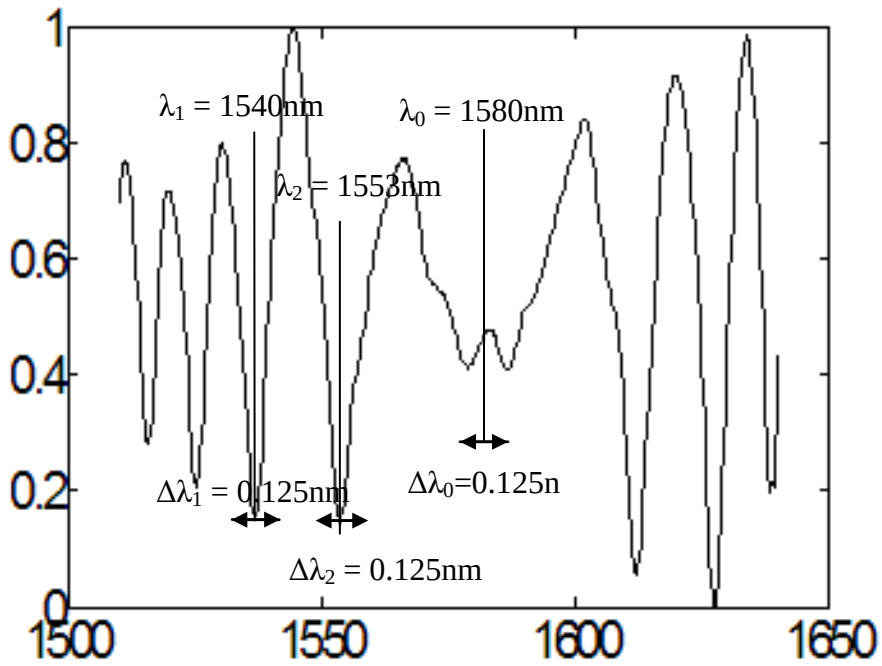

Fig. 5-8: Error in calculating *B* due to the error in locating the peaks of the interferogram

A numerical example of the error associated with the measurement of the dispersion parameters in the plots of the previous three sections is now presented for one of the SMF28^{TM} measurements. The single mode fiber was measured to be 0.395$\pm$0.001 m. Thus the human error in the measurement of the fiber length is estimated to be ΔL_f = $\pm$0.001 m. One of the interferograms from the measurement is shown in Fig. 5-8. The wavelength window size used in the experiments was 0.25nm therefore $\Delta\lambda_{0,1,2}$=0.125nm. From Fig. 5-8 we can see that λ_0 = 1580nm, λ_1 = 1540nm and λ_2 = 1553nm. Thus from Eq. 5-11, ΔA = 0.0082nm. Substitution of ΔA= 0.0082nm and ΔL_f = $\pm$0.001 m into Eq. 5-10 (assuming m = 1 separation is used as in Fig 5-8) yields,

$\Delta B = \sqrt{3.913x10^{15} + 1.268x10^{14}} = 6.356x10^{7} / m$ which shows that the error in locating the peaks of the envelope has a larger effect than the human error in measuring the length of the fiber. Substitution of this value into Eq. 5-7 yields:

$\Delta D = \sqrt{1.917x10^{-18} + 1.12x10^{-13}} = 0.334\, ps / nm - km$. Which shows that the error in measuring *B,* has a larger effect than the error in determining the central wavelength. Thus ΔD is mainly determined by the error in measuring *B* regardless of whether or not λ_0 and B are independent. This value for ΔD is consistent with the observed spread in the dispersion pattern in Fig. 5-3.

In conclusion, the experimental results of Single Arm Interferometry confirm the theory developed in chapter 4. They show that the dispersion parameter can be calculated from the envelope of the fringe pattern produced by the interference of 3 waves in a balanced SAI. The experiments on Single mode fiber (SMF28^{TM}) and Dispersion

Compensating Fiber (DCF) were used to confirm the theory behind the technique and once the technique was confirmed it was used to measure the unknown dispersion parameter plot for THF. The length of Twin hole fiber used in the experiment was larger than allowed by Eq. 4-28 so the technique of wavelength windowing, described in sections 4.5.1 - 4.5.3, had to be used. This technique was shown theoretically and via simulation to extend the maximum length of fiber that can be characterized by this technique. Ultimately the largest length of fiber that can be characterized is limited by the largest air path that can be produced in the experiment and the laser linewidth.

Chapter 6: Conclusions

6.1 Expected Significance to Academia

The single arm interferometer is introduced as an alternative to the Michelson or the Mach Zehnder configuration for interferometric measurements of the dispersion parameter. It will be most useful for measurements of the dispersion parameter in short lengths of fiber. The technology will be used to eliminate the need for the arm balancing required by dual arm interferometers and by doing so allow for greater ease in the commercialization of Interferometric dispersion measurement techniques.

The new interferometer is significant for Academia since it can be studied and used alongside the earlier types of interferometers like the Michelson, the Mach-Zehnder and the Fabry Perot. This new interferometer provides academia with another tool for studying dispersion in short length fibers and waveguides which will be useful in the development of specialty fibers. These specialty fibers require simple and accurate short length characterization since they are generally made in very small quantities and their geometry tends to vary as a function of position along the fiber.

Another significant academic achievement of the Single Arm Interferometer is that a paper has been written for this technique and it will be submitted shortly for review to the Journal 'Optics Express'. If it is accepted for publication the new technique will be accessible to anyone interested in measuring dispersion on short length fibers. This technique increases the ease of dispersion characterization and as a result it will lead to a greater number of dispersion measurements being performed, especially in the area of specialty fiber.

6.2 Expected Significance to Industry

The new interferometer is significant to Industry since it eliminates the need to compensate for unwanted reflections by eliminating the need for a coupler altogether. As a result this interferometer is a simpler (less expensive) interferometric dispersion measurement device capable of characterizing the dispersion of short length optical fiber. As a result it is a viable commercial competitor to the current Modulation Phase Shift (MPS) based devices currently on the market. The new interferometer, however, has an advantage over MPS based devices since it has the ability to measure short length fiber with high accuracy.

Also, since it can measure short lengths of fiber it has the ability for another type of measurement as well. Dispersion is a function of both material and dimensional (waveguide) properties of a fiber but if the dimensions, particularly the diameter of the fiber, vary then the dispersion will vary. If several small sections can be cut from various points on a long length fiber and the dispersion is measured in each of them then the variation in the dispersion can be plotted as a function of position in the fiber. This can then be directly related to the variation in the fiber diameter. The main point here is that a great deal of accuracy in measuring the fiber diameter can be achieved by measuring it indirectly via the dispersion and it would be an easy way for a fiber drawing company to perform quality control.

Greater commercial interest in this device will enable measurement of dispersion in smaller lengths of fiber since larger bandwidth tunable lasers will be developed. Also the advancement in the speed of the tunable laser and scanning process will make each measurement faster to obtain.

6.3 Patent Application

One of the most interesting features of a single arm interferometer is the ease with which it can be built. This ease of construction lends itself very nicely to economical commercial assembly of a dispersion measurement device. An idea which is currently under patent is to produce a cheap add-on module for a tunable laser system to allow it to make dispersion measurements. A conceptual design of such a module is illustrated in Fig. 5-9:

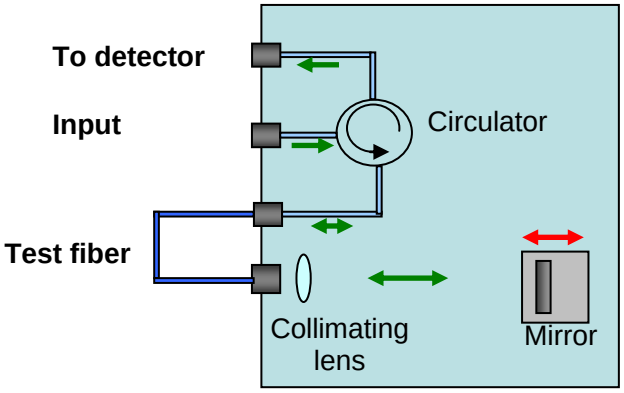

Fig. 5-9: Conceptual design for a dispersion measurement module for a tunable laser system. The connector labeled 'To detector' is the input to a power detector, the connector labeled input is connected to the output of a tunable laser. The test fiber can then be connected as shown in the diagram in order to perform the dispersion measurement.

* [U of T Invention Disclosures: RIS ID #10001509 & RIS ID #10001591 Patent applications now underway]

This dispersion measurement module could be produced to work with, for example, the Agilent 8164A or 8164B Lightwave measurement system mainframe depicted in Fig. 5-10:

Fig. 5-10: Agilent 8164A/B Lightwave measurement system mainframe.

The Agilent 8164A or 8164B Lightwave measurement mainframe is a mainframe which controls modules such as tunable lasers and measurement devices that are inserted into the slots on the mainframe. The cost of the mainframe and a tunable laser module is $20,000. A dispersion characterization system sold by Agilent, namely the Agilent 86038A/B Photonic Dispersion and Loss Analyzer depicted below in Fig. 5-11 costs $130,000.

Fig. 5-11: Agilent 86038 A/B Photonic Dispersion and Loss Analyzer

Since this system includes the mainframe and tunable laser their value must be subtracted. This leaves about $110,000 for the dispersion and loss characterization devices in the system. Since an SAI has a higher precision, can characterize both short and long length fiber and it is less expensive to implement it is very easy to see that this technology is disruptive to the industry. As a result the commercial potential of this characterization technology is quite extraordinary.

6.4 Conclusions

In this paper we presented a novel fiber-based SAI to measure directly the dispersion coefficient in short lengths of fiber (< 50 cm) with a standard deviation (precision) as low as 0.0001 ps/nm. The technique utilizes the spectral interferogram created by three reflections and extracts the second-order dispersion from the envelope of the interferogram. The technique is shown to be a simpler alternative to the Michelson or Mach Zehnder interferometers. By eliminating one of the interferometer arms, the technique does not require calibration and are less susceptible to polarization and phase fluctuations. The constraints on the operating parameters of this technique, such as wavelength resolution, fiber length, and measurable bandwidth, were discussed in detail.

We verified the technique experimentally by performing a dispersion measurement on SMF28^{TM} and DCF. Our measured dispersion results on SMF28^{TM} showed good agreement with the simulated dispersion values based on published fiber geometry and material properties. Our measurement results on DCF agreed well with the measurement performed on a much longer DCF using a commercial dispersion measurement system. In addition to SMF28^{TM} and DCF, single arm interferometry was used to measure the dispersion parameter of a twin-hole fiber for the first time.

The operating parameters of this technique were discussed in detail and it was shown that the range of measurable fiber lengths can be extended using wavelength windowing and a tunable laser with a random step size. This method can also be used to measure the dispersion of any waveguide in general and is not limited to optical fiber.

Appendix A: Matlab Code

A.1: Generating the Interference Pattern and the Envelope

```
% Envelope and Interference pattern program

clear all
close all
clc

% Parameters
step_size = 1*10^-12;% 1 pm step size
Lf = 0.395;            % Length of fiber in meters
Lair = 1.472469*Lf;    % 1.47235 is the group index
Uo=1;                % First Fresnel reflection
gamma=1;             % Fraction of first Fresnel reflection
                     % reflected from first facet
alpha=1;             % Fraction of the first Fresnel
                     % reflection reflected from the mirror

% Interference pattern
load neff2.mat        % neff for single mode fiber
neff_fit = polyfit(lambda1, neff, 3); % Interpolated
lambda = 1510*10^-9:step_size:1640*10^-9; % Interpolated
neff_sim = polyval(neff_fit, lambda);     % Interpolated
beta = (2*pi./lambda) .* neff_sim;        % Beta values interpolated
ko=2*pi./lambda;

% Entire interference pattern
I=abs(1+alpha*exp(i*beta*2*Lf)+gamma*exp(i*(beta*2*Lf+ko*2*Lair))).^2;

% Envelope of the interference pattern
envelope_full = Uo^2*(1 + alpha^2 + gamma^2 + 4*alpha*abs(cos(beta*Lf -
ko*Lair)) + 2*alpha*(gamma-1) + 2*gamma);
figure
plot(lambda,I,lambda,envelope_full, 'x');
xlabel('lambda (nm)')
ylabel('Intensity (a.u.)')
```

A.2 Calculating Neff

```
clc;
clear;
warning off;

global Ks Ko r0 rj n_j tj m beta w l eps0 mu0 ns no lambda0 V Uj Wj Rs
R1 p a
% Fiber parameters ================================================
```

```
for lambda_i=0:100

    lambda_i
    lambda0=1.5e-6+.1e-6*lambda_i/100
    lambda1(lambda_i+1)=lambda0;
    ko=2*pi/lambda0
    % SMF parameters
    m=1;
    %NA=.122;
    NA=0.112
    Delta_n=0.0036;
    n1=silica_index2(lambda0*1e6,1); % Taken from data file
    n2=silica_index2(lambda0*1e6,0); % Taken from data file
    Dn=n1-n2;
    % Source fiber
    Rs=2.3e-6;
    V=ko*Rs*sqrt(n1^2-n2^2);
    ws=Rs*(0.65+1.619*V^-1.5+2.879*V^-6);
    no=n1;
    ns=n2;
    Uo=fzero(@LP,V-.4);    % Function LP defined below
    Xo=Uo/Rs;
    Wo=sqrt(V^2-Uo.^2);
    beta(lambda_i+1) = sqrt(ko^2*n1^2-(Uo/Rs).^2);
    neff(lambda_i+1) = beta(lambda_i+1)/ko;
end

save neff2 lambda1 beta neff

%%%%%%%%%%%%%%%%%%%%%%%%%%%%%%%%%%%%%%%%%%%%%%%%%%%%


function S1=LP(U)

global V no ns m

W=sqrt(V^2-U.^2);
Jp=(besselj(m-1,U)-besselj(m+1,U))/2;
Kp=(besselk(m-1,W)+besselk(m+1,W))/2;
J=besselj(m,U);
K=besselk(m,W);

%S1=(Jp./(U.*J) + Kp./(W.*K)).*((ns/no)^2*Jp./(U.*J)+Kp./(W.*K)) -
m^2*(1./U.^2+1./W.^2).*((ns/no)^2./U.^2+1./W.^2);
S1=besselj(0,U)./(U.*besselj(1,U)) - besselk(0,W)./(W.*besselk(1,W));
end
```

A.3: Probability vs. Several other Parameters

A.3.1: Probability vs. window size

```
% Probability versus WINDOW SIZE

clear all
close all
warning off
clc

% Independent parameters that may be varied
%%%%%%%%%%%%%%%%%%%%%%%%%%%%%%%%%%%%%%%%%%%%%%%%

Lf = 0.395;              % Fiber length in meters
step_size = 1*10^(-12);  % Average wavelength step of the tunable laser
tolerance = 0.02;        % Tolerance in locating the peak (gives >99.9%
                         %  of peak)

%%%%%%%%%%%%%%%%%%%%%%%%%%%%%%%%%%%%%%%%%%%%%%%%%%%%%%%%%%%%%%%%%%%%%%%%%%%%%%%

sigma = 0.17*10^-12;
for i = 1:30
    coarse_sampling_bandwidth(i) = i* 0.01*10^-9;   % Width of window
    Pnone_average1(i) = 1 - Probability(Lf,
            coarse_sampling_bandwidth(i), step_size, tolerance, sigma)
end
% Convert to nm
coarse_sampling_bandwidth = coarse_sampling_bandwidth * 10^9;

% Plot the curve
figure
plot(coarse_sampling_bandwidth,Pnone_average1, 'b')
xlabel('Window Size in nm')
ylabel('Probability')

%%%%%%%%%%%%%%%%%%%%%%%%%%%%%%%%%%%%%%%%%%%%%%%%%%%%%%%%%%%%%%%%%%%%%%%%%%%%%%%

sigma = 0.5*10^-13;                          % sigma = 0
% Probability vs window size
for i = 1:30
    coarse_sampling_bandwidth(i) = i* 0.01*10^-9;   % Width of window
    Pnone_average2(i) = 1 - Probability(Lf,
    coarse_sampling_bandwidth(i), step_size, tolerance, sigma)
end
% Convert to nm
coarse_sampling_bandwidth = coarse_sampling_bandwidth * 10^9;

% Plot the curve
hold on
plot(coarse_sampling_bandwidth,Pnone_average2, 'g')
```

```
%%%%%%%%%%%%%%%%%%%%%%%%%%%%%%%%%%%%%%%%%%%%%%%%%%%%%%%%%%%%%%%%%%%%%%%%%%%%

sigma = 1*10^-12;
% Probability vs window size
for i = 1:30
    coarse_sampling_bandwidth(i) = i* 0.01*10^-9;   % Width of window
    Pnone_average3(i) = 1 - Probability(Lf,
    coarse_sampling_bandwidth(i), step_size, tolerance, sigma)
end
% Convert to nm
coarse_sampling_bandwidth = coarse_sampling_bandwidth * 10^9;

% Plot the curve
hold on
plot(coarse_sampling_bandwidth,Pnone_average3, 'r')
```

A.3.2: Probability vs. average step size

```
% Probability versus STEP SIZE

clear all
close all
warning off
clc

% Independent parameters that may be varied
%%%%%%%%%%%%%%%%%%%%%%%%%%%%%%%%%%%%%%%%%%%%%%%%
Lf = 0.395;                          % Fiber length in meters
tolerance = 0.02;                    % Tolerance in locating the peak
coarse_sampling_bandwidth = 0.25*10^-9;              % Width of window
for finding peak of envelope


%%%%%%%%%%%%%%%%%%%%%%%%%%%%%%%%%%%%%%%%%%%%%%%%%%%%%%%%%%%%%%%%%%%%%%%%%%%%
sigma = 0.05*10^-12;
% Test program
for i = 1:20
   step_size(i) = i*0.1*10^-12
   Pnone_average(i) = 1 - Probability(Lf, coarse_sampling_bandwidth,
   step_size(i), tolerance, sigma)
end

% Convert to pm
step_size = step_size * 10^12;

% Plot the curve
figure
plot(step_size,Pnone_average, 'g')
xlabel('Step Size in picometers')
ylabel('Probability')
```

```
hold on
%%%%%%%%%%%%%%%%%%%%%%%%%%%%%%%%%%%%%%%%%%%%%%%%%%%%%%%%%%%%%%%%%%%%%%%%%%%%%%%%
%%%%%%%%%%%%%%%%%%%%%%%%%%%%%%%%%%

sigma = 0.17*10^-12;
% Test program
for i = 1:20
    step_size(i) = i*0.1*10^-12
     Pnone_average(i) = 1 - Probability(Lf, coarse_sampling_bandwidth,
     step_size(i), tolerance, sigma)
end

% Convert to pm
step_size = step_size * 10^12;

% Plot the curve
plot(step_size,Pnone_average, 'b')

%%%%%%%%%%%%%%%%%%%%%%%%%%%%%%%%%%%%%%%%%%%%%%%%%%%%%%%%%%%%%%%%%%%%%%%%%%%%%%%%

sigma = 1*10^-12;
% Test program
for i = 1:20
    step_size(i) = i*0.1*10^-12
    Pnone_average(i) = 1 - Probability(Lf, coarse_sampling_bandwidth,
    step_size(i), tolerance, sigma)
end

% Convert to pm
step_size = step_size * 10^12;

% Plot the curve
plot(step_size,Pnone_average, 'r')
%%%%%%%%%%%%%%%%%%%%%%%%%%%%%%%%%%%%%%%%%%%%%%%%%%%%%%%%%%%%%%%%%%%%%%%%%%%%%%%%
```

A.3.3: Probability vs. fiber length

```
% Probability versus FIBER LENGTH
clear all
close all
warning off
clc

% Independent parameters that may be varied
%%%%%%%%%%%%%%%%%%%%%%%%%%%%%%%%%%%%%%%%%%%%%%%%

tolerance = 0.02;                % Tolerance in locating the peak
coarse_sampling_bandwidth = 0.25*10^-9; % Width of window
step_size = 1*10^(-12); % Average wavelength step of the tunable laser


%%%%%%%%%%%%%%%%%%%%%%%%%%%%%%%%%%%%%%%%%%%%%%%%%%%%%%%%%%%%%%%%%%%%%%%%%%%%%%%%
sigma = 0.05*10^-12;
```

```
%Pnone_average = Probability(Lf, coarse_sampling_bandwidth, step_size,
tolerance)
% % Probability vs Fiber length
for i = 1:150
    Lf(i) = 0.01*i;
    Pnone_average(i) = 1 - Probability(Lf(i),
coarse_sampling_bandwidth, step_size, tolerance, sigma);
    i
end

% Plot the curve
figure
plot(Lf,Pnone_average, 'g' )
xlabel('Fiber Length in meters')
ylabel('Probability')
hold on
%%%%%%%%%%%%%%%%%%%%%%%%%%%%%%%%%%%%%%%%%%%%%%%%%%%%%%%%%%%%%%%%%%%%%%%%%%%

%%%%%%%%%%%%%%%%%%%%%%%%%%%%%%%%%%%%%%%%%%%%%%%%%%%%%%%%%%%%%%%%%%%%%%%%%%%
sigma = 0.17*10^-12;
% % Probability vs Fiber length
for i = 1:150
    Lf(i) = 0.01*i;
    Pnone_average(i) = 1 - Probability(Lf(i),
     coarse_sampling_bandwidth, step_size, tolerance, sigma);
end

% Plot the curve
plot(Lf,Pnone_average, 'b')
%%%%%%%%%%%%%%%%%%%%%%%%%%%%%%%%%%%%%%%%%%%%%%%%%%%%%%%%%%%%%%%%%%%%%%%%%%%

%%%%%%%%%%%%%%%%%%%%%%%%%%%%%%%%%%%%%%%%%%%%%%%%%%%%%%%%%%%%%%%%%%%%%%%%%%%
sigma = 1*10^-12;
% Probability vs Fiber length
for i = 1:150
    Lf(i) = 0.01*i;
    Pnone_average(i) = 1 - Probability(Lf(i),
    coarse_sampling_bandwidth, step_size, tolerance, sigma);
end

% Plot the curve
plot(Lf,Pnone_average, 'r')
%%%%%%%%%%%%%%%%%%%%%%%%%%%%%%%%%%%%%%%%%%%%%%%%%%%%%%%%%%%%%%%%%%%%%%%%%%%
```

A.3.4: Probability vs. tolerance

```
% Probability vs. Tolerance

clear all
close all
warning off
clc
```

```
% Independent parameters that may be varied size
%%%%%%%%%%%%%%%%%%%%%%%%%%%%%%%%%%%%%%%%%%%%%%%%
Lf = 0.395;                         % Fiber length in meters
step_size = 1*10^(-12);             % Average wavelength step
tolerance = 0.02;                   % Tolerance in locating the peak
coarse_sampling_bandwidth = 0.25*10^-9;    % Width of window

%%%%%%%%%%%%%%%%%%%%%%%%%%%%%%%%%%%%%%%%%%%%%%%%%%%%%%%%%%%%%%%%%%%%%%%%%%%%%%%
sigma = 0.05*10^-12;     % Standard deviation of the source
for i = 1:50
    tolerance(i) = i* 0.001;  % Width of window
    Pnone_average(i) = 1 - Probability(Lf, coarse_sampling_bandwidth,
    step_size, tolerance(i), sigma)
end
% Convert to %
tolerance = tolerance * 100;

% Plot the curve
figure
plot(tolerance,Pnone_average, 'g')
xlabel('Tolerance: % of the peak spacing of the carrier ')
ylabel('Probability')
hold on
%%%%%%%%%%%%%%%%%%%%%%%%%%%%%%%%%%%%%%%%%%%%%%%%%%%%%%%%%%%%%%%%%%%%%%%%%%%%%%%

%%%%%%%%%%%%%%%%%%%%%%%%%%%%%%%%%%%%%%%%%%%%%%%%%%%%%%%%%%%%%%%%%%%%%%%%%%%%%%%
sigma = 0.17*10^-12;        % Standard deviation of the source
for i = 1:50
    tolerance(i) = i* 0.001;   % Width of window
    Pnone_average(i) = 1 - Probability(Lf, coarse_sampling_bandwidth,
    step_size, tolerance(i),sigma)
end
% Convert to %
tolerance = tolerance * 100;

% Plot the curve

plot(tolerance,Pnone_average, 'b')

%%%%%%%%%%%%%%%%%%%%%%%%%%%%%%%%%%%%%%%%%%%%%%%%%%%%%%%%%%%%%%%%%%%%%%%%%%%%%%%

%%%%%%%%%%%%%%%%%%%%%%%%%%%%%%%%%%%%%%%%%%%%%%%%%%%%%%%%%%%%%%%%%%%%%%%%%%%%%%%
sigma = 1*10^-12;     % Standard deviation of the source
for i = 1:50
    tolerance(i) = i* 0.001;   % Width of window
    Pnone_average(i) = 1 - Probability(Lf, coarse_sampling_bandwidth,
    step_size, tolerance(i), sigma)
end
% Convert to %
tolerance = tolerance * 100;

% Plot the curve
plot(tolerance,Pnone_average, 'r')
%%%%%%%%%%%%%%%%%%%%%%%%%%%%%%%%%%%%%%%%%%%%%%%%%%%%%%%%%%%%%%%%%%%%%%%%%%%%%%%
```

A.3.5: The Probability calculating function

```
function Pnone_average =
Probability(Lf,coarse_sampling_bandwidth,step_size,tolerance,sigma)


% Dependent parameters
N = coarse_sampling_bandwidth/step_size;
   % n = Step number, N = number of steps of the tunable laser

% Dependent on fiber
load neff2.mat    % neff for single mode fiber calc from prog in A.2.6
neff_fit = polyfit(lambda1, neff, 4);  % Interpolated
lambda = 1510*10^-9:step_size:1640*10^-9;
neff_sim = polyval(neff_fit, lambda);

beta = (2*pi./lambda) .* neff_sim;
ko=2*pi./lambda;
lambda_p = lambda.^2./(2*neff_sim*Lf);
                  % Fringe period as a function of wavelength

% Determine M
summation = 0;
M = 1;
while summation < coarse_sampling_bandwidth
    summation = summation + lambda_p(M);
    M = M+1; % m = Peak number, M = number of peaks of
             % carrier in the coarse sampling bandwidth
end
lambda_p = summation/M;
           % lambda_p is now the average carrier period
% Dep on required tolerance
epsilon = tolerance*lambda_p;

% Probability calculation
lambda0 = 0:lambda_p/100:lambda_p;
      % Average of Pnone for different lambda0's over the period
      % of one carrier wave using 100 slots

Pnone = 1;        % Initialize
for m = 1:M
    for n = 0:N-1
        t_upper = ((m*lambda_p+(epsilon/2))-
                  (n*step_size+lambda0))/((2)^0.5*sigma);
        t_lower = ((m*lambda_p-(epsilon/2))-
                  (n*step_size+lambda0))/((2)^0.5*sigma);
        Pmn = 0.5*(erf(t_upper)-erf(t_lower));
        Pnone = Pnone .* (1 - Pmn);
    end
end
Pnone_average = (1/100) * sum(Pnone);
% Equivalent to taking (1/period) * integral --> Averaging
% function
end
```

A.4: Determining the Precision of the Measurements

A.4.1: Standard deviation of the SMF28™ Measurement

```
% Standard deviation of measured points for SMF

clear all
close all
clc

lambda = [1561.75 1562 1568.00625 1568.933 1570.6 1574.56 1578.92
1582.33 1582.5 1587.75 1591.85 1585.9 1585.179 1584.5 1582.0625 1578.35
1575.525];
D = [16.82755171 17.18662336 17.77326099 17.20098046 17.59624122
18.2471311 17.68196927 18.2652686 17.92272445 18.70175776 18.92026714
18.39241202 17.89563351 18.398473 17.65587929 17.87261432 17.83568272];

D_eq = polyfit(lambda, D, 1);
D_fit = polyval(D_eq, lambda);

figure
plot(lambda, D, '.', lambda, D_fit)

x = D - D_fit;
mu = mean(x)
sigma = std(x)
```

A.4.2: Standard deviation of the DCF Measurement

```
% Standard deviation of measured points for DCF

clear all
close all
clc

lambda = [1589.58 1577.06 1571.69 1567.09 1561.29 1556.3875 1552.03
1549.04 1545.5 1549.45 1553.21 1556.94 1560.6 1563.96 1566.76 1569.38];
D = [-116.7629518 -111.959276 -112.4753801 -111.047913 -107.8351303 -
107.2692935 -108.0823711 -105.6770865 -103.8157538 -107.9982834 -
108.7332739 -108.7422301 -108.4420574 -110.2654607 -110.2692982 -
111.0290457];

D_eq = polyfit(lambda, D, 1);
D_fit = polyval(D_eq, lambda);
figure
plot(lambda, D, '.', lambda, D_fit)

x = D - D_fit;
mu = mean(x)
sigma = std(x)
```

A.4.3: Standard deviation of the THF Measurement

```
% Standard deviation of measured points for THF

clear all
close all
clc

lambda = [1616 1605.5 1597 1559.5 1557.5 1550 1557 1570 1578.5 1585
1587 1588.5 1588 1583 1580.5 1573.5 1568 1574 1576 1584.5];
D = [13.8648 13.0351 13.0996 12.3733 12.7532 12.9702 12.6568 12.7846
12.7902 12.8739 12.7401 12.6646 13.5784 13.2361 12.6629 12.4485 13.1504
13.6222 13.6876 13.3069];

D_eq = polyfit(lambda, D, 1);
D_fit = polyval(D_eq, lambda);

figure
plot(lambda, D, '.', lambda, D_fit)

x = D - D_fit;
mu = mean(x)
sigma = std(x)
```

Appendix B Corning SMF28™ Data Sheet

Corning® SMF-28™ Optical Fiber
Product Information

PI1036
Issued: April 2002
Supersedes: December 2001
ISO 9001 Registered

Corning® Single-Mode Optical Fiber

The Standard For Performance

Corning® SMF-28™ single-mode optical fiber has set the standard for value and performance for telephony, cable television, submarine, and utility network applications. Widely used in the transmission of voice, data, and/or video services, SMF-28 fiber is manufactured to the most demanding specifications in the industry. SMF-28 fiber meets or exceeds ITU-T Recommendation G.652, TIA/EIA-492CAAA, IEC Publication 60793-2 and GR-20-CORE requirements.

Taking advantage of today's high-capacity, low-cost transmission components developed for the 1310 nm window, SMF-28 fiber features low dispersion and is optimized for use in the 1310 nm wavelength region. SMF-28 fiber also can be used effectively with TDM and WDM systems operating in the 1550 nm wavelength region.

Features And Benefits

- Versatility in 1310 nm and 1550 nm applications
- Enhanced optical properties that optimize transmission performance
- Outstanding geometrical properties for low splice loss and high splice yield
- OVD manufacturing reliability and product consistency
- Optimized for use in loose tube, ribbon, and other common cable design

The Sales Leader

Corning SMF-28 fiber is the world's best selling fiber. In 2001, SMF-28 fiber was deployed in over 45 countries around the world. All types of network providers count on this fiber to support network expansion into the 21st Century.

Protection And Versatility

SMF-28 fiber is protected for long-term performance and reliability by the CPC®coating system. Corning's enhanced, dual acrylate CPC coatings provide excellent fiber protection and are easy to work with. CPC coatings are designed to be mechanically stripped and have an outside diameter of 245 µm. They are optimized for use in many single- and multi-fiber cable designs including loose tube, ribbon, slotted core, and tight buffer cables.

Patented Quality Process

SMF-28 fiber is manufactured using the Outside Vapor Deposition (OVD) process, which produces a totally synthetic ultra-pure fiber. As a result, Corning SMF-28 fiber has consistent geometric properties, high strength, and low attenuation. Corning SMF-28 fiber can be counted on to deliver excellent performance and high reliability, reel after reel. Measurement methods comply with ITU recommendations G.650, IEC 60793-1, and Bellcore GR-20-CORE.

Optical Specifications

Attenuation

Wavelength	Attenuation* (dB/km)	
(nm)	Premium	Standard
1310	≤0.34	≤0.35
1550	≤0.20	≤0.22

*Alternate attenuation values available upon request

Point Discontinuity

No point discontinuity greater than 0.10 dB at either 1310 nm or 1550 nm.

Attenuation at the Water Peak

The attenuation at 1383 ± 3 nm shall not exceed 2.1 dB/km.

Attenuation vs. Wavelength

Range (nm)	Ref. λ (nm)	Max. α Difference (dB/km)
1285 - 1330	1310	0.05
1525 - 1575	1550	0.05

The attenuation in a given wavelength range does not exceed the attenuation of the reference wavelength (λ) by more than the value α.

Attenuation with Bending

Mandrel Diameter (mm)	Number of Turns	Wavelength (nm)	Induced Attenuation* (dB)
32	1	1550	≤0.50
50	100	1310	≤0.05
50	100	1550	≤0.10
60	100	1550	≤0.05

*The induced attenuation due to fiber wrapped around a mandrel of a specified diameter.

Cable Cutoff Wavelength (λ_{ccf})

$\lambda_{ccf} \leq 1260$ nm

Mode-Field Diameter

9.2 ± 0.4 µm at 1310 nm

10.4 ± 0.8 µm at 1550 nm

Dispersion

Zero Dispersion Wavelength (λ_0):

1302 nm ≤ λ_0 ≤ 1322 nm

Zero Dispersion Slope (S_0):

≤ 0.092 ps/(nm²•km)

$$\text{Dispersion} = D(\lambda) := \frac{S_0}{4}\left[\lambda - \frac{\lambda_0^4}{\lambda^3}\right] \text{ps/(nm•km)},$$

for 1200 nm ≤ λ ≤ 1600 nm

λ = Operating Wavelength

Polarization Mode Dispersion

Fiber Polarization Mode Dispersion (PMD)

	Value (ps/√km)
PMD Link Value	≤ 0.1*
Maximum Individual Fiber	≤ 0.2

* Complies with IEC 60794-3:2001, section 5.5, Method 1, September 2001.

The PMD link value is a term used to describe the PMD of concatenated lengths of fiber (also known as the link quadrature average). This value is used to determine a statistical upper limit for system PMD performance.

Individual PMD values may change when cabled. Corning's fiber specification supports network design requirements for a 0.5 ps/√km maximum PMD.

Environmental Specifications

Environmental Test Condition	Induced Attenuation 1310 nm/1550 nm (dB/km)
Temperature Dependence -60°C to +85°C*	≤0.05
Temperature-Humidity Cycling -10°C to +85°C*, up to 98% RH	≤0.05
Water Immersion, 23°± 2°C*	≤0.05
Heat Aging, 85° ± 2°C*	≤0.05

*Reference temperature = +23°C

Operating Temperature Range

-60°C to +85°C

Dimensional Specifications

Length (km/reel): fiber lengths available up to 50.4*

* Longer spliced lengths available at a premium.

Glass Geometry

Fiber Curl: ≥ 4.0 m radius of curvature
Cladding Diameter: 125.0 ± 0.7 µm
Core-Clad Concentricity: ≤ 0.5 µm
Cladding Non-Circularity: ≤ 1.0%

Defined as: $\left[1-\frac{\text{Min. Cladding Diameter}}{\text{Max. Cladding Diameter}}\right] \times 100$

Coating Geometry

Coating Diameter: 245 ± 5 µm
Coating-Cladding Concentricity: <12 µm

Mechanical Specifications

Proof Test

The entire fiber length is subjected to a tensile proof stress ≥ 100 kpsi (0.7 GN/m²)*.

* Higher proof test levels available at a premium.

Performance Characterizations

Characterized parameters are typical values.

Core Diameter: 8.2 µm

Numerical Aperture: 0.14

NA is measured at the one percent power level of a one-dimensional far-field scan at 1310 nm.

Zero Dispersion Wavelength (λ_0): 1313 nm

Zero Dispersion Slope (S_0): 0.086 ps/(nm²•km)

Refractive Index Difference: 0.36%

Effective Group Index of Refraction, (N_{eff} @ nominal MFD):

1.4677 at 1310 nm
1.4682 at 1550 nm

Fatigue Resistance Parameter (n_d): 20

Coating Strip Force:

Dry: 0.6 lbs. (3N)
Wet, 14-day room temperature: 0.6 lbs. (3N)

Rayleigh Backscatter Coefficient (for 1 ns pulse width):

1310 nm: -77 dB
1550 nm: -82 dB

Refractive Index Profile (typical fiber)

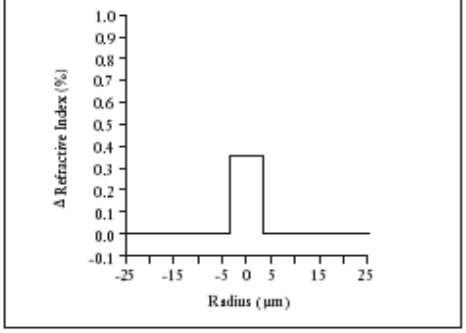

Spectral Attenuation (typical fiber)

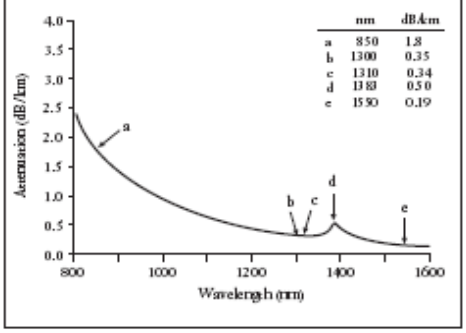

Ordering Information

To order Corning® SMF-28™ fiber, contact your sales representative, or call the Optical Fiber Customer Service Department at **607-248-2000** or **+44-1244-287-437** in Europe. Please specify the following parameters when ordering.

Fiber Type: Corning® SMF-28™ Fiber

Fiber Attenuation: dB/km

Fiber Quantity: km

Other: (Requested ship date, etc.)

Corning Incorporated
www.corning.com/opticalfiber

One Riverfront Plaza
Corning, NY 14831
U.S.A.

Phone: 800-525-2524 (U.S. and Canada)
607-786-8125 (International)

Fax: 800-539-3632 (U.S. and Canada)
607-786-8344 (International)

Email: cofic@corning.com

Europe

Phone: 00 800 6620 6621 (U.K.*, Ireland, Italy, France, Germany, The Netherlands, Spain and Sweden)

+1 607 786 8125 (All other countries)

Fax: +1 607 786 8344

Asia Pacific

Australia
Phone: 1-800-148-690
Fax: 1-800-148-568

Indonesia
Phone: 001-803-015-721-1261
Fax: 001-803-015-721-1262

Malaysia
Phone: 1-800-80-3156
Fax: 1-800-80-3155

Philippines
Phone: 1-800-1-116-0338
Fax: 1-800-1-116-0339

Singapore
Phone: 800-1300-955
Fax: 800-1300-956

Thailand
Phone: 001-800-1-3-721-1263
Fax: 001-800-1-3-721-1264

Latin America

Brazil
Phone: 000817-762-4732
Fax: 000817-762-4996

Mexico
Phone: 001-800-235-1719
Fax: 001-800-339-1472

Venezuela
Phone: 800-1-4418
Fax: 800-1-4419

Greater China

Beijing
Phone: (86)10-6505-5066
Fax: (86) 10-6505-5077

Hong Kong
Phone: (852)2807-2723
Fax: (852) 2807-2152

Shanghai
Phone: (86)21-3222-4668
Fax: (86) 21-6288-1575

Taiwan
Phone: (886)2-2716-0338
Fax: (886) 2-2716-0339

E-mail: GCCofic@corning.com

References and links

1. Hect Eugene, 'Optics: 4th Ed', Addison Wesley (2002)
2. Agrawal G. P., 'Fiber-Optic Communication Systems: 3rd Ed', Wiley-Interscience (2002)
3. Liu Jia-Ming, 'Photonic Devices', Cambridge University Press (2005)
4. M. Saleh & C. Teich, "Fundamentals of Photonics", John Wiley and Sons, Inc (2001)
5. K.C Chan and H.F. Liu, "Effect of third order dispersion on soliton-effect pulse compression," Opt. Lett., vol. 19, no. 11, pp. 49-51 (1994)
6. L. F. Mollenauer, R. H. Stolen, and J. P. Gordon, "Experimental observation of picosecond pulse narrowing and solitons in optical fibers," Phys. Rev. Lett. 45, 1095-1098 (1980).
7. W.J. Thomlinson, R.H. Stolen, and C.V. Shank, "Compression of optical pulses chirped by self-phase modulation in fibers," J. Opt. Soc. Amer. B, vol.1 no. 2, pp 139-149 (1984)
8. L.F. Mollenauer, R.H. Stolen, J.P. Gordon, and W.J. Tomlinson, "Extreme picosecond pulse narrowing by means of soliton effect in single mode optical fibers," Opt. Lett. Vol. 8, no. 5, pp. 289-291 (1983)

9. T. Mizunami, T. Tsukada, "Quasi phase-matched second-harmonic generation in thermally poled twin-hole fiber by periodic UV depoling," 30th European Conference on Optical Communication. ECOC 2004, pt. 2, p240-1, vol. 2. (2004)

10. T. Mizunami, T. Tsukada, Y. Noi, K. Horimoto "Second-harmonic generation in thermally poled twin-hole fiber using nanosecond and femtosecond laser pulses", 2003 IEEE LEOS Annual Meeting Conference Proceedings (IEEE Cat. No. 03CH37460), pt.1, p.413-14 vol. 1 (2003)

11. T. Mizunami, T. Tsukada, Y. Noi, K. Horimoto, "Second-order nonlinearity and phase matching in thermally poled twin-hole fiber", Proc. SPIE – The International Society for Optical Engineering, v. 5350, Optical Component and Materials, p.115-122, (2004)

12. D. Liu, W. Tong, S. Liu and H Liu, "Study on the Fabrication Techniques of Photonic Crystal Fiber and PCF based Structures," Proc. SPIE – The International Society for Optical Engineering, v.5722, no. 1, p.123-9 (2005)

13. T. Matsui, K. Nakajima and I. Sankawa, "Dispersion Compensation Over All the Telecommunication Bands With Double-Cladding Photonic Crystal Fiber", Jour. Lightwave Tech. Vol. 25, no. 3 (2007)

14. D.J. Richardson et al, "Advances in microstructured fiber technology", Proc. WFOPC2005 – 4th IEEE/LEOS Workshop on Fibres and Optical Passive Components, p. 1-9 (2005)

15. E. Desurvire, Erbium Doped Fiber Amplifiers: Principles and Applications, A Wiley-Interscience Publication (1994).

16. P. Merrit, R. P. Tatam, and D.A. Jackson, "Interferometric chromatic dispersion measurements on short lengths of Monomode optical fiber," J. Lightwave Technol. 7, 703-716 (1989).

17. L. G. Cohen. "Comparison of single-mode fiber dispersion measurement techniques," J. Lightwave Technol. 3, 958-966 (1985).

18. J. H. Wiesenfeld and J. Stone, "Measurement of dispersion using short lengths of an optical fiber and picosecond pulses from semiconductor film lasers," J. Lightwave Technol., vol. LT-2, p.464, (1984).

19. B. Costa, D. Mazzoni, M. Puleo, E. Vezzoni, " Phase Shift Technique for the measurement of Chromatic Dispersion in Optical Fibers using LED's", IEEE Transactions on Microwave Theory and Techniques, vol. 82, Issue 10, p. 1497-1503 (1982).

20. Agilent White Paper, "Agilent 86038B Photonic Dispersion and Loss Analyzer", January 2007.

21. J. Brendel, H. Zbinden, and N. Gision, "Measurement of chromatic dispersion in optical fibers using pairs of correlated photons," Opt. Commun. 151, 35-39 (1998).

22. L. Cherbi, M. Mehenni, and R. Aksas, "Experimental Investigation of the Modulation Phase-Shift Method for the Measure of the Chromatic Dispersion in a Single-Mode fiber coiled on a cover spool," Microwave and Optical Tech. Letts. Vol. 48, No. 1 (January 2006).

23. R. Cella and W. Wood, "Measurement of chromatic Dispersion in erbium doped fiber using low coherence interferometry," *Proceedings of the Sixth Optical Fiber Measurement Conference,* 207-210 (2001).

24. Y.O. Noh, D.Y. Kim, S.K. Oh, U.C. Pack. "Dispersion measurements of a short length optical fiber using Fourier transform spectroscopy", ThB5, Cleo, Pacific Rim '99 pp. 599-600, 1999. P. J. Harshman, T. K. Gustafson, P. Kelley, "Title of paper," J. Chem. Phys. **3,** (to be published).

25. D. D Shellee and K. B. Rochford, "Low-coherence interferometric measurements of the dispersion of multiple fiber bragg gratings," IEEE Photon. Technol. Lett. 13, 230-232 (2001).

26. J. Gehler and W. Spahn, "Dispersion measurement of arrayed-waveguide grating by Fourier transform spectroscopy," Electron. Lett. 36, 338-340 (2000).

27. P. Hamel, Y. Jaouen and R. Gabet, "Optical low-coherence reflectometry for complete chromatic dispersion characterization of few-mode fibers," Opt. Letts. Vol. 32, No. 9 (2007).

28. F. Hakimi, H. Hakimi. “Measurement of optical fiber dispersion and dispersion slope using a pair of short optical pulses and Fourier transform property of dispersive medium”, Optical Engineering, Vol. 40 No. 6, (June 2001).

29. C. Palavicini, Y. Jaouën, G. Debarge, E. Kerrinckx, Y. Quiquempois, M. Douay, C. Lepers, A.-F. Obaton, G. Melin, “Phase-sensitive optical low-coherence reflectometry technique applied to the characterization of photonic crystal fiber properties,” Optics Letts., 30, .361 (2005)

30. A. Wax, C. Yang, and J.A. Izatt, “Fourier-domain low-coherence interferometry for light-scattering spectroscopy,” Opt. Lett. 28, 1230-1232 (2003).

31. K. Takada, I. Yokohama, K. Chida, and J. Noda, “New measurement system for fault location in optical waveguide devices based on an interferometric technique,” Appl. Opt. 26, 1603-1605 (1987).

32. R. K. Hickernell, T. Kaumasa, M. Yamada, M. Shimizu, M. Horiguchi. “Pump-induced dispersion of erbium-doped fiber measured by Fourier-transform spectroscopy”, Opt. Lett. Vol. 18. no. 1, (1993).

33. C. D. Dorrer, N. Belabas, J. P. Likforman, and M. Joffre, “Spectral resolution and sampling in Fourier transform spectral interferometry,” J. Opt. Soc. Am. B 17, 1795-1802 (2000).

34. C. Dorrer, “Influence of the calibration of the detector on spectral interferometry”, J.Opt. Soc. Am. B, 16, No. 7 (1999).

35. P. Hlubina, "White-light spectral interferometry to measure intermodal dispersion in two-mode elliptical core optical fibers, Opt. Commun. 218, 283-289 (2003).

36. P. Hlubina, T. Martynkien, and W. Urbanczyk, "Dispersion of group and phase modal birefringence in elliptical-core fiber measured by white-light spectral interferometry," Opt. Express 11, 2793-2798 (2003).

37. J. Tignon, M. V Marquezini, T. Hasch, and D. S. Chemals, "Spectral interferometry of semiconductor nanostructures," IEEE J. Quantum Electron. 35, 510-522 (1999).

38. A. B. Vakhtin, K. A. Peterson, W. R. Wood, and D. J. Kane, "Differential spectral interferometry and imaging technique for biomedical applications," Opt. Lett. 28, 1332-1334 (2003).

39. A. F. Fercher, C. K. Hitzenberger, G. Kamp, and S. Y. Elzaiat, "Measurement of Intraocular Distances by Backscattering Spectral Interferometry," Opt. Commun. 117, 43-48 (1995).

40. R. Leitgeb, W. Drexler, A. Unterhuber, B. Hermann, T. Bajraszewski, T. Le, A. Stingl, and A. Fercher, "Ultra high resolution Fourier domain optical coherence tomography," Opt. Express 12, 2156-2165 (2004).

41. D. Huang, E. A. Swang, C. P. Lin, J. S. Schuman, W. G. Stinson, W. Chang, M. R. Hee, T. Flotte, K. Gregory, C. A. Puliafito, and J. G. Fugimoto, "Optical coherence tomography," Science 254, 1178-1181 (1991).

42. M. Wojtkowski, R. Leitgeb, A. Kowalczyk, T. Bajraszewski, and A. F. Fercher, "In vivo human retinal imaging by Fourier domain optical coherence tomography," J. Biomed. Opt. 7, 457-463 (2002).

43. M. Wojtkowski, A. Kowalczyk, R. Leitgeb, and A. F. Fercher, "Full range complex spectral optical coherence tomography technique in eye imaging," Opt. Lett. 27, 1415-1417 (2002).

44. G. Hausler and M. W. Lindner, "Coherence Radar and Spectral Radar – New tools for dermatological diagnosis," J. Biomed. Opt. 3, 21-31 (1998).

45. R. Leitgeb, C. Hitzenberger, and A. Fercher, "Performance of Fourier domain vs. time domain optical coherence tomography," Opt. Express 11, 889-894 (2004).

46. B. Auguie, A. Mussot, A. Boucon, E. Lantz, and T. Sylvestre, "Ultralow Chromatic Dispersion Measurement of Optical Fibers With a Tunable Fiber Laser," IEEE Photon. Tech. Lett. Vol. 18, no. 17, 1825-1827 (2006).

47. J. Y. Lee and D. Y. Kim, "Versatile chromatic dispersion measurement of a single mode fiber using spectral white light interferometry," Opt. Express, Vol. 14, no. 24, 11608-11615 (2006).

48. P. Blazkiewicz, W. Xu, D. Wong, S. Fleming, and T. Ryan, "Modification of Thermal Poling Evolution Using Novel Twin-Hole Fibers," J. Lightwave Technol. **19**, 1149- (2001).

49. H.T. Shang, "Chromatic dispersion measurement by white light interferometry on meter length single-mode optic fibers," Electron. Letts., vol. 17, p. 603 (1981).

50. Andrei B. Vakhtin, Daniel J. Kane, William R. Wood, and Kirsten A. Peterson. "Common-path interferometer for frequency-domain optical coherence tomography", Applied Optics, vol 42, No. 34, p6953 (December 2003.)

51. U. Sharma, N.M. Fried, J.U. Kang, "All-fiber common-path optical coherence tomography: sensitivity optimization and system analysis", IEEE Journal of Selected Topics in Quantum Electronics, Vol. 11, Issue 4, p799-805 (2005).

52. P.G. Kazansky, L. Dong, and P.S.J. Russell, "High second-order nonlinearities in poled silicate fibers," Opt. Lett, **19**, 701-703 (1994).

53. M. Fokine, L. E. Nilsson, Ã. Claesson, D. Berlemont, L. Kjellberg, L. Krummenacher, and W. Margulis, " Integrated fiber Mach-Zehnder interferometer for electro-optic switching," Opt. Lett. **27**, 1643-1645 (2002).